U-Pb Geochronology & Geochemistry of Apatite within the Marshall Shear Zone of the Ernest Henry Deposit, NW Queensland.

Thesis submitted in accordance with the requirements of the University of Adelaide for an Honours Degree in Geology

Alistair Griffin

October 2018

U-PB GEOCHRONOLOGY & GEOCHEMISTRY OF APATITE WITHIN THE MARSHALL SHEAR ZONE OF THE ERNEST HENRY DEPOSIT, NW QUEENSLAND.

RUNNING TITLE: **Geochronology and Geochemistry of Marshall Shear Zone Apatite**

ABSTRACT

Ernest Henry is the largest known Iron Oxide Copper Gold (IOCG) deposit within the Eastern Fold Belt of the Proterozoic Mount Isa Inlier. The deposit is hosted in meta-andesitic volcanics, the temporal equivalent of the Mount Fort Constantine volcanics. The orebody formed in a hydrothermally altered and brecciated system with the four shear zones: Hangingwall Shear Zone (HWSZ), Footwall Shear Zone, Inter-lens and the Marshall Shear Zone (MSZ). The Marshall Shear Zone has been overlooked due to its relative distance to the orebody. However, it plays an important role in improving our understanding of the timing of alteration, formation and mineralisation within the deposit. This study uses geochronology and geochemistry techniques to investigate apatite grains within the MSZ and E1 deposits.

Apatite from the MSZ provided U-Pb ages between 1508 ± 45 Ma and 1463 ± 38 Ma, synchronous with the late stage of Cu-Au mineralisation and regional D_3 deformation event of the Isan Orogeny. The E1-North apatite dated at 1550 ± 16 Ma, synchronous with early K (-Ba)-feldspar, apatite, biotite and magnetite of the stage 2 alteration at E1 and pre-mineralisation at Ernest Henry. However, investigations into the paragenesis and fluid chemistry of apatite within the MSZ suggest the apatite could have undergone fluid induced resetting and could be older than the age found in this study.

Trace element compositions of the MSZ and E1 apatite suggest the source of fluids that formed the apatite were likely magmatic and hydrothermal in origin, rich in S + REE, but sourced from different magmatic bodies, similar to the Williams and Naraku Batholiths. The metasomatising fluid affecting the MSZ and E1-North apatite populations are likely a combination of the magmatic-hydrothermal fluids mentioned before, and a highly saline upper crustal brine, or a S bearing fluid form the Corella Formation.

KEYWORDS

Apatite, U-Pb Geochronology, Geochemistry, Marshall Shear Zone, Ernest Henry Deposit, Trace Elements,

TABLE OF CONTENTS

LIST OF FIGURES AND TABLES

LIST OF EQUATIONS

1. INTRODUCTION

The Ernest Henry Iron Oxide Copper-Gold (IOCG) deposit is located within the Eastern Fold Belt of the Mount Isa Inlier, Queensland, 35km NW of Cloncurry (Figure 1). Drilling of large magnetic anomalies lead to its discovery in 1991 beneath 35 – 60m of Phanerozoic sedimentary material where it contained a pre-mining resource of 166Mt at 1.1% Cu and 0.54 g/t (Lilly, Case, & Miller, 2017). Hosted within the heavily altered Mount Fort Constantine (intermediate) volcanics, the pipe-like orebody is the largest deposit in the Eastern Succession, and second largest IOCG deposit in Australia after Olympic Dam. The orebody is bound by two magnetite-biotite dominated shear zones trending NE called the Hangingwall Shear Zone (HWSZ) and the Footwall Shear Zone (FWSZ) that dip roughly 45^{o} SSE. At greater depths, the orebody is separated into two distinct lenses by a strongly foliated zone known as the Inter-lens (Cave, Lilly, Glorie, & Gillespie, 2018; O'Brien, 2016). Previous paragenetic and geochronology studies (Cave, 2017; O'Brien, 2016) have determined that the Inter-lens predates mineralisation by ca. 50Ma. The Marshall Shear Zone (MSZ) is an additional shear zone to the south of the HWSZ, and dips SSE at ca. 60°. The composition of the MSZ is comparable to that of the other shear zones; dominated by many overprinting alteration events, and infill that consists of magnetite, biotite, amphibole and K-feldspar with coarse-grained apatite and garnet, possibly as a result of the original metasediment or metavolcanic protolith. The shear zones are all affected by minor and relatively late cross-cutting calcite, quartz, biotite, pyrite and chalcopyrite from the main ore stage and post-ore chlorite and sericite alteration and calcite-quartz veins. However, little is currently known about the MSZ, and no links have been made with any relationships to mineralisation or other nearby IOCG deposits.

The E1 deposit, located 8km east of Ernest Henry, is a small stratabound IOCG deposit that contains similar chemical and mineralogical characteristics, and a similar paragenesis to the Ernest Henry deposit. Such characteristics could imply a possible spatial/temporal relationship regarding their origins and formation models. Any existing paragenetic, geochemical or geochronological relationships between the apatite populations at the Ernest Henry and E1 IOCG deposits, will increase our understanding of how these deposits form, and the relationships the deposits might have to each other.

This study aims to resolve the following questions

- Can apatite from the Marshall Shear Zone be dated using the apatite U-Pb dating method?
- How does the Marshall Shear Zone apatite correlate geochronologically, paragenetically and geochemically with the apatite found within the orebody and Inter-lens?
- What trace elements are present in the apatite from the MSZ, and how do they correlate with those in the orebody and Inter-lens apatite?
- How does the trace element composition of apatite from the MSZ and Inter-lens compare to apatite from the E1 deposit?

In this study, I will analyse apatite grains from within the Marshall Shear Zone to determine their age and trace element composition, and therefore constrain the relation of the Marshall Shear Zone to the orebody and other local structures. This study makes use of techniques involving petrology, Mineral Liberation Analysis (MLA) and cathodoluminescence (CL) techniques using scanning electron microscopes (SEM) and U-Pb dating methods using Laser-Ablation Inductively Coupled Plasma-Mass Spectrometry (LA-ICP-MS).

2. BACKGROUND GEOLOGY

2.1 Regional Geology

The Ernest Henry deposit is located in the Proterozoic Eastern Fold belt of the Mount Isa Inlier, Northwest Queensland, Australia (Figure 1). The Mount Isa Inlier is comprised of three broad tectonic divisions: the Western fold Belt, the Kalkadoon-Leichhardt Belt, and the Eastern Fold Belt. Throughout these divisions, thick layers of early to middle Proterozoic sedimentary and igneous rocks of post-Barramundi Orogeny event are divided into multiple sequences known as Cover Sequence (CS) 1, CS2 and CS3 (Blake, 1987; D. Foster & Austin, 2008). The subaerial felsic volcanics of CS 1 are dated at ca. 1875–1850 Ma, and are overlain by the ca. 1790–1760 Ma bimodal volcanic and calc-silicate rocks comprising CS 2 and the silicalastic sedimentary rocks of CS 3 (Blake, 1987; D. Foster & Austin, 2008; Mark et al., 2006; Page & Sun, 1998). CS 2 and 3 both outcrop in the Eastern Fold Belt and host the majority of IOCG deposits (D. Foster & Austin, 2008). The cover sequences were later deformed by thrusting, faulting and tight to open upright folding and metamorphosed into greenschists to amphibolite facies during the Isan Orogeny and associated deformation events: D_1, D_2 and D_3 between ~1610–1500 Ma (Blake, 1987; D. Foster & Rubenach, 2006; Page & Sun, 1998; Williams, Holwell, Lilly, Case, & McDonald, 2015).

The smaller E1 deposit is located 8km east of Ernest Henry and had a pre-mining resource of 47 Mt at 0.71% Cu and 0.21 g/t Au (Williams et al., 2015). The E1 deposit is split into three main orebodies: E1 North (E1-N), E1 South and E1 East. E1-N contains the majority of the Cu and Au grade and tonnes (Case, 2016), and was mined between 2013 and 2015. The E1 host rocks are primarily metasiltstones, psammites, marble with minor amounts of meta-volcanoclastic tuffs, meta-andesites, meta-basalts, and hydrothermal breccias (Williams et al., 2015). Mineralisation is hosted within the steeply dipping and folded

calcareous meta-sediments and meta-volcanic units of the Soldiers Cap Group (CS3) (Williams et al., 2015).

Multiple granitic intrusions dated between 1860 Ma −1500 Ma are found within the Mount Isa Inlier (Blake, 1987; Mark et al., 2006; Page & Sun, 1998). The Williams and Naraku batholiths (ca. 1550 Ma−1500 Ma) represent the youngest of the felsic intrusions in the Cloncurry region (Wyborn, 1998), and are spatially and temporally associated with regional mineralisation events. Outcropping over 2400m^2 and believed to extend north and south of the Mount Isa Inlier, these batholiths are comprised of alkaline to subalkaline, K-rich, magnetite bearing granitoids occurring over three phases (Mark, Oliver, Williams, Valenta, & Richard, 2000). Examples of Granites that formed within this batholith are the Malakoff granites to the west of Ernest Henry and E1, Mount Margaret granites to the east and multiple to the south including Wimberu and Saxby granites (Page & Sun, 1998; Williams et al., 2015; Wyborn, 1998).

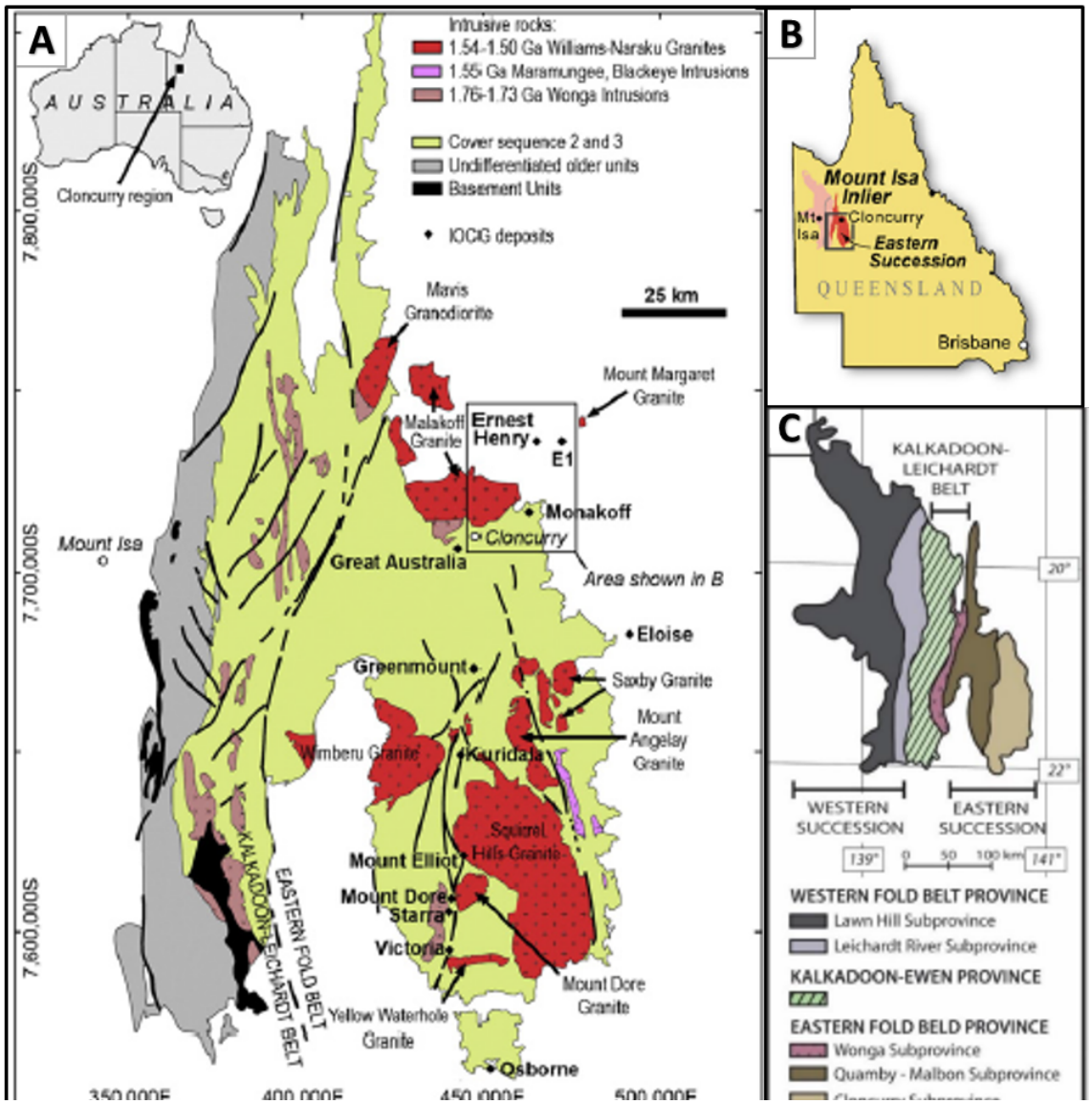

Figure 1: A) Location of the Mount Isa Inlier in Queensland with Ernest Henry, E1 and other notable deposits marked from Foster & Austin (2008). B) Sub-divisions of the Mount Isa inlier from Hutton et al (2012). C) Simplified geological map of the Eastern Succession adapted from William et al. (2015).

2.2 Ernest Henry Deposit Geology

2.2.1 HOST ROCKS & STRUCTURE

The Ernest Henry orebody is hosted in a brecciated and plagioclase-phyric altered meta-andesitic (intermediate) volcanic rocks, interpreted to the temporal equivalent of the Mount Fort Constantine Volcanics (1746 ± 9 Ma (Page & Sun, 1998)), intercalated with metasediments and medium-grained metadiorite intrusions (Mark et al., 2006).

The orebody is structurally bound by two magnetite and biotite-rich, strongly foliated shear zones known as the Hangingwall Shear Zone (HWSZ) and the Footwall Shear Zone (FWSZ). The pipe-like structure of the orebody dips at roughly 45° SSE, and contains a pre-ore, strongly foliated biotite and magnetite-rich shear zone termed the Inter-lens (Cave, 2017; Cave et al., 2018). The Marshall Shear Zone (MSZ) is another shear zone that lies to the south of the HWSZ, and dips SSE at an angle of ca. 60° (Figure 2). The composition is comparable to that of the other shear zones; dominated by overprinting alteration and infill of magnetite, biotite, amphibole and K-feldspar with coarse-grained apatite and garnet and relatively late cross-cutting calcite, quartz, pyrite and chalcopyrite from the main ore stage with post-ore alteration (Mark et al., 2006; Twyerould, 1997).

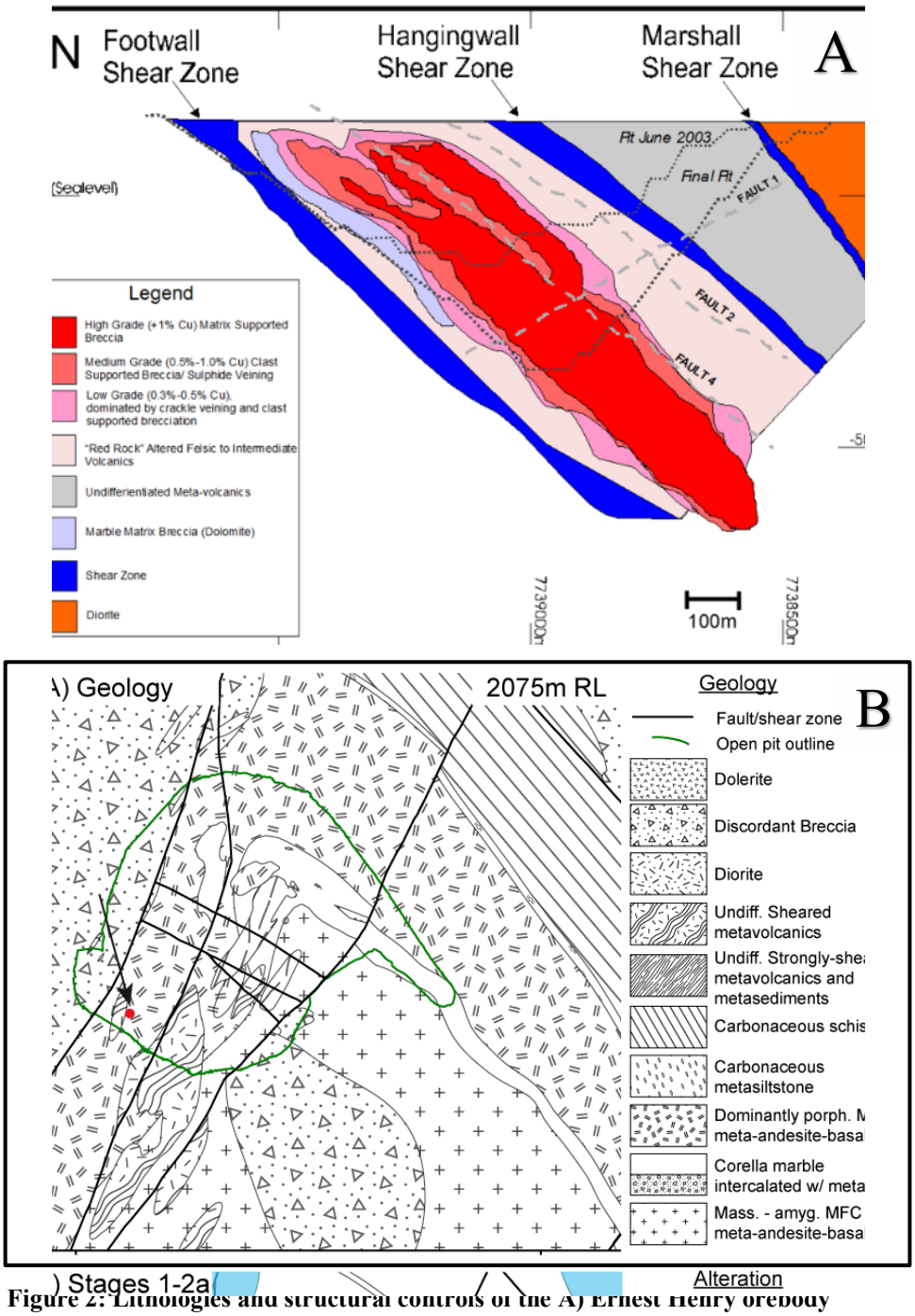

Figure 2: Lithologies and structural controls of the A) Ernest Henry orebody (adapted from Lilly et al., 2017) and B) the E1 North orebody with the location of the sample highlighted by the red dot.

2.2.2 ALTERATION AND MINERALISATION

The Ernest Henry deposit formed within a zoned, post peak hydrothermal alteration system dominated by brecciation and veining (Mark et al., 2006). The history of the alteration (Figure 3) is described in detail in previous articles by Mark et al. (2006) and Twyerould (1997), with the extent of the alteration controlled by NE trending faults, fault zones adjacent to metadiorite intrusions and several shear zones that bound the orebody (Oliver, Valenta, & Wall, 1990). The main alteration events can be summed up into four main stages: regional Na-Ca alteration, pre-ore K-(Mn-Ba)-rich alteration, main stage Cu-Au mineralisation and the post-ore veining and alteration (Mark et al., 2006).

2.2.2.1 REGIONAL NA-CA ALTERATION

The initial Na and Na-Ca alteration event experienced by the Ernest Henry region is predominately albitisation with minor amounts of actinolite, diopside, magnetite, pyrite and quartz (Mark et al., 2006). Albitisation is preserved outside the bounds of the mine lease due to overprinting by later alteration stages of alteration. The sodic-calcic alteration was the result of a hypersaline fluid (400-500°C) (Jong & Williams, 1995) passing along the NE trending contacts between the metadiorite and metasedimentary rocks, indicating that the fluids were structurally controlled by faults, fractures and lithological contacts (Oliver et al., 1990).

2.2.2.2 PRE-ORE K-(MN-BA)-RICH ALTERATION

Commonly known as ‘pre-ore alteration’, this stage is split into two separate alteration types: dark rock alteration and red rock alteration. The initial dark rock stage involves the formation of fine-grained Mn-rich biotite and magnetite assemblages that overprint the sodic-calcic rocks produced during regional Na-Ca alteration (Mark et al.,

2006). The later red rock stage involves the formation of coarse-grained Mn-rich garnet, Ba-rich K-feldspar and biotite-rich assemblages with minor pyrite (Mark et al., 2006). This alteration is best observed in the plagioclase-phyric meta-igneous rocks, but is at its greatest intensity in the ferromagnesian-rich metadioritic rocks (Mark et al., 2006).

2.2.2.3 MAIN STAGE CU-AU

Cu-Au mineralisation is proposed to be a caused by the mixing between magmatic fluids sourced from nearby 'A-type' granites and sedimentary fluids sourced from an upper crust high saline brine (Kendrick, Mark, & Phillips, 2007; Mark et al., 2006; Rusk et al., 2010). However, it is more likely that the mineralisation was a result of a combination of the fluid mixing, changes in pressure and temperature and wall rock reactions rather than the fluid mixing alone (Baker et al., 2008).

Cu-Au mineralisation is hosted within a clast and matrix supported breccia system that evolves into a crackle-style hydrothermal veining system towards the edges of the ore deposit (Mark et al., 2006). The breccia is composed of rounded K-feldspar altered meta-andesite host rocks with subhedral to euhedral phenocrysts of plagioclase and a groundmass comprised of biotite, magnetite, quartz, calcite, pyrite, chalcopyrite and accessory apatite, biotite, specular hematite and K-feldspar (Mark et al., 2006). Copper and gold mineralisation exists as chalcopyrite forming as infill between the breccia clasts and predominately as free gold respectively (A. R. Foster, Williams, & Ryan, 2007; Hewett, 2017; Lilly et al., 2017).

2.2.2.4 POST-ORE VEINING AND ALTERATION

The post ore alteration consists of minor carbonate-rich veining and matrix supported breccias comprised of calcite, dolomite, and quartz and retrograde chlorite-sericite overprinting all previous stages (Mark et al., 2006).

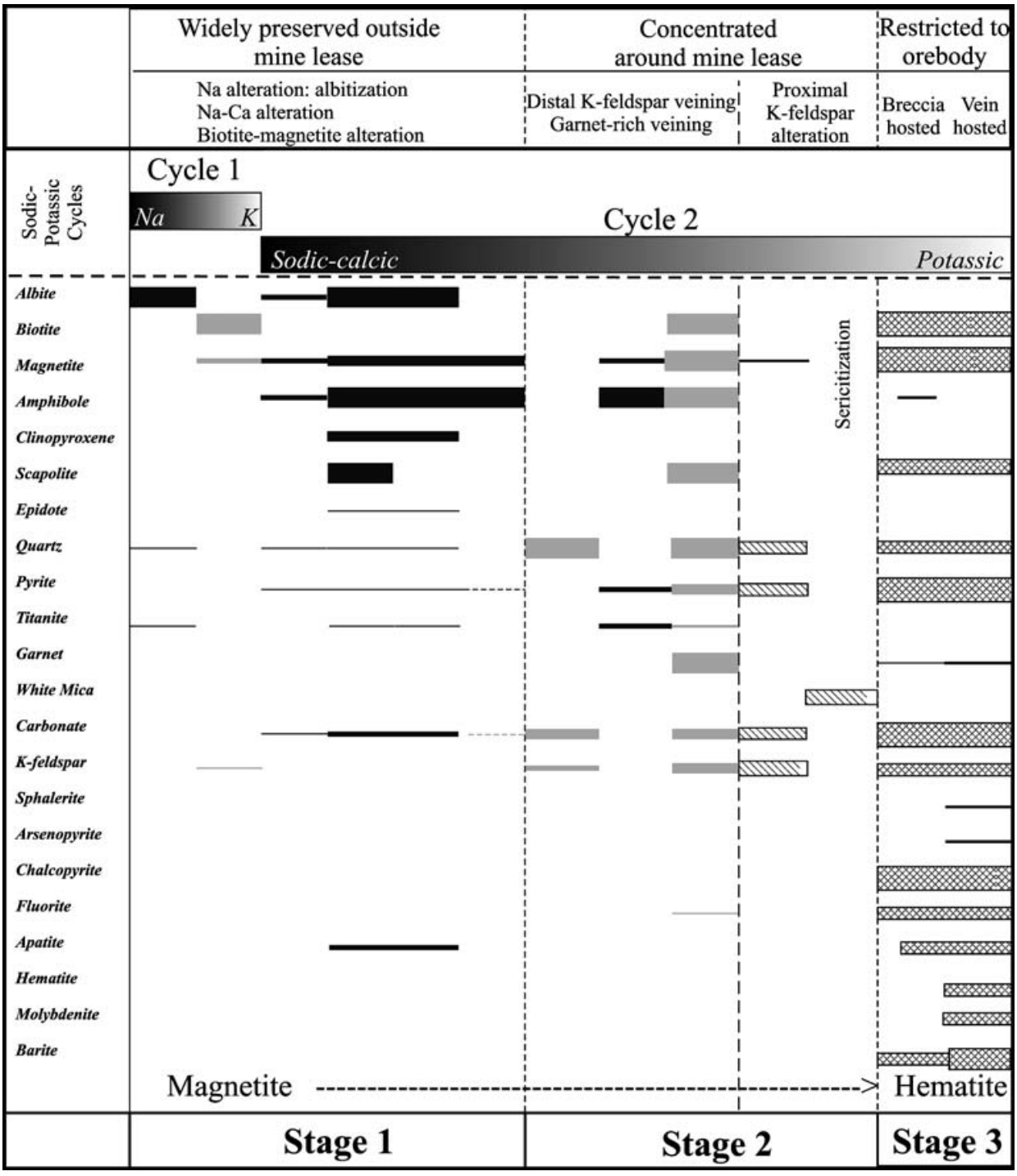

Figure 3: Paragenetic sequence of the regional Na-Ca alteration (stage 1), 'pre-ore' alteration (stage 2) and the ore stage alteration (stage 3) experienced within the Ernest Henry term lease as summarised by Mark et al. (2006). Thickness of individual lines refers to the relative abundance of the specific mineral.

2.2.3 DEPOSIT GEOCHRONOLOGY

Extensive geochronology has been completed throughout the Ernest Henry deposit and nearby sequences in order to understand the history of the area and to assign dates to hydrothermal events. The meta-andesite host rocks are comparable to the Mount Fort Constantine (intermediate) Volcanics and were dated using zircon U-Pb data at 1746 ± 9 Ma (Page & Sun, 1998). In the same study, Page & Sun (1998) used zircon U-Pb data to constrain the peak metamorphic conditions at 1584 ± 17 Ma .The Isan Orogeny deformation events were dated at 1610 ± 13 Ma (Page & Bell, 1986) , 1595–1975 Ma (Page & Sweet, 1998) and 1532–1480 Ma (Betts et al., 2006) for D_1, D_2 and D_3 respectively. Mark et al. (2006) performed U-Pb geochronology on titanite from Na-Ca and biotite-magnetite altered rocks, which resulted in ages of 1529 ± 11 and 1514 ± 24 respectively. Twyerould (1997) analysed $^{40}Ar/^{39}Ar$ from biotite in the Cu-Au mineralisation and post-ore alteration and recorded ages of 1504 ± 3 Ma and 1514 ± 6 Ma respectively. Cave et al. (2018) used U-Pb dating to determine the age of apatite within the Inter-lens and attained ages of 1584 ± 22 Ma and 1587 ± 22 Ma.

Minor geochronology studies at E1-N have been conducted, with only a handful of dates recorded from the deposit and surrounding area. Case (2016) used U-Pb dating to date Stage 3 monazites within early Stage 2 apatites of a host rock with a comparable composition to that of the Ba-rich K-feldspar, magnetite, and biotite ‘pre-mineralisation’ alteration at Ernest Henry. These monazites produced an age of 1456 ± 44 Ma which are within error of the regional mineralisation event at ca. 1500 Ma (Case, 2016). Further ages have been calculated for nearby structures such as the Mount Margaret Granite, 2 km east of E1, which was dated by Page & Sun (1998) at 1530 ± 8 Ma and the diorite intrusions, possibly related to

the Ernest Henry diorites, were dated at 1660 ± 13 Ma using U-Pb data from titanate by Pollard & McNaughton (1998).

2.3 Ernest Henry and E1 apatite

Apatite at Ernest Henry is predominately found as an accessory mineral with records of apatite occurring in the alteration events, orebody and the HWSZ, FWSZ, MSZ and Inter-lens (Cave, 2017; Mark et al., 2006; O'Brien, 2016; Twyerould, 1997). Apatite crystals within the MSZ range from fine-grained up to several centimetres in diameter and can be multiple colours including red and green (Figure 4). Studies by Rusk et al. (2010) have shown that the apatites within the Ernest Henry deposit are more enriched with fluorine and arsenic compared to those in other IOCG deposits. Along with this, individual apatite grains from high grade mineralized areas have been observed to show a strong zonation with variable concentrations of sulfur (0.5 wt% in the form of SO_3) and arsenic (5 wt% in the form of As_2O_5) comprising the core and rim respectively (Cleverley, 2006; Liu et al., 2017). Multiple generations of apatite have been proposed to exist within this deposit; the first being an early stage existing within the initial host rocks, the second forming during the pre-mineralisation alteration around ~1580 Ma, such as that seen within the Inter-lens, and a third and final formed during the main orebody mineralisation around ~1530 Ma (Cave et al., 2018; Mark et al., 2006).

Apatite within E1-N is found exclusively within the early to middle part of the second stage alteration where it forms alongside the magnetite-biotite-K (-Ba)-feldspar alteration (Case, 2016). The size of apatites are similar to that found in Ernest Henry with grains ranging between fine-grained (<100 μm) to very coarse-grained (> 1cm). The chemistry also appears to be similar to that at Ernest Henry with the apatite grains relatively enriched in fluorine and termed fluoro-apatite (Case, 2016).

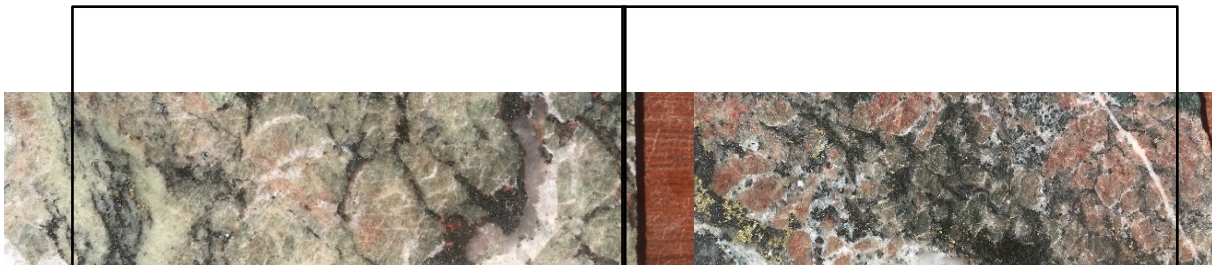

Figure 4: Hand samples of A: MSZ-5 and B: MSZ-6 showing the multiple colours of apatite.

3.1 Sample collection

Samples were collected over 14m from the recently drilled core (EH969) that intersected the Marshall Shear Zone over a distance of approximately 80m. Sections within the core showing large abundances of apatite were highlighted and made into a total of 7 slabs with dimensions of roughly 5.0cm x 10.0cm x 5mm. The slabs were then sent to Adelaide Petrographic Laboratories and cut into 9 polished thin section measuring 2.5cm x 4.5cm x 40µm. An additional thin section collected by George Case from drill hole EMMD026 (221.3m) at the nearby E1 deposit containing apatite grains was included in this study to compare the geochronology and geochemistry of the Ernest Henry samples. Further sample details are included in Appendix A.

3.2 Optical Petrography

Optical petrography of the 10 polished thin sections was conducted at the University of Adelaide on the Olympus BX51 microscope with an attached Olympus DP51 microscope camera. Chosen apatite grains were then selected for further analysis on the SEM and LA-ICP-MS. Petrographic descriptions of these thin sections are included in Appendix B.

3.3 Scanning Electron Microscope (SEM)

Selected apatite grains from all samples were imaged and analysed under a cathodoluminescence detector attached to the Quanta SEM 600 located at Adelaide Microscopy. An external blue/UV light filter was applied to cathodoluminescence detector in order to minimise the transmission of longer wavelengths to improve image quality (Reed & Milliken, 2003). Table 1 outlines the settings used during cathodoluminescence (CL) imaging

Setting	Value
Beam Energy	15.00 kV
Working Distance	15mm

Table 1: Settings of the SEM while performing the analysis.

3.4 Laser Ablation Inductively Coupled Plasma Mass Spectrometry (LA-ICP-MS)

Six of the ten samples were chosen for analysis on the Agilent 7900x ICP-MS with a RESOlution LR 193nm Excimer laser at Adelaide Microscopy. Each thin section contained three - eight separate locations comprising of either a larger single apatite grain or multiple smaller yet zoned apatite grains. The larger apatite grains were subjected to multiple single spot ablations running through the grain (Figure 4.C), whereas the ablations on the smaller grains were separated into cores and rims (Figure 4.C). A detailed description of the parameters used during the analysis can be found in Table 2. An additional distribution of the ablation spot locations and descriptions for each sample can be found in Appendix C.

LA-ICP-MS studies were completed using a method adapted from Chew, Petrus, & Kamber (2014) with changes made to suit the equipment at Adelaide Microscopy. Selected elements and isotopes were chosen based on their role in either the geochronology or geochemistry studies (Table 2).

ICP-MS	
Parameter	Value
Brand & model	Agilent 7900x ICP-MS
Forward power	1350W
Cool (Ar)	15
Auxiliary (Ar)	0.89
Carrier (He)	0.35
Sample (Ar)	1.06
Laser	
Type of laser	ArF Excimer
Brand and model	Resolution LR (Resonetics)
Laser wavelength	193nm
Pulse duration	20ns
Spot Size	29µm
Repetition rate	5 Hz
Laser fluency	3.5 J/cm^2
Data Acquisition Parameters	
Data acquisition protocol	Time-resolved analysis
Cleaning method	5 pulses followed by washout
Scanned Masses	^{27}Al, ^{29}Si, ^{31}P, ^{35}Cl, ^{43}Ca, ^{51}V, ^{55}Mn, ^{88}Sr, ^{89}Y, ^{90}Zr, ^{139}La, ^{140}Ce, ^{141}Pr, ^{146}Nd, ^{147}Sm, ^{153}Eu, ^{157}Gd, ^{159}Tb, ^{163}Dy, ^{165}Ho, ^{166}Er, ^{169}Tm, ^{172}Yb, ^{175}Lu, ^{201}Hg, ^{204}Pb, ^{206}Pb, ^{207}Pb, ^{208}Pb, ^{232}Th, ^{238}U
Detection mode	Pulse counting
Background collection	30 sec
Ablation time	30 sec
Washout	20 sec
Sampling period	0.542 sec
Dwell time	^{27}Al, ^{29}Si, ^{31}P, ^{35}Cl, ^{43}Ca = 0.005 sec per isotope ^{206}Pb, ^{207}Pb = 0.1 sec per isotope ^{232}Th, ^{238}U = 0.2 sec per isotope ^{51}V, ^{55}Mn, ^{88}Sr, ^{89}Y, ^{90}Zr, ^{139}La, ^{140}Ce, ^{141}Pr, ^{146}Nd, ^{147}Sm, ^{153}Eu, ^{157}Gd, ^{159}Tb, ^{163}Dy, ^{165}Ho, ^{166}Er, ^{169}Tm, ^{172}Yb, ^{175}Lu, ^{201}Hg, ^{204}Pb, ^{208}Pb = 0.01 sec per isotope.
Ablation sequence	2 x Madagascar, 2 x OD306, 2 x 401, 2 x McClure Mountain, 2 x NIST612
Standardisation and Data Reduction	
Primary standard	McClure & NIST612
Secondary standard	401, OD306, Madagascar, NIST612
Data reduction software	Iolite, In house Excel add-in

Table 2: ICP-MS, laser and data acquisition parameters used during the LA-ICP-MS study at Adelaide Microscopy.

3.5 Data Reduction

The Iolite software package (Paton, Hellstrom, Paul, Woodhead, & Hergt, 2011) with the VizualAge_UcomPbine data reduction scheme (DRS) (Patron et al., 2011) was used for reducing U-Pb age data while the Trace Element_IS DRS (Patron et al., 2011) was used to reduce trace element data using the method outlined in (Chew, Petrus, & Kamber, 2014). This allowed for the downhole fractionation and instrumental drift to be corrected for (Chew et al., 2014). IsoplotR and the in house Excel add in was used to construct the Tera-Wasserburg concordia plots and to compute the common lead corrected $^{238}U/^{206}Pb$ age for each sample. McClure Mountain apatite (U-Pb TIMS 523.51 ± 1.47 Ma) (Schoene, Crowley, Condon, Schmitz, & Bowring, 2006)) was used as a primary standard for the U-Pb analysis, and NIST612 as the primary standard with an internal standard value of 39.36 wt % Ca for the trace element analysis. 401 apatite (U-Pb LA-ICP-MS 530.3 ± 1.5 Ma (Thompson et al., 2016)) was used as a secondary standard to test the accuracy of the results.

U-bearing minerals such as apatite can contain significant concentrations of common lead which is corrected for during the data reduction stage in the Iolite software package (Chew et al., 2014). The initial levels of common lead in the apatite is represented as the y-intercept on a Tera-Wasserburg plot while the U-Pb age is represented as the lower intercept on the concordia curve (Chew et al., 2014). This age either represents the age of apatite formation or that at which the grains were reset by intrusive fluids (Kirkland et al., 2018). This resetting is a result of the closure temperature of apatite (350^{o}C – 550^{o}C) being exceeded, leading to the loss of common lead (Chew & Spikings, 2015).

4. OBSERVATIONS AND RESULTS

4.1 Apatite Petrography and Paragenesis

Samples MSZ-1 to MSZ-7 contained varying concentrations of fine- (<100 μm) to coarse- grained (>1cm) apatite in a groundmass dominated by fine- to coarse-grained quartz and calcite and fine- to medium-grained biotite, chlorite, magnetite, pyrite and chalcopyrite. Apatite grains were independent in their spatial position relative to the surrounding minerals and contained minimal to substantial amounts of brecciation and intrusive veining as a result of coarse- and fine-grained calcite veining respectively (Figure 5A & 5B). Fine-grained apatite predominantly appeared within the coarse-grained calcite veins proximal to the coarse-grained apatite and were interpreted to be fragments from the larger crystals entrained in the calcite (Figure 5C & 5D). In hand samples, apatite occasionally appeared as two different colours: red and green, indicating potential geochemical differences in these apatite populations. The coarse calcite veining, typically found proximal to the apatite grains, ranged up to several centimetres thick and contained traces of quartz, magnetite, biotite, chlorite and pyrite/chalcopyrite (Figure 5E & 5F). A second, later stage of calcite veins is present that cross-cuts the coarse-grained calcite veining and all other minerals. Petrological observations concur with the paragenesis described in more detail by Mark et al. (2006) and Cave et al (2018).

The single E1-N sample contained coarse-grained apatite (> 1 cm), magnetite, chalcopyrite and pyrite with a groundmass of fine-grained quartz, calcite and biotite. The apatite grains appeared spatially independent of all other minerals and mostly intact with only a small portion broken into fragments as a result of coarse calcite veins or have any cross cutting fine-grained calcite veins. The calcite appeared predominately as veins throughout the sample, usually proximal to the apatite, magnetite and pyrite/chalcopyrite.

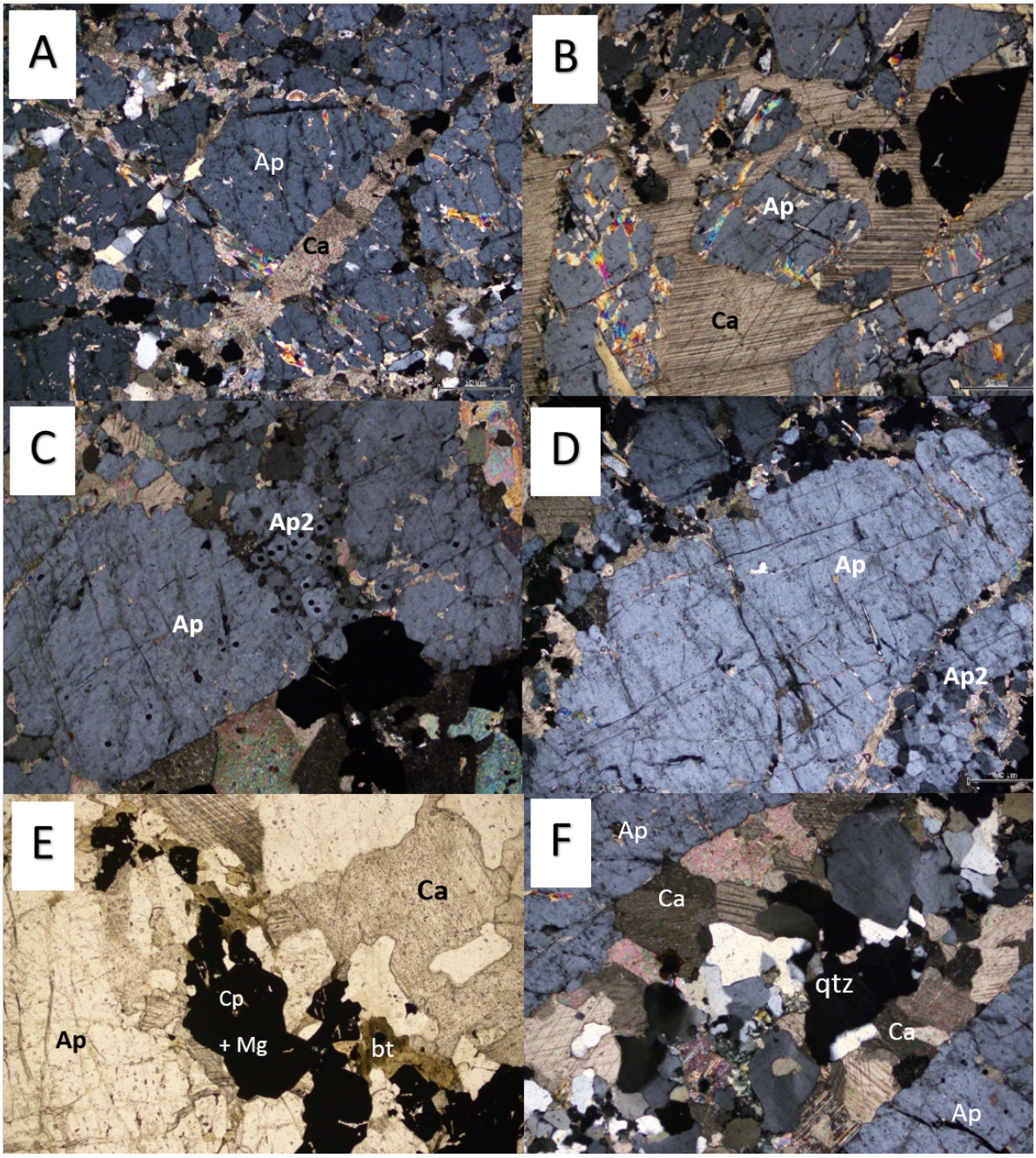

Figure 5: Petrographic images of apatite (Ap) grains and other associated minerals within the MSZ samples. A) & B): Coarse-grained apatite experiencing high amounts of both brecciation by coarse-grained calcite and intrusive veining by fine-grained calcite. C) Fine-grained apatite (Ap2) within coarse-grained calcite veins proximal to coarse-grained apatite. Black spots are craters as a result of the LA-ICP-MS process where coarse-grained apatite was sampled across the grain and fine-grained apatite was sampled in the cores and rims. D) Fine-grained apatite within coarse-grained calcite veins proximal to coarse-grained apatite. E) Coarse-grained calcite vein containing additional biotite, magnetite and pyrite F) Coarse-grained calcite vein between apatite and comprising of calcite on the edge and quartz in the centre.

4.2 SEM and Cathodoluminescence

Cathodoluminescence studies of apatite grains within the MSZ revealed the presence of concentric zonations in the fine-grained apatites highlighted by the light and brighter coloured cores with darker and dimmer rims (Figure 6). Coarse-grained apatite rarely showed this zonation and would be too narrow to analyse if present. Samples MSZ-2 and MSZ-6 contain data solely on the coarse, unzoned apatite whereas samples MSZ-3.1, MSZ-4 and MSZ-5.2 all contained enough fine-grained apatite to collect sufficient data on the cores and rims (Figure 6A, 6B and 6C respectively). The sample from E1-N comprised of predominately coarse-grained apatite with a single zoned grain (Figure 6D), all with abundant monazite inclusions throughout the grain (Figure 6.E & F).

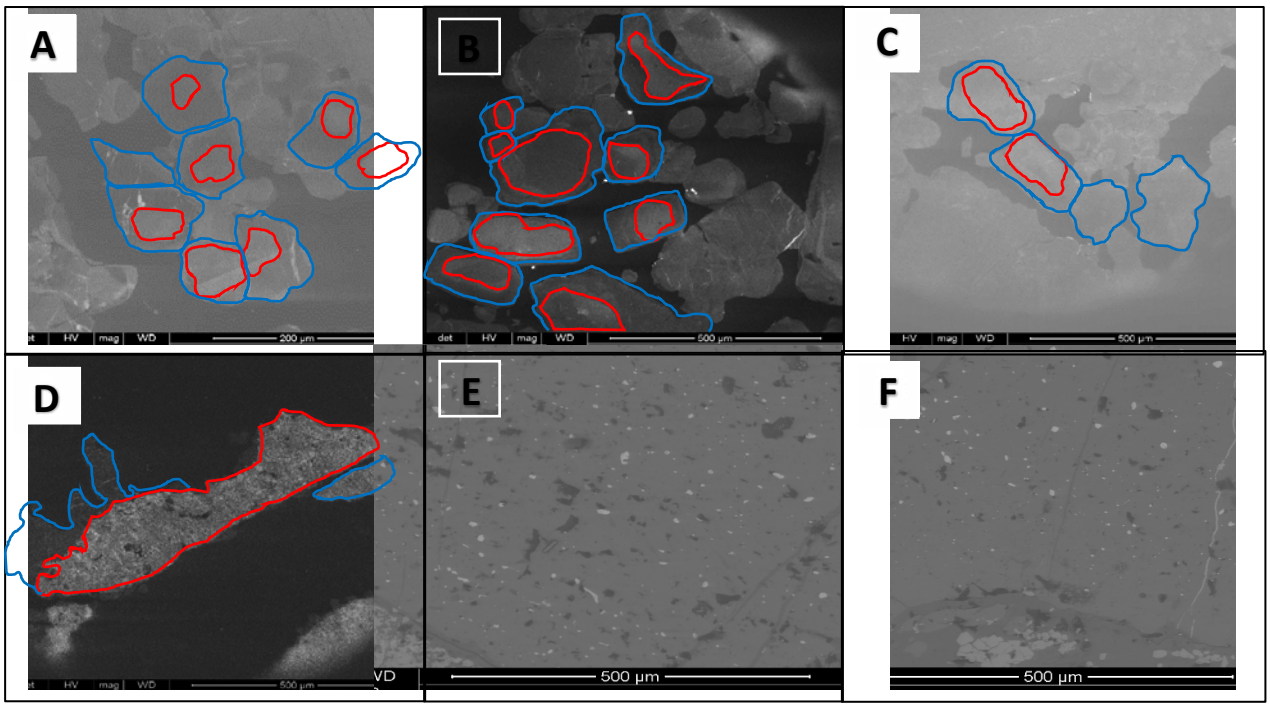

Figure 6: A, B and C) CL image of MSZ-3.1 section 2, MSZ-4 section 1 and MSZ-5.2 section 1 respectively highlighting the zonation in multiple finer grained apatite caused by the discrepancy in CL reflectance. D) CL image of a single grain within the E1-N sample, section 4, with zonation present highlighted by the lighter cores and darker rims. The red outlines highlight the edges of the cores and the blue outlines highlight the edges of the rims. E) & F) BSED images of monazite (white) and calcite (black) inclusions within apatite grains (grey)

4.3 Apatite Geochronology

4.3.1 DATA ACCURACY

Primary and secondary apatite standards were analysed using the standard sample bracketing approach to confirm the accuracy of the data. A new and unused piece of the Madagascar apatite sample was initially used as the primary standard along with the McClure Mountain, OD306 and 401 apatite as secondaries. The Madagascar apatite produced a concordant age of 488 ± 78 Ma whilst the McClure Mountain, OD306 and 401 apatite samples produced concordant and disconcordant ages of 553.5 ± 7.9 Ma, 1558 ± 20 Ma and 578 ± 16 Ma (Appendix D). The Madagascar apatite primary standard age fell within error of the published 473.5 ± 0.7 Ma (Chew et al., 2014). However, the secondary standards fall outside the published ages of 524.6 ± 3.2 Ma (Schoene et al., 2006), 1596.7 ± 7.1 Ma (Thompson et al., 2016) and 530.3 ± 1.5 Ma (Thompson et al., 2016) for McClure, OD306 and 401 apatite respectively, indicating the possibility of imprecise data. To resolve this issue, the McClure Mountain apatite replaced the Madagascar apatite as the primary standard with 401 apatite being the only secondary standard utilised. McClure mountain apatite now produced a concordant age of 526 ± 36 Ma (Figure 7A), and the 401 apatite produced an age of 530.3 ± 2.4 Ma (Figure 7B). These ages agree with the published ages and suggest the new unknown ages are accurate and can be used with confidence.

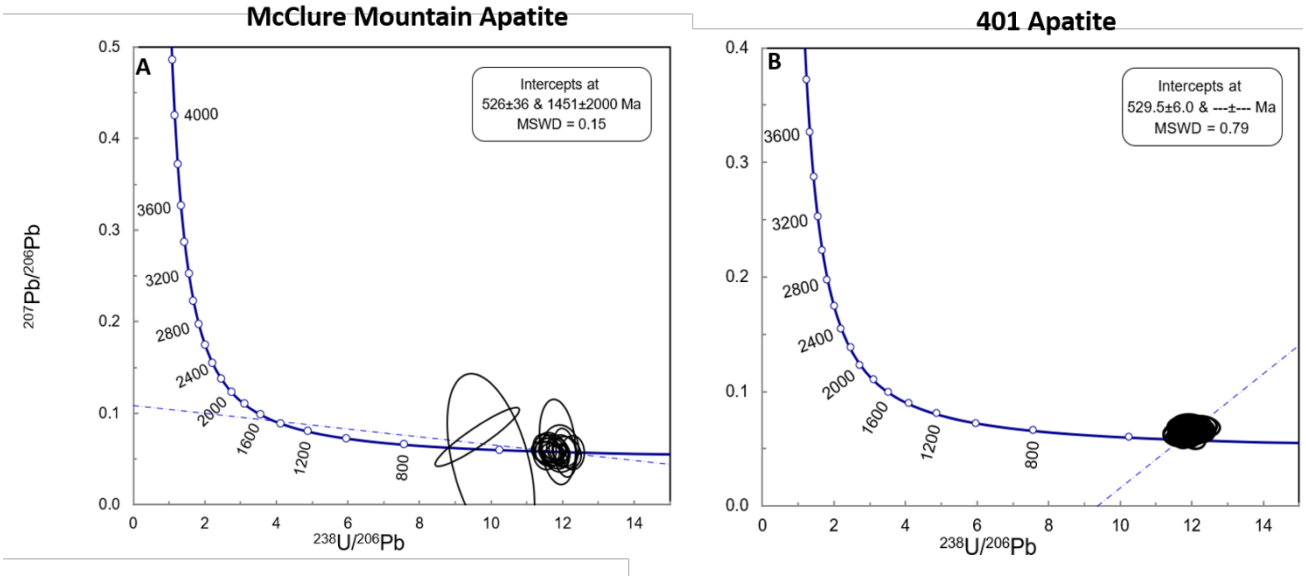

Figure 7: A) Tera-Wasserburg concordia plot of the McClure Mountain Apatite primary standard. B) Tera-Wasserburg concordia plot of the 401 apatite secondary standard.

4.3.2 UNKNOWN SAMPLES

Three separate ages for Samples MSZ-3.1, MSZ-4, MSZ-5.2 and E1-N were calculated as all contained data from unzoned, coarse-grained apatite and fine-grained apatite with core and rim zonation. All calculated ages for unzoned grains, cores and rims were deemed to be cogenetic as the 2σ propagated error range of each sample overlapped due to the large errors associated with both the cores and rims. This led to the calculation of a single age per sample after the three data sets were combined. The individual Tera-Wasserburg plots can be found in Appendix D.

4.3.2.1 MSZ APATITE

Sample MSZ-2 produced a common lead corrected age of 1508 ± 45 Ma (MSWD = 0.90 & probability = 0.21) with a $^{207}Pb/^{206}Pb$ common lead ratio of 0.91 from samples containing solely unzoned apatite (Figure 8A). The precision for this sample was high due to the large sample population where n = 62 and the consistent ratio of $^{207}Pb/^{206}Pb$ (0.28-0.38

ppm) and $^{238}U/^{206}Pb$ (2.36-2.91 ppm) over all but one of the data points. The effect of this single data point with a slightly higher $^{207}Pb/^{206}Pb$ and lower $^{238}U/^{206}Pb$ is negligible as the age without the point is still within the current uncertainty range. However, it may have had some effect on the position of the common lead line.

Sample MSZ-3.1 produced a common lead corrected age of 1497 ± 34 Ma (MSWD = 1.4 & probability = 0.000) with a $^{207}Pb/^{206}Pb$ common lead ratio of 0.85 from samples containing both apatite with and without zonation (Figure 8B). Highly variable $^{207}Pb/^{206}Pb$ (0.28-0.69 ppm) and $^{238}U/^{206}Pb$ (0.93-2.84 ppm) data resulted in a well resolved common lead line. However, uncertainties in the data were the likely cause for the resulting uncertainty in the age.

Sample MSZ-4 produced a common lead corrected age of 1479 ± 19 Ma (MSWD = 0.95 & probability = 0.000) with a $^{207}Pb/^{206}Pb$ common lead ratio of 0.86 from samples containing both apatite with and without zonation (Figure 8C). Highly variable $^{207}Pb/^{206}Pb$ (0.28-0.73 ppm) and $^{238}U/^{206}Pb$ (0.81-2.97 ppm) data resulted in a well resolved common lead line.

Sample MSZ-5.2 produced a common lead corrected age of 1463 ± 38 Ma (MSWD = 0.94 & probability = 0.089) with a $^{207}Pb/^{206}Pb$ common lead ratio of 0.89 from samples containing both apatite with and without zonation (Figure 8D). Highly variable $^{207}Pb/^{206}Pb$ (0.26-0.81 ppm) and $^{238}U/^{206}Pb$ (0.19-3.00 ppm) data resulted in a well resolved common lead line. Multiple data points containing minimum levels of ^{238}U (<0.5ppm) or abundant common lead were removed from the set of data due to plotting outside of concordant space.

Sample MSZ-6 produced a common lead corrected age of 1472 ± 35 Ma (MSWD = 1.07 & probability = 0.040) with a $^{207}Pb/^{206}Pb$ common lead ratio of 0.85 from samples containing both apatite with and without zonation (Figure 8E). Highly variable $^{207}Pb/^{206}Pb$

(0.25-0.61 ppm) and $^{238}U/^{206}Pb$ (1.15-3.07 ppm) data resulted in a well resolved common lead line.

4.3.2.2 E1-N APATITE

The E1-N sample produced a common lead corrected age of 1550 ± 16 Ma (MSWD = 1.5 & probability = 0.064) with a $^{207}Pb/^{206}Pb$ common lead ratio of 0.50 from samples containing both apatite with and without zonation (Figure 8F). Highly variable data with large uncertainties resulted in the Tera-Wasserburg plot displaying distributed data that greatly affected the position of the final common lead trend line and the final common lead ratio. Multiple data points in this sample contained insufficient levels of ^{238}U or abundant levels of common lead and were removed. The low level of common lead in this sample is attributed to the abundant alteration that the E1 deposit has experienced.

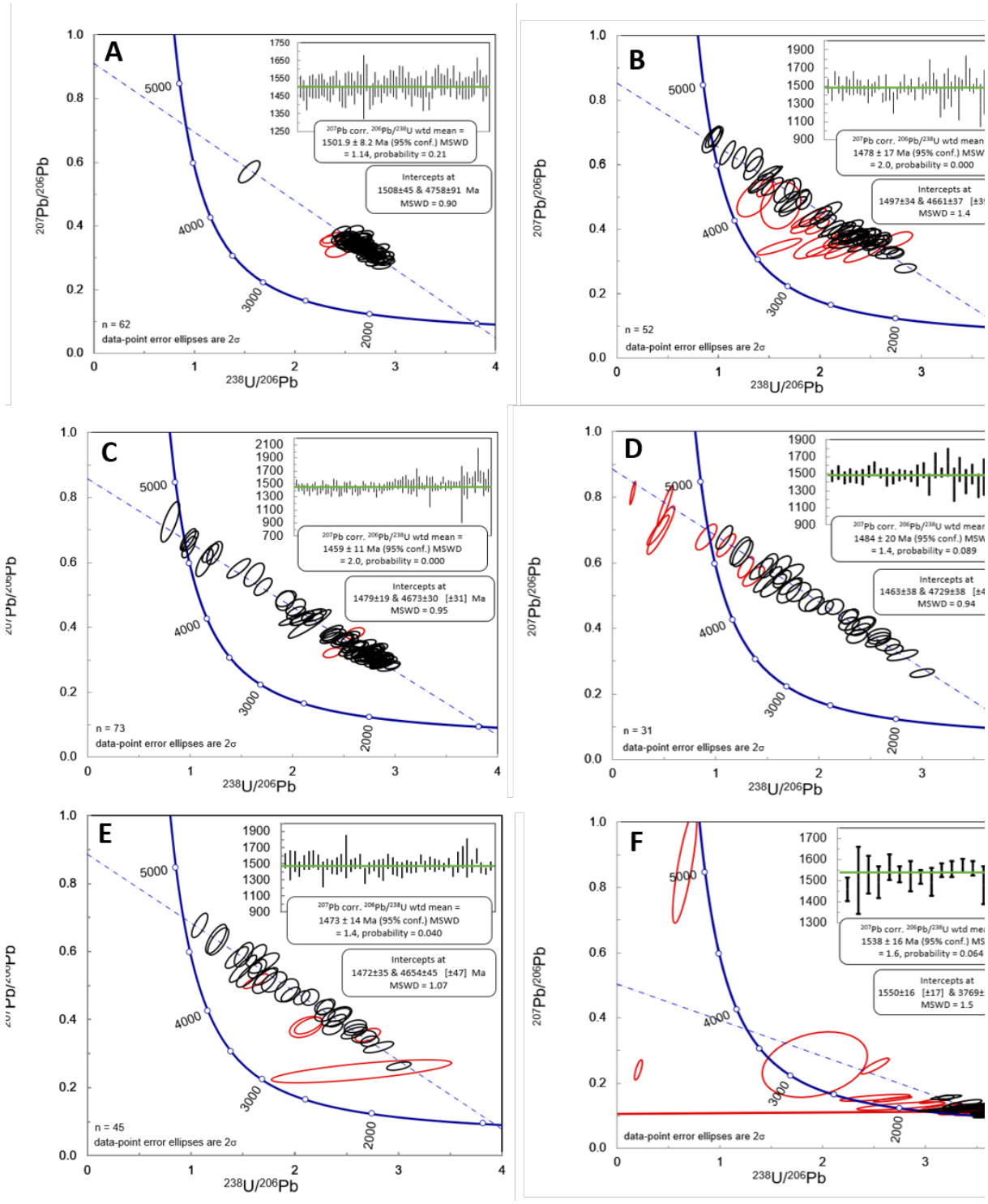

Figure 8: Tera-Wasserburg plots for the MSZ and E1-N apatite samples with associated weighted mean U-Pb ^{207}Pb corrected $^{206}Pb/^{238}U$ ages: A) MSZ-2. B) MSZ-3.1. C) MSZ-4. D) MSZ-5.2. E) MSZ-6. F) E1. The ellipses represent the 2σ error range for the $^{238}U/^{206}Pb$ and $^{207}Pb/^{206}Pb$ values of each data point. Black ellipses signify the sample points utilised in the creation of the common lead line whereas the red ellipses signify the sample points considered as outliers and were removed from further investigation. The lower intercept of the common lead line represents the point in which the apatite grains formed or ceased common lead diffusion at ~350-550°C (Chew et al., 2015). The listed weighted mean ages are inaccurate as they lack any common lead correction therefore, they will not be utilised in further investigations.

4.4 Apatite Geochemistry

4.4.1 CHONDRITE - NORMALISED REE PLOTS

REE plots of apatite normalised to chondrite standards (Sun & McDonough, 1989) show a variation in the mean REE concentration over each sample. In all cases, a depletion of all REE is observed in the rim relative to that in the core with the one exception of the E1-N apatite rim showing a slight enrichment of HREE relative to that in the core (Figure 9). All MSZ samples containing core and rim data (MSZ-3.1, MSZ-4 and MSZ-5.2) showed a similar pattern of LREE enrichment relative to the MREE & HREE with a consistent overall REE concentration between samples. The one exception to this is the slightly lower levels of all REE in MSZ-5.2 (Figure 9C) compared to that in MSZ-3.1 (Figure 9A) and MSZ-4 (Figure 9B). The E1-N sample (Figure 9D) also shows a LREE enrichment pattern in the core; However, shows the opposite trend in the rim where the HREE become enriched in comparison to the LREE. Caution must be advised with the E1-N sample as only a single grain showed zonations and was only large enough to obtain 7 points in the core and 5 points in the rim, suggesting that the obtained data may not be representative of the deposit as a whole.

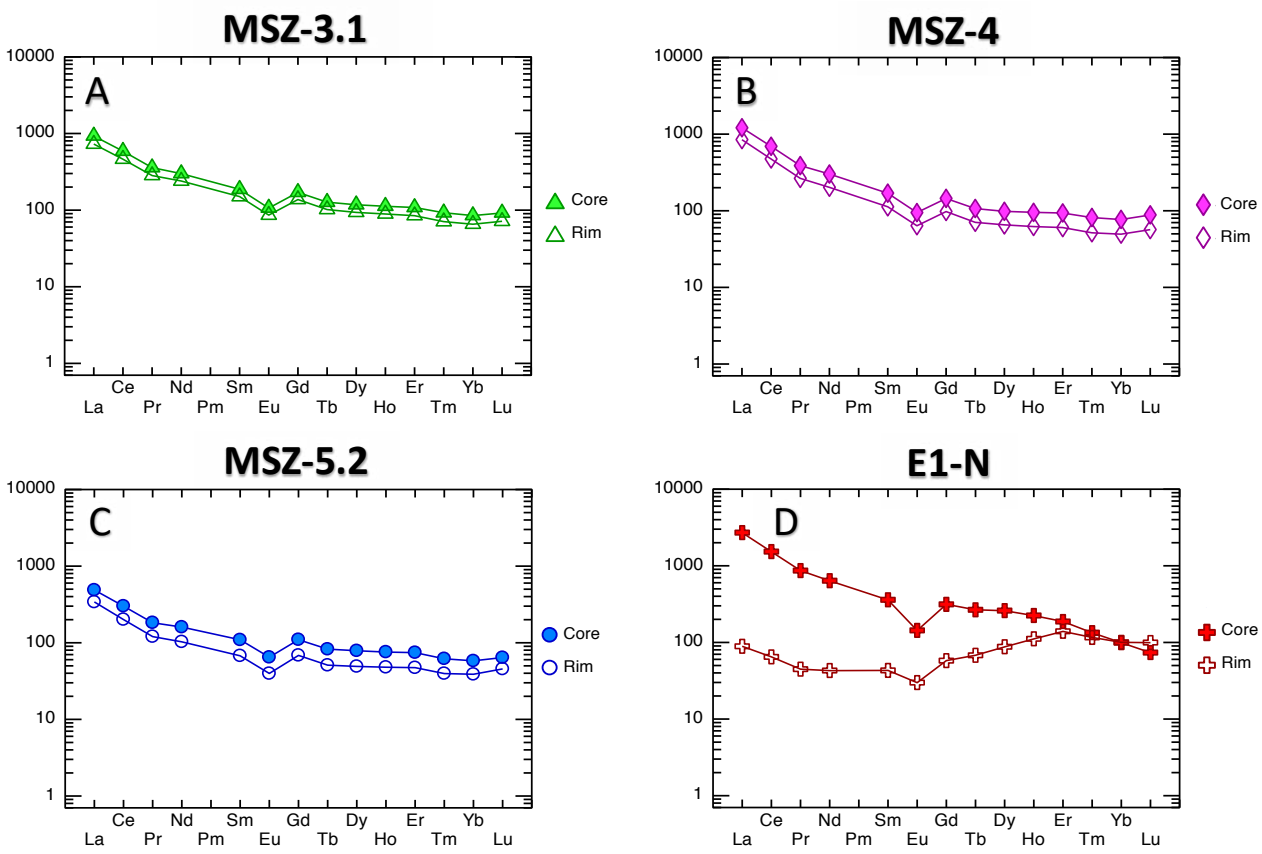

Figure 9: chondrite-normalised REE spidergram diagrams for A) MSZ-3.1. B) MSZ-4. C) MSZ-5.2. D) E1-N. Solid shapes indicate the concentration of REE within the core and outlined shape indicate the concentration within the Rim. The 2σ error range for each sample was not included due to the resulting value being too small to cause any deviation in the overall concentration.

4.4.2 DISCRIMINATION PLOTS

Discrimination plots from Belousova et al. (2002) were used to plot the apatite geochemical data from this study along with orebody and Inter-lens apatite data from Cave (2017) in order to constrain and compare their potential source.

The Sr vs. Y plot (Figure 10) shows a relatively consistent concentration of Sr with the exception of a portion of the Inter-lens samples containing slightly lower levels relative to the samples of this study. A greater variation is present in the Y with the E1-N sample showing increased levels relative to the EHM samples that results in the E1-N data plotting in the mafic rocks & iron ores field and the MSZ and orebody and Inter-lens data plotting in the granitoids section.

The Y vs. Eu/Eu* (Figure 11) plots shows slight differences in the overall abundance of Eu/Eu* with E1-N having the lowest concentration, the Ernest Henry orebody and Inter-lens samples having the highest and the MSZ falling in the middle. The Y concentrations are more consistent, with the exception of the E1-N data showing a slightly higher concentration. This results in the E1-N data again, plotting in the mafic rocks & iron ores field and the MSZ and orebody and Inter-lens data now plotting half way between the carbonatites and granitoids section.

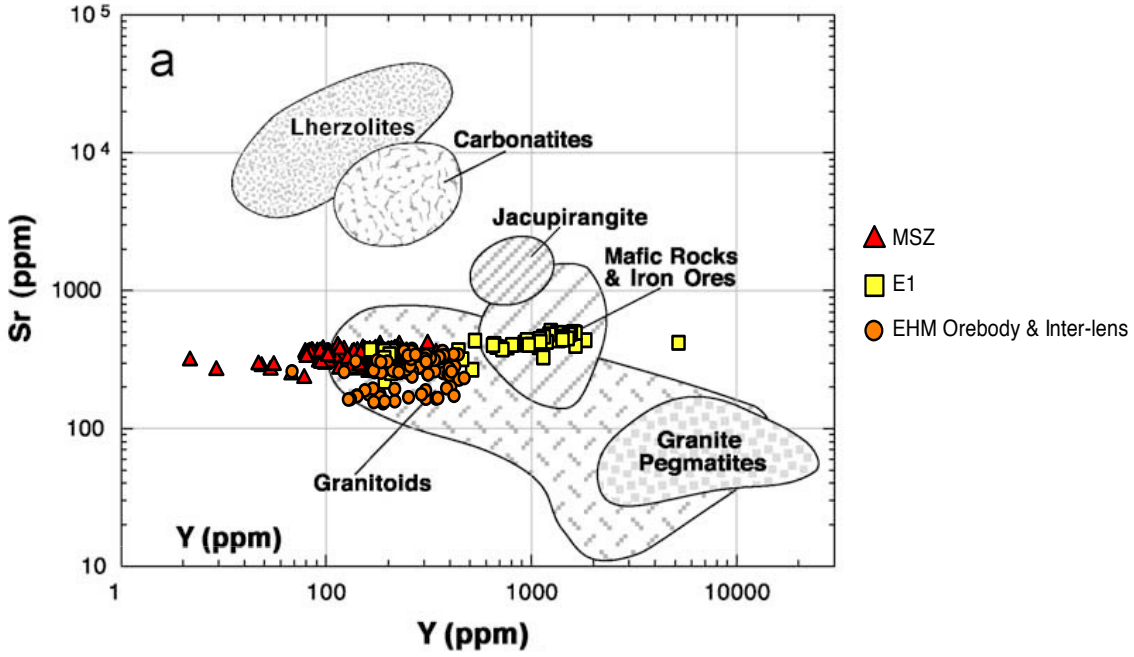

Figure 10: Y (ppm) vs Sr (ppm) discriminant plots with respective fields from Belousova et al. (2002) highlighting the different compositions of the source rock. MSZ, E1-N and Ernest Henry orebody and Inter-lens data are all chondrite-normalised values in log form. Eu* represents the mean of the sum of chondrite-normalised Sm & Gd values.

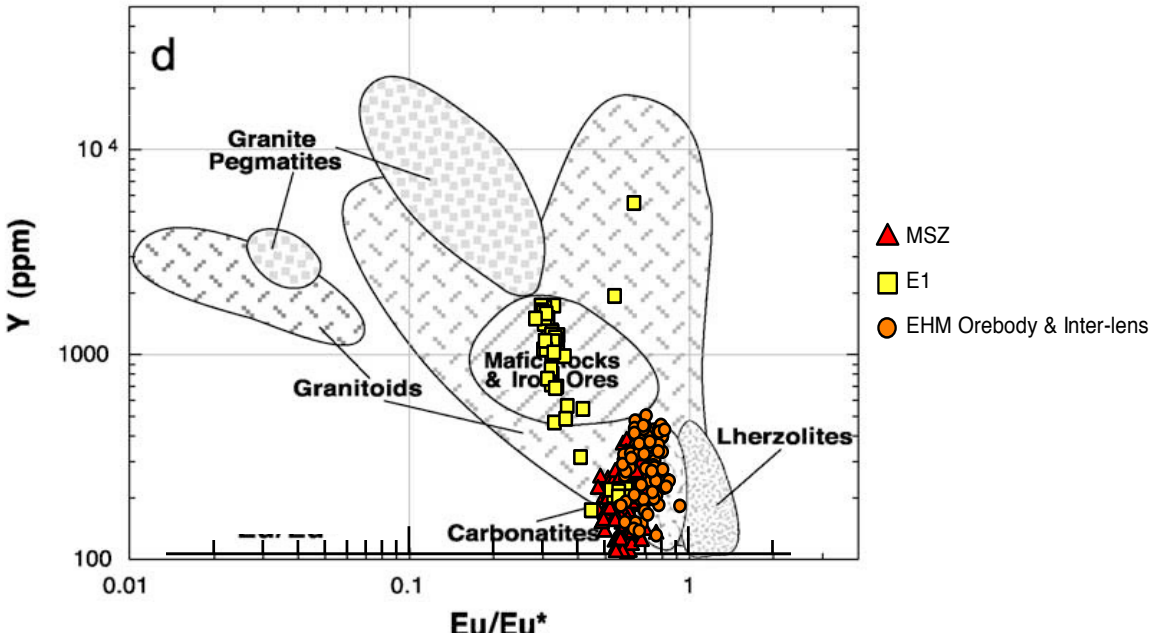

Figure 11: Y (ppm) vs Eu/Eu* discriminant plots with respective fields from Belousova et al. (2002) highlighting the different compositions of the source rock. MSZ, E1-N and Ernest Henry orebody and Inter-lens data are all chondrite-normalised values in log form. The value for Eu* was calculated using the mean of the sum of chondrite-normalised Sm & Gd values.

4.4.3 GEOCHEMICAL PLOTS

Apatite is known to contain variations in certain trace elements throughout the grain including: REE, Sr, Y, Mn and Th depending on the parent rock or events that rock type has experienced (Belousova, Griffin, O'Reilly, & Fisher, 2002; Belousova, Walters, Griffin, & O'Reilly, 2001). Figure 12 shows plots of U vs. Th, Sr vs. Mn and Sr vs. Y. The U vs.Th plots (Figure 12 A & B) shows consistent concentrations of both unzoned and zoned apatite grains throughout all samples with a greater concentration in the zoned E1-N apatites. A negative linear correlation of both U and Th from the cores to the rims is present in all samples with the E1-N zoned grain showing the largest difference. The Sr vs. Mn plot (Figure 12 C & D) shows a comparatively lower concentration of Mn, but greater Sr in the E1-N apatite compared to the MSZ apatite with the MSZ samples concentrated in one spot with the exception of the MSZ-2 samples that are enriched with Mn. No obvious depletion in

Mn or Sr is observed in the MSZ samples; however, a slight depletion of Sr is seen within the E1-N sample. The Sr vs. Y plot (Figure 12 E & D) shows all MSZ apatite contains consistent concentrations of Sr and Y with the E1-N apatite showing greater variation and higher abundance than the MSZ. No obvious depletion in Sr or Y in the zoned samples is observed, with the exception of the E1-N samples showing decreased levels in the zoned samples compared to the unzoned samples. A comparison between all graphs reveals not only trace element differences between deposits, but also between unzoned and zoned grains from the same samples.

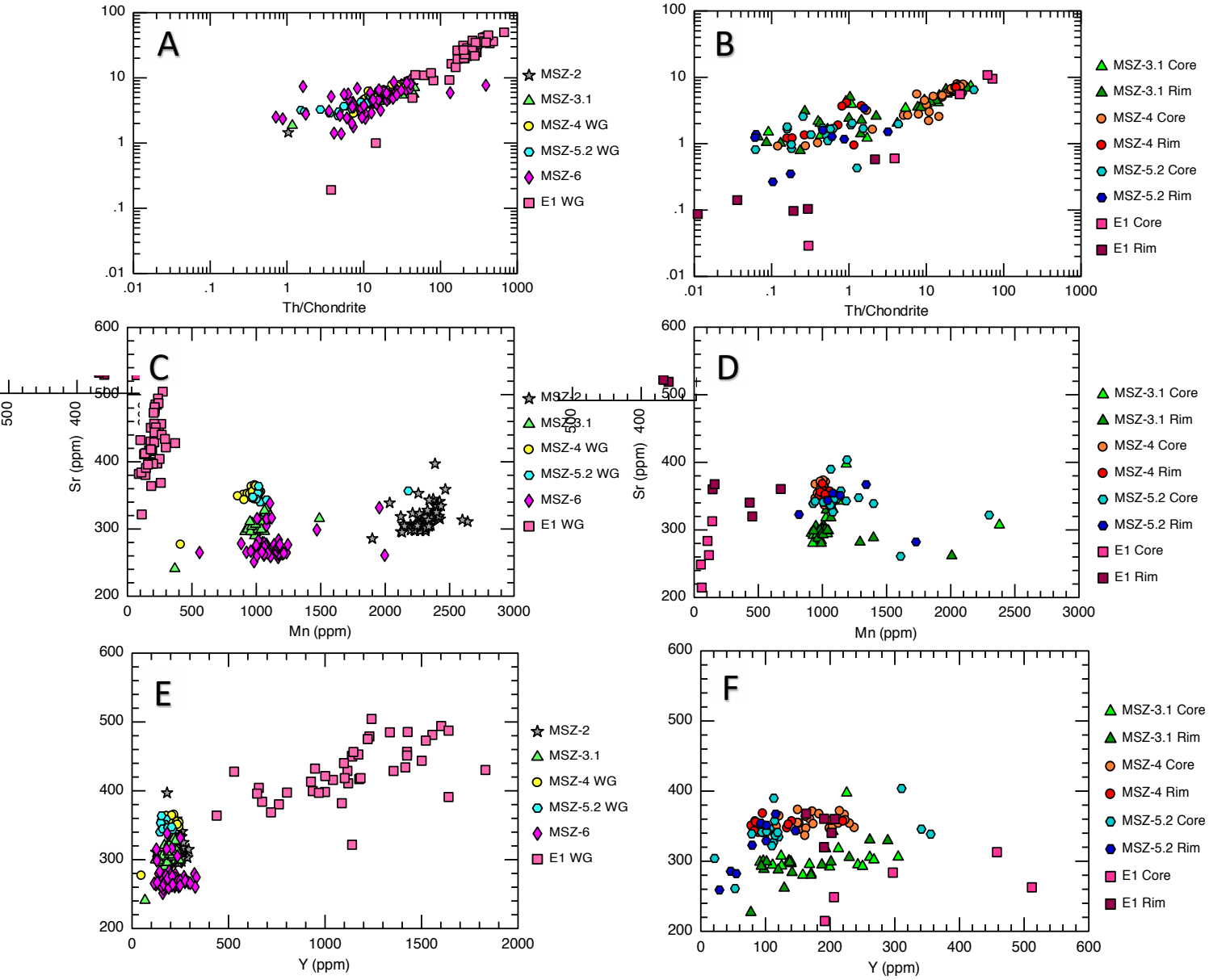

Figure 12: Geochemical Diagrams depicting trace element trends across the MSZ and E1-N apatite samples. A: Chondrite-normalised U vs. Th plot of data from unzoned apatite grains. B: Chondrite-normalised U vs. Th plot of data from zoned apatite grains. C: Sr (ppm) vs. Mn (ppm) plot of data from unzoned apatite grains. D: Sr (ppm) vs. Mn (ppm) plot of data from data from zoned apatite grains. E: Sr (ppm) vs. Y (ppm) plot of data from unzoned apatite grains. F: Sr (ppm) vs. Y (ppm) plot of data from zoned apatite grains.

4.4.4 GREEN VS. RED APATITES

The different coloured apatite grains are seen in multiple samples, with the most pronounced in MSZ-6 (Figure 13B). The trace element data from the different coloured apatite was collected and plotted on Figure 13A, which showed only minor to no differences in the overall concentration of all trace elements.

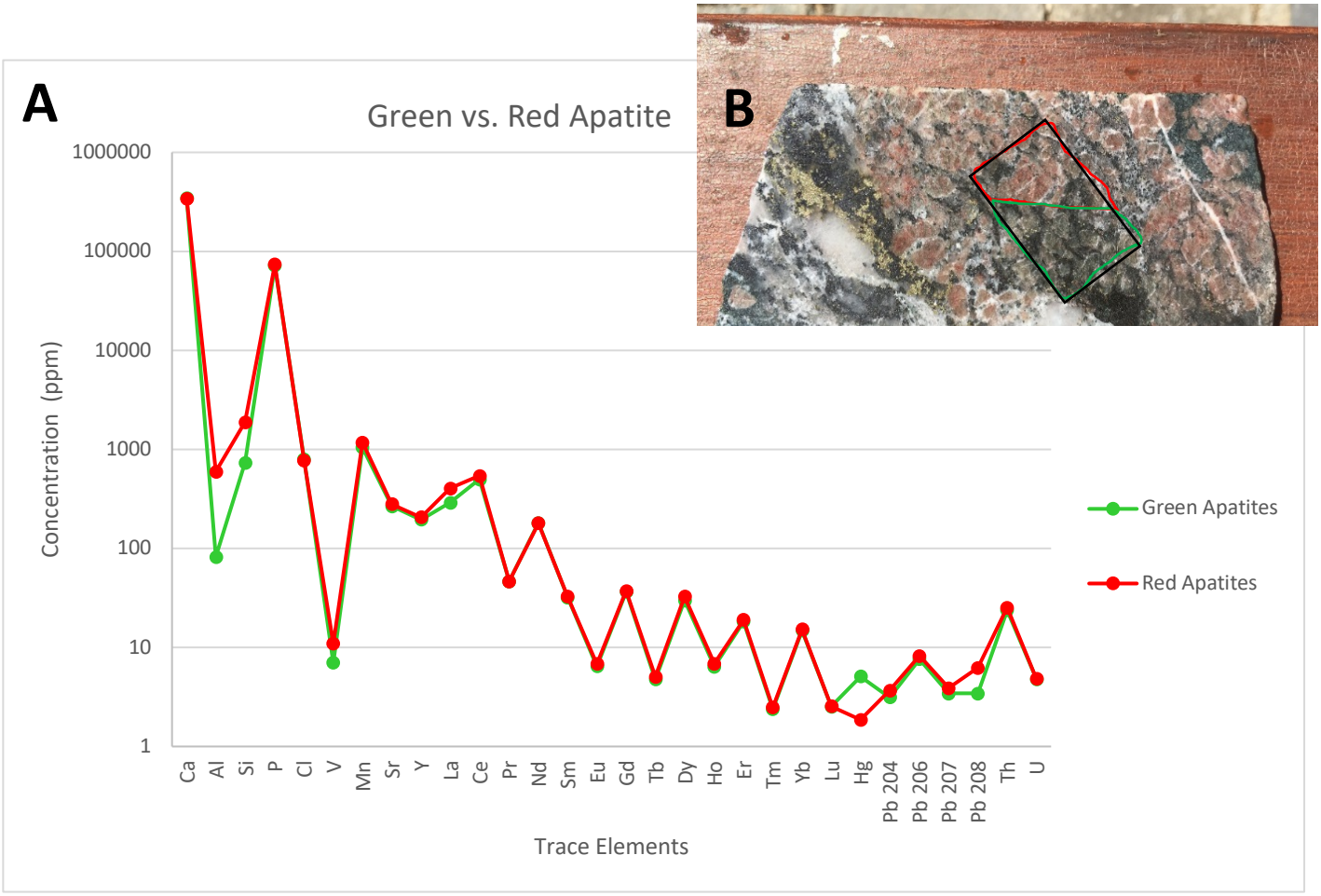

Figu
high
apatites.

5. DISCUSSION

5.1.1 DATA ACCURACY

The source of inaccuracies within the secondary standards when the Madagascar apatite was the primary standard remains unknown. However, incorrectly performing the data reduction can be ruled out as the data was processed on Iolite multiple times by different staff from Adelaide Microscopy and University of Adelaide to produce the same age within error for every test. Another test was completed by Adelaide Microscopy that compared the secondary standard ages produced by the new Madagascar apatite from this study with ages produced by a previously used Madagascar standard. The results of this test found that the original Madagascar standard produced secondary standard ages that were more accurate and concordant than the newer Madagascar apatite, with the only difference being the new standard was prepared as chips mounted in pipette tips, which contained more common lead than the old standard prepared in a resin block. This increased the concentration of common lead often requires more correction, which in turn increases the uncertainty of the overall age. Following this, the data was processed using McClure Mountain as the primary standard with Madagascar, OD306 and 401 apatite acting as secondary standards to find that McClure Mountain and 401 apatite both produced accurate and concordant ages.

Overall, the likely cause of the inaccuracies in the initial tests was the increased uncertainty caused by higher levels of common lead in the newer Madagascar apatite standard. This was corrected for when the McClure Mountain apatite was utilised as the primary standard.

5.1.2 APATITE GEOCHRONOLOGY

The U-Pb ages of the MSZ apatite samples were found to be between ~1508 ± 45 Ma – 1463 ± 38 Ma which coincided with events locally within the deposit (Mark et al., 2006) and regionally within the Eastern Fold Belt (Figure 14). This suggests that an age of formation or a date of fluid induced resetting can be constrained, and a comparison can be made between the other structures within the deposit. All MSZ samples contain ages that are synchronous with the D_3 deformation from 1532−1480 Ma (Betts et al., 2006), biotite from the ore stage at ~1478 Ma (Perkins & Wyborn, 1998) post peak metamorphic conditions, monazite inclusions from E1-N (Case, 2016) and the intrusion of fluids that likely formed the orebody during or following the main stage Cu-Au alteration event. If this was the case, there is potential for the MSZ to intersect the orebody at depth. However, the separate ages do show a high variability that could suggest the possibility of multiple stages of apatite growth or resetting events. Even though this could explain the different sizes of apatite present within many samples, this is unlikely as all ages do have an overlapping 2σ error range and were sampled over a 10m length of core that showed no evidence of more than one stage of apatite growth. This would imply that the finer apatite observed ware likely part of the existing coarse apatite that was broken off and entrained in the calcite veins and are therefore co-genetic in nature.

The U-Pb ages of the E1-N apatite sample was found to be 1550 Ma ± 16 Ma; However, the common lead ratio of 0.5 (Figure 8) is unusually low and puts uncertainty in the age. This age is relatively old in comparison to the MSZ samples; however, it agrees with the younger 1456 ± 44 Ma age of monazite grains from E1-N dated by Case (2016) as the monazites are found as inclusions within the apatite grains and thus, must be younger than the apatite. The age is also synchronous with the Mount Margaret granite at 1530 ± 8 (Page &

Sun, 1998) that is in close proximity to the E1 deposit and the pre-ore alteration event at Ernest Henry ~1530 Ma (Mark et al., 2006) that contains comparatively similar rocks comprising of Ba-rich K-feldspar, magnetite, biotite, apatite and pyrite.

The presence of zonation and apparent cores and rims during cathodoluminescence within both MSZ and E1-N apatite samples suggests a deviation in the overall composition of trace elements, in particular Mn^{2+} or REE (Gros et al., 2016). A deviation in REE is the likely cause as there is an equal drop in all REE concentrations within the rim relative to that in the core (Figure 8); whereas there is no apparent change in the Mn^{2+} concentration (Figure 11). The cause of this REE variation is likely the effects of metasomatism, similar to that observed in the Ernest Henry orebody and Inter-lens apatite study (Cave et al., 2018) Unlike the previous study, the zonations were solely found within finer grained apatite with cores and rims commonly no larger than 100 μm with the E1-N sample only containing a single zoned grain. However, the core and rim age data across all samples contained overlapping 2σ error ranges (Appendix D) and never produced statistically significant ages that could constrain the ages of each zonation. The cause of this could be attributed to a low sample size, low precision of data, contamination between core, rim or adjacent minerals when sampling, rapid alteration or low temperature cooling.

Caution must be taken with the age of the MSZ samples as there is a possibility that the apatite had undergone fluid induced resetting as documented by Kirkland (2018), as multiple observations from previous authors (Cave et al., 2018; Mark et al., 2006) suggest that the MSZ is older than the dates produced by this study. The petrological analysis of the samples show that the apatite was one of the first minerals to form, with minerals such as calcite, quartz, magnetite and biotite forming afterwards. This indicates that the later forming minerals would have formed < ~1480 Ma, during the last stage of alteration. However,

petrological studies by Mark et al. (2006) and Cave et al. (2018) indicates that none of these minerals formed in sufficient quantities during this event. If the age for the original formation of MSZ apatite was roughly around peak metamorphism, the timing of the calcite, quartz, biotite and magnetite would agree with the paragenesis in the literature. Multiple fluid inclusions within the Ernest Henry deposit have been shown to contain temperatures within the closure temperature of range of 350°C – 550°C (Chew et al., 2014). These fluid inclusion temperatures range between 200°C - 600°C (Kendrick et al., 2007) and 375 ± 50°C (Mark et al., 2000). Additionally, the fluid is likely to be ≥ 300°C based on the REE depletion trends that suggest the fluid has high levels of sulphate ions (SO_4^{2-}), which are most stable at this temperatures (Cave et al., 2018; Migdisov, Williams-Jones, Brugger, & Caporuscio, 2016).This shows that there is a possibility that the closure temperature between could have been reached and the loss of Pb could have occurred (Chew & Spikings, 2015). To prove or disprove this, thermochronology studies chould be undertaken to determine if the age of the apatites of the MSZ have been reset. Additionally, the study by Twyerould (1997) speculated that the MSZ belonged to the D_2 deformation events (~1580 Ma) due to its peak-metamorphic textures, amphibolite facies alteration, intense ductile nature and general NE trend, which supports an age of formation during the D2 deformation and thus, the resetting of the MSZ apatite.

Assuming the MSZ apatites were reset and were indeed formed around peak metamorphic conditions, it is likely that the two apatite populations could have originated form the same paragenetic stage. This is due to the similar ages of both the MSZ (~1580 Ma) and E1-N (~1550 Ma) apatite and the similar host rocks comprised of the K-(Ba)-feldspar, biotite, magnetite, quartz and apatite red rock alteration of the ‘pre-ore’ alteration event.

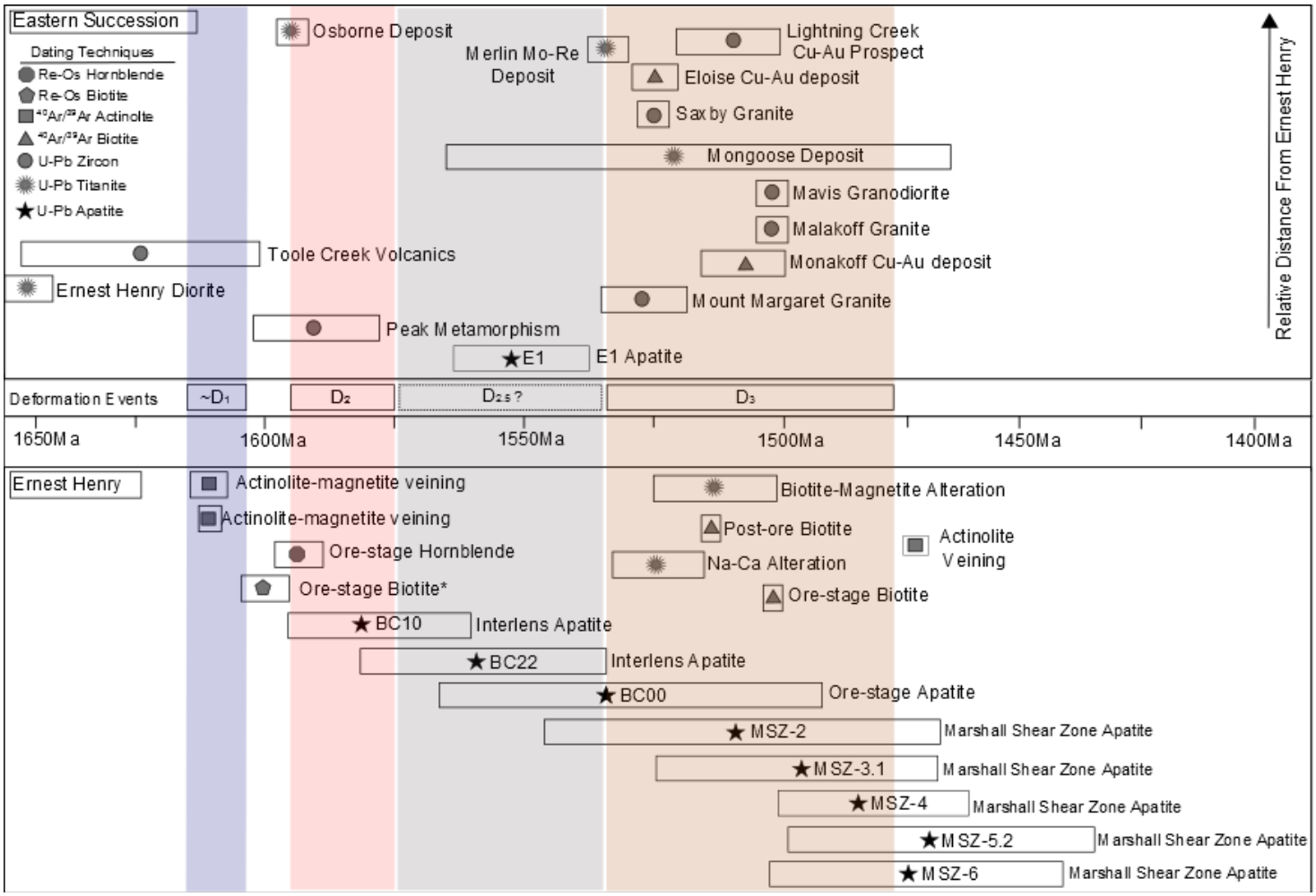

Figure 14: Summary of the geochronology studies completed by various authors within the Eastern Succession adapted from Cave (2017). The top half consists of data from the Eastern Succession and the lower half is based on the Ernest Henry deposit. The length of boxes represents the 2σ error present with each age and the symbol represents the dating technique utilised. Starting at the top, the ages for each event were sourced from the following studies: Osborne Deposit (1595 ± 6 Ma(Gauthier, Hall, Stein, & Schaltegger, 2001)), Merlin Mo-Re Deposit (1535 ± 6 Ma(Babo et al., 2017)), Lightening Creek Prospect (~1508 Ma(Perring, Pollard, & Nunn, 2001)), Eloise Cu-Au deposit (1530 ± 3 Ma(Baker, Perkins, Blake, & Williams, 2001)), Saxby Granite (1527 ± 4 Ma(Rubenach, Foster, Evins, Blake, & Fanning, 2008)), Mongoose Deposit (1515 ± 55 Ma(Maughan, 2016)), Mavis Granidiorite (1505 ± 3 Ma(Davis, Pollard, Lally, Blake, & Williams, 2001)), Malakoff Granite (1505 ± 5 Ma(Page & Sun, 1998)), Monakoff Cu-Au deposit (1508 ± 10 Ma(Polland & Perkins, 1997)), Toole Creek Volcanics (1625 ± 27 Ma(Griffin, Belousova, Walters, & O'Reilly, 2006)), Ernest Henry Diorite (1660 ± 13 Ma(Pollard & McNaughton, 1997)), Mount Margaret Granite (1530 ± 8 Ma(Page & Sun, 1998)), Peak Metamorphism (1584 ± 17 Ma(Page & Sun, 1998)), E1-N Apatite (1550 ± 16 Ma (This Study)), D_1 (1610 ± 13 Ma (Page & Bell, 1986)) , D_2 (1595-1975 Ma (Page & Sweet, 1998)), D_3 (1532-1480 Ma (Betts et al., 2006)), actinolite - magnetite veining (1610 ± 2 Ma & 1611 ± 4 Ma(Twyerould, 1997)), ore-stage biotite (1504 ± 3 Ma(Twyerould, 1997)), post-ore biotite (1514 ± 3 Ma(Twyerould, 1997)), and actinolite veining (1476 ± 3 Ma(Twyerould, 1997)), Na-Ca alteration (1529 ± 11Ma(Mark, Oliver, & Williams, 2006)), biotite-magnetite alteration (1514 ± 29Ma(Mark et al., 2006)), ore-stage biotite* (1595 ± 6 Ma(Gauthier et al., 2001)), ore-stage hornblende (1600 ± 6 Ma(Gauthier et al., 2001)), Interlens Apatite (1581 ± 16 Ma & 1557 ± 23 Ma (Cave, 2017), Ore-Stage Apatite (1529 ± 39 Ma (Cave, 2017) and Marshall Shear Zone Apatite (1508 ± 45 Ma, 1497 ± 34 Ma, 1479 ± 19 Ma, 1463 ± 38 Ma and 1472 ± 35 Ma (This Study)). The MSZ samples from this study correlate with the D_3 deformation, multiple granitic intrusions and mineralisation events throughout the Eastern Succession event whilst the E1-N sample correlates with the late D_2 and hypothesised $D_{2.5}$ deformation event.

5.1.3 APATITE GEOCHEMISTRY

Apatite from the Marshall Shear Zone and E1-N show different chemical characteristics and overall different trace element compositions. These variations allow for the apatite grains to be used as indicators for the type of host rock and fluids responsible for the alteration (Belousova et al., 2002; D. E. Harlov, 2015). The samples of this study show distinct variations in Y, Sr, Eu/Eu*, resulting in the MSZ samples plotting as granitoids/carbonatites and the E1-N sample plotting as mafic rocks/iron ores on the discrimination plots (Figure 9). This could suggest that the apatites were sourced from fluids that originated from different rock types, with the MSZ likely sourced from the metasediments and metavolcanic of the protolith rock and the E1-N sample from the mafic meta-andestie basalt of the host rock (Figure 2). Apatite data from the Ernest Henry orebody and Inter-lens (Cave, 2017) roughly fall in the same discrimination sections as the MSZ samples (Figure 10), suggesting all three locations could be sourced from the same granitoids/carbonatites. The few data points that contain less Sr than the rest represent the metasomatized rims of the Inter-lens samples, indicating Sr was likely stripped away during metasomatism and likely redeposited in a later mineral stage.

The study by Cave et al. (2018) showed that the fluids interacting with the Ernest Henry system caused fluid induced metasomatism, resulting in the textural differences within apatite grains caused by a depletion of certain trace elements. Similar metasomatism likely affected the MSZ apatite as the similar trends and textural changes of REE depletion and zonation are observed in this study. The concentration of REE in apatite grains can be linked to the abundance of monazite inclusions as they specifically require LREE to form, which are commonly metasomatically removed from apatite grains (D. E. Harlov, 2015) during metasomatic reactions with a high Na and/or Ca fluid (D. E. Harlov & Förster, 2003; D. E.

Harlov, Förster, & Nijland, 2002; Daniel E. Harlov, Wirth, & Förster, 2005). As the E1 apatite sample from this study possessed varying amounts of fine-grained monazite inclusions, it is implied that the metasomatising fluids removed partial amounts of LREE to form these inclusions (Equation 1), Resulting in a LREE depletion in the rim. However, The MSZ apatite samples show a depletion of REE with minimal amounts of monazite inclusions. This is characteristic of a fluid comprised of Na and/or Ca as these cations act to stabilise the apatite grains and inhibits the REE exchange reactions from progressing (D. E. Harlov, 2015; D. E. Harlov & Förster, 2003). This is supported by a variably high (35-70 wt%) NaCl salinity in the Ernest Henry fluid inclusion studies (Kendrick et al., 2007; Mark et al., 2000; Rusk et al., 2010) and variably low (15-40 wt%) NaCl salinity within the E1-N fluid inclusions (Case, 2016).

$$REE^{3+} + Na^{+} \leftrightarrow 2Ca^{2+}$$

Equation 1: Atomic Substitution equation showing how REE is substituted out of the apatite grain (left side of the equation) and into the fluid where it will then either be transported away or used to form minerals such as monazite. (right side). (Harlov, 2015)

Variations in REE trends in the MSZ and E1-N apatite (Figure 8) could imply the fluids in question had differing compositions and sources. The consistent enrichment of LREE relative to HREE (Figure 8) across all samples is typical of a magmatic-hydrothermal fluid system (D. E. Harlov, Andersson, et al., 2002), Suggesting the fluids that formed both the MSZ and E1-N apatite are likely hydrothermal and magmatic in nature. This would imply that apatite from E1-N and the MSZ would have likely originated from the magmatic and hydrothermal fluids documented in both the E1 and Ernest Henry deposits (Case, 2016; Kendrick et al., 2007). However, differences do exist between the fluids with the MSZ fluid likely forming at greater depths due to Br/Cl and I/Cl values of fluid inclusions resembling a

mantle derived source (Kendrick et al., 2007), the abundant CO_2 in Ernest Henry deposit relative to E1 and the larger concentrations of REE in the unaltered E1-N apatite in comparison to the MSZ apatite (Figure 8). Overall, the likelihood that both fluids were sourced from magmatic intrusions similar to that of the Williams and Naraku batholiths is high. However, it is unlikely that both fluids were sourced from the same intrusion as their chemical compositions are too different and it is unlikely that the varying levels of compounds and trace elements such as CO_2, Y, Sr and Mn would arise solely from the mixing with surrounding rocks/fluids.

The fluid induced metasomatism that affected both the MSZ and E1-N apatite appear to be similar but again, contain slight geochemical differences. The MSZ samples show a consistent depletion of all REE, which is typical of a fluid abundant in $-SO^4$ as it acts as a stable ligand for all REE in alkaline conditions at ≥ 300°C (Cave et al., 2018; Migdisov et al., 2016). The source of this S could be attributed to the source rock comprising of a S-rich alkaline igneous intrusion, similar to that of the Williams and Naraku batholiths (Fuss, 2014), a S-rich brine or possibly a combination of two fluids. The depletion of REE in the E1-N sample appear to favour the LREE. This is typical of a hydrothermal system where monazite inclusions are present as they (D. E. Harlov, 2015). However, a fluid abundant in Cl-ligands also causes the same result as LREE-Cl compounds are more stable in acidic conditions at ≥ 250°C (Cave et al., 2018; Migdisov et al., 2016). As fluid inclusions within E1-N exhibit only moderate Na:Cl levels, it is more likely that the LREE depletion was predominately caused by the growth of the fine-grained monazite inclusions with only minor contributions by a Cl-rich fluid. The HREE enrichment in the rim of the E1-N sample is unlikely indicative of any process and more likely an error in the results. This is due to the minimal number of data points recorded form the rim (n=5) and the slight difference in appearance compared to the core of the grain and other rim samples from the MSZ apatite. Overall, it is probable that

the fluids responsible for the apatite grains alteration were a combination of the magmatic/hydrothermal fluids responsible apatite formation and an additional fluid possibly from the S bearing fluid from the Corella Formation for E1 (Case, 2016) and an upper crustal saline brine for the MSZ that mixed together (Kendrick et al., 2007). This would also explain the additional S noted in the E1 system brought in with the shallow fluid from the Corella Formation and the additional Cl in the MSZ transported in by the upper crustal brine.(Kendrick et al., 2007).

The comparison of the trace elements within the red and green apatite show no distinct differences with only minor variations in Al, Si, Hg, ^{208}Pb and La. These variations are not large enough to confidently conclude that these trace elements are the cause for the different coloured apatite. However, the elements tested in this study were limited and the potential for untested elements such as the common halogens (F or OH) in the different forms of apatite to be the cause is plausible.

6. CONCLUSIONS

- Apatite from the MSZ is dated between 1508 ± 45 Ma and 1463 ± 38 Ma, linking its formation to after Cu-Au mineralisation and towards the end of the D_3 deformation event. Apatite from E1-N is dated at 1550 ± 16 Ma, synchronous with the formation of the Mount Margaret granite at 1530 ± 8, and the pre-ore alteration event at Ernest Henry ~1530 Ma.

- U-Pb geochronology revealed no distinct date for the altered and unaltered zones of the metasomatised MSZ and E1-N apatite grains.

- The theory of the MSZ apatite grains undergoing fluid induced resetting by the introduction of fluids during the late D_3 or post orebody formation is likely. If this is true, it is also possible that the two populations are from the same paragenetic stage.

- The REE composition of the MSZ and E1-N apatite revealed the fluids that formed the apatite were likely magmatic-hydrothermal in origin, contained enriched levels of S and REE, were alkaline in nature and sourced from different magmatic intrusions, both similar in composition to that of the Williams and Naraku Batholiths.

- The metasomatising fluids affecting the MSZ apatite were likely rich in Na and/or Ca due to the lack of monazite inclusions in comparison to that in E1-N, which contained abundant monazite inclusions.

- Geochemical studies conducted on the red and green apatite revealed no differences in composition of elements analysed.

7. ACKNOWLEDGEMENTS

Firstly, I would like to thank the team up at Ernest Henry Mine, especially Brad Miller and Elizabeth Philippa for their assistance with the project, as well as Mount Isa Mines for funding this exciting project. I would also like to thank the honours cohort for making this year an enjoyable experience and overall, slightly less stressful. At Adelaide Microscopy, I would like to give a huge thank you to Dave Kelsey and Sarah Gilbert who provided me with invaluable insight and technical support into my project. I would also like to thank Gilby Jepson for going out of his way to assist me with the apatite dating process and Stijn Glorie for providing the necessary apatite standards. Finally, I would like to give a huge thanks to Brad Cave for his assistance with numerous aspects of my project and last but certainly not least, my supervisor, Richard Lilly, who has provided the geological and academic knowledge required to make this project possible.

8. REFERENCES

Babo, J., Spandler, C., Oliver, N., Brown, M., Rubenach, M., & Creaser, R. (2017). The High-Grade Mo-Re Merlin Deposit, Cloncurry District, Australia: Paragenesis and Geochronology of Hydrothermal Alteration and Ore Formation. *Economic Geology, 112*(2), 397-422.

Baker, T., Mustard, R., Fu, B., Williams, P. J., Dong, G., Fisher, L., . . . Ryan, C. G. (2008). Mixed messages in iron oxide–copper–gold systems of the Cloncurry district, Australia: insights

from PIXE analysis of halogens and copper in fluid inclusions. *Mineralium Deposita, 43*(6), 599-608. doi: 10.1007/s00126-008-0198-y

Baker, T., Perkins, C., Blake, K., & Williams, P. J. (2001). Radiogenic and stable isotope constraints on the genesis of the Eloise Cu-Au deposit, Cloncurry district, northwest Queensland. *Economic Geology, 96*(4), 723 - 742.

Belousova, E. A., Griffin, W. L., O'Reilly, O. S., & Fisher, N. I. (2002). Apatite as an indicator mineral for mineral exploration: trace-element compositions and their relationship to host rock type. *Journal of Geochemical Exploration, 76*(1), 45 - 69.

Belousova, E. A., Walters, S., Griffin, W. L., & O'Reilly, O. S. (2001). Trace-element signatures of apatites in granitoids from the Mt Isa Inlier, northwestern Queensland. *Australian Journal of Earth Sciences, 48*(4), 608 - 619.

Betts, P. G., Giles, D., Mark, G., Lister, G. S., Goleby, B. R., & Aillères, L. (2006). Synthesis of the proterozoic evolution of the Mt Isa Inlier. *Australian Journal of Earth Sciences, 53*(1), 187-211. doi: 10.1080/08120090500434625

Blake, D. (1987). *Geology of the Mount Isa Inlierand environs, Queensland and Northern Territory*. Australia: Bureau of Mineral Resources, Geology and Geophysics.

Case, G. (2016). *Genesis of the E1 Group of Iron oxide-Copper-Gold deposits, Cloncurry District, north West Queensland.* (Doctor of Philosophy), James Cook University.

Cave, B. (2017). *U-Pb geochronology and Trace Element Analysis of Apatite and Calcite from the Ernest Henry Deposit, NW Queensland.* (Bachelor of Science (Honours)), University of Adelaide.

Cave, B., Lilly, R., Glorie, S., & Gillespie, J. (2018). Geology, Apatite Geochronology, and Geochemistry of the Ernest Henry Inter-Lens: Implications for a Re-Examined Deposit Model. *Minerals, 8*(9), 405. doi: 10.3390/min8090405

Chew, D. M., Petrus, J. A., & Kamber, B. S. (2014). U–Pb LA–ICPMS dating using accessory mineral standards with variable common Pb. *Chemical Geology, 363*, 185-199. doi: 10.1016/j.chemgeo.2013.11.006

Chew, D. M., & Spikings, R. A. (2015). Geochronology and Thermochronology Using Apatite: Time and Temperature, Lower Crust to Surface. *Elements, 11*(3), 189-194. doi: 10.2113/gselements.11.3.189

Cleverley, J. (2006). Using the chemistry of apatite to track fluids in Fe-oxide Cu-Au systems. *Geochimica et Cosmochimica Acta, 70*(18), 105.

Davis, B., Pollard, P. J., Lally, J., Blake, K., & Williams, P. J. (2001). Deformation history of the Naraku Batholith, Mt Isa Inlier, Australia: implications for pluton ages and geometries from structural study of the Dipvale Granodiorite and Levian Granite. *Australian Journal of Earth Sciences, 48*(1), 113 - 129.

Foster, A. R., Williams, P. J., & Ryan, C. G. (2007). Distribution of Gold in Hypogene Ore at the Ernest Henry Iron Oxide Copper-gold Deposit, Cloncurry District, NW Queensland. *Exploration and mining Geology, 16*(3-4), 125-143.

Foster, D., & Austin, J. (2008). The 1800–1610Ma stratigraphic and magmatic history of the Eastern Succession, Mount Isa Inlier, and correlations with adjacent Paleoproterozoic terranes. *Precambrian Research, 163*(1-2), 7-30. doi: 10.1016/j.precamres.2007.08.010

Foster, D., & Rubenach, M. J. (2006). Isograd pattern and regional low-pressure, high-temperature metamorphism of pelitic, mafic and calc-silicate rocks along an east – west section through the Mt Isa Inlier. *Australian Journal of Earth Sciences, 53*(1), 167-186. doi: 10.1080/08120090500434617

Fuss, M. (2014). *Isotopic (87Sr/86Sr, δ13C and δ18O) indicators of fluid source from carbonates in the Ernest Henry deposit, Queensland, Australia: implications for genesis and exploration.* (Bachelor of Science (Honours)), James Cook University.

Gauthier, L., Hall, G., Stein, H., & Schaltegger, U. (2001). The Osborne deposit, Cloncurry district: a 1595 Ma Cu–Au skarn deposit. *Contributions of the Economic Geology Research Unit, James Cook University, 59*, 58-59.

Griffin, W. L., Belousova, E. A., Walters, S. G., & O'Reilly, S. Y. (2006). Archaean and Proterozoic crustal evolution in the Eastern Succession of the Mt Isa district, Australia: U – Pb and Hf-isotope studies of detrital zircons *. *Australian Journal of Earth Sciences, 53*(1), 125-149. doi: 10.1080/08120090500434591

Gros, K., Słaby, E., Förster, H.-J., Michalak, P. P., Munnik, F., Götze, J., & Rhede, D. (2016). Visualization of trace-element zoning in fluorapatite using BSE and CL imaging, and EPMA and µPIXE/µPIGE mapping. *Mineralogy and Petrology, 110*(6), 809-821. doi: 10.1007/s00710-016-0452-4

Harlov, D. E. (2015). Apatite: A Fingerprint for Metasomatic Processes. *Elements, 11*(3), 171-176. doi: 10.2113/gselements.11.3.171

Harlov, D. E., Andersson, U. B., Förster, H.-J., Nyström, J. O., Dulski, P., & Broman, C. (2002). Apatite–monazite relations in the Kiirunavaara

magnetite–apatite ore, northern Sweden. *Chemical Geology, 191*(1-3), 47-72.

Harlov, D. E., & Förster, H.-J. (2003). Fluid-induced nucleation of (Y+REE) phosphate minerals within apatite: Nature and experiment. Part II. Fluorapatite. *American Mineralogist, 88*(8-9), 1209-1229.

Harlov, D. E., Förster, H.-J., & Nijland, T. G. (2002). Fluid-induced nucleation of (Y + REE)-phosphate minerals within apatite: Nature and experiment. Part I. Chlorapatite. *American Mineralogist, 87*(2-3), 245-361.

Harlov, D. E., Wirth, R., & Förster, H.-J. (2005). An experimental study of dissolution–reprecipitation in fluorapatite: fluid infiltration and the formation of monazite. *Contributions to Mineralogy and Petrology, 150*(3), 268-286. doi: 10.1007/s00410-005-0017-8

Hewett, J. (2017). *Gold Distribution and the Relationship to Pyrite Trace Element Geochemistry at the Ernest Henry Deposit, Queensland.* (Bachelor of Science (Honours)), University of Adelaide.

Jong, G. D., & Williams, P. J. (1995). Giant metasomatic system formed during exhumation of mid-crustal Proterozoic rocks in the vicinity of the Cloncurry Fault, northwest Queensland. *Australian Journal of Earth Sciences, 42*(3), 281-290. doi: 10.1080/08120099508728202

Kendrick, M. A., Mark, G., & Phillips, D. (2007). Mid-crustal fluid mixing in a Proterozoic Fe oxide–Cu–Au deposit, Ernest Henry, Australia: Evidence from Ar, Kr, Xe, Cl, Br, and I. *Earth and Planetary Science Letters, 256*(3-4), 328-343. doi: 10.1016/j.epsl.2006.12.032

Kirkland, C. L., Yakymchuk, C., Szilas, K., Evans, N., Hollis, J., McDonald, B., & Gardiner, N. J. (2018). Apatite: a U-Pb thermochronometer or geochronometer? *Lithos, 318-319*, 143-157. doi: 10.1016/j.lithos.2018.08.007

Lilly, R., Case, G., & Miller, B. (2017). Ernest Henry iron oxide copper-gold deposit. *Australian Ore Deposits, 1-6*.

Liu, W., Mei, Y., Etschmann, B., Brugger, J., Pearce, M., Ryan, C. G., . . . Falkenberg, G. (2017). Arsenic in hydrothermal apatite: Oxidation state, mechanism of uptake, and comparison between experiments and nature. *Geochimica et Cosmochimica Acta, 196*, 144-159. doi: 10.1016/j.gca.2016.09.023

Mark, G., Oliver, N., Williams, P. J., Valenta, R. K., & Richard, C. A. (2000). The Evolution of the Ernest Henry Fe-Oxide-(Cu-Au) hydrothermal System. *PGC Publishing, 1*, 123-126.

Mark, G., Oliver, N. H. S., & Williams, P. J. (2006). Mineralogical and chemical evolution of the Ernest Henry Fe oxide–Cu–Au ore system, Cloncurry district, northwest Queensland, Australia. *Mineralium Deposita, 40*(8), 769-801. doi: 10.1007/s00126-005-0009-7

Maughan, J. (2016). *Geochemistry of the Mafic Sequences in the Cloncurry District,*

Queensland: Implications for crustal accretion and prospectivity. (Bachelor of Science (Honours)), University of Adelaide.

Migdisov, A., Williams-Jones, A. E., Brugger, J., & Caporuscio, F. A. (2016). Hydrothermal transport, deposition, and fractionation of the REE: Experimental data and thermodynamic calculations. *Chemical Geology, 439*, 13-42. doi: 10.1016/j.chemgeo.2016.06.005

O'Brien, S. (2016). *Structural and Mineralogical Controls on the Formation of the 'Inter-lens' at the Ernest Henry Deposit, Queensland.* (Bachelor of Science (Honours)), University of Adelaide.

Oliver, N., Valenta, R. K., & Wall, V. J. (1990). The effect of heterogeneous stress and strain on metamorphic fluid flow, Mary Kathleen, Australia, and a model for large-scale fluid circulation. *Journal of Metamorphic Geology, 8*(3), 311-331. doi: 10.1111/j.1525-1314.1990.tb00475.x

Page, R. W., & Bell, T. H. (1986). Isotopic and Structural Responses of granite to Successive Deformation and Metamorphism. *The Journal of Geology, 94*(3), 365-379.

Page, R. W., & Sun, S. S. (1998). Aspects of geochronology and crustal evolution in the Eastern Fold Belt, Mt Isa Inlier∗. *Australian Journal of Earth Sciences, 45*(3), 343-361. doi: 10.1080/08120099808728396

Page, R. W., & Sweet, I. P. (1998). Geochronology of basin phases in the western Mt Isa Inlier, and correlation with the McArthur Basin. *Australian Journal of Earth Sciences, 45*(2), 219-232. doi: 10.1080/08120099808728383

Paton, C., Hellstrom, J., Paul, B., Woodhead, J., & Hergt, J. (2011). Iolite: Freeware for the visualisation and processing of mass spectrometric data. *Journal of Analytical Atomic Spectrometry, 26*(12), 2508. doi: 10.1039/c1ja10172b

Perkins, C., & Wyborn, L. (1998). <Perkins and Wyborn - orebody biotite age.pdf>. *The age of Cu-Au mineralisation, Cloncurry district, Mount Isa Inlier, as determined by 40Ar/39Ar dating, 45*(2), 233-246.

Perring, C., Pollard, P. J., & Nunn, A. (2001). Petrogenesis of the Squirrel Hills granite and associated magnetite-rich sill and vein complex: Lightning Creek prospect, Cloncurry district, northwest Queensland. *Precambrian Research, 106*(3), 213 - 238.

Polland, P., & Perkins, C. (1997). 40Ar/39Ar geochronology of alteration and Cu–Au–Co mineralization in the Cloncurry district, Mount Isa Inlier. *P438 Cloncurry Base Metals and Gold Final Report, Section, 3.*

Pollard, P. J., & McNaughton, N. J. (1997). U/Pb geochronology and Sm/Nd isotope characteristics of Proterozoic intrusive rocks in the Cloncurry district, Mount Isa Inlier, Australia. *AMIRA P438 Cloncurry base Metals and Gold Final Report, section 4*, 19.

Reed, R. M., & Milliken, K. I. (2003). HOW TO OVERCOME IMAGING PROBLEMS ASSOCIATED WITH CARBONATE MINERALS ON SEM-BASED CATHODOLUMINESCENCE SYSTEMS. *Journal Of Sedimentary Research, 73*(2), 328-332.

Rubenach, M., Foster, D., Evins, P., Blake, K., & Fanning, C. (2008). Age constraints on the tectonothermal evolution of the Selwyn Zone, Eastern fold belt, Mount Isa Inlier. *Precambrian Research, 163*(1), 81 - 107.

Rusk, B., Oliver, N., Cleverley, J., Blenkinsop, T., Zhang, D., Williams, P. J., & Habermann, P. (2010). Physical and chemical characteristics of the Ernest Henry Iron Oxide Copper Gold deposit, Australia; Implications for IOCG genesis. *PGC Publishing*.

Schoene, B., Crowley, J. L., Condon, D. J., Schmitz, M. D., & Bowring, S. A. (2006). Reassessing the uranium decay constants for geochronology using ID-TIMS U–Pb data. *Geochimica et Cosmochimica Acta, 70*(2), 426-445. doi: 10.1016/j.gca.2005.09.007

Sun, S. S., & McDonough, W. F. (1989). Chemical and Isotopic Systematics of Oceanic Basalts: Implications for Mantle Composition and processes. *Geological Society, London, Special Publications, 42*(1), 313-345.

Thompson, J., Meffre, S., Maas, R., Kamenetsky, V., Kamenetsky, M., Goemann, K., . . . Danyushevsky, L. (2016). Matrix effects in Pb/U measurements during LA-ICP-MS analysis of the mineral apatite. *Journal of Analytical Atomic Spectrometry, 31*(6), 1206-1215. doi: 10.1039/c6ja00048g

Twyerould, S. C. (1997). *The Geology and Genesis of the Ernets Henry Fe-Cu-Au Deposit, NW Queensland Australia.* (Doctor of Philisophy), University of Oregon.

Williams, M. R., Holwell, D. A., Lilly, R. M., Case, G. N. D., & McDonald, I. (2015). Mineralogical and fluid characteristics of the fluorite-rich Monakoff and E1 Cu–Au deposits, Cloncurry region, Queensland, Australia: Implications for regional F–Ba-rich IOCG mineralisation. *Ore Geology Reviews, 64*, 103-127. doi: 10.1016/j.oregeorev.2014.05.021

Wyborn, L. (1998). Youngerca1500 Ma granites of the Williams and Naraku Batholiths, Cloncurry district, eastern Mt Isa Inlier: Geochemistry, origin, metallogenic significance and exploration indicators∗. *Australian Journal of Earth Sciences, 45*(3), 397-411. doi: 10.1080/08120099808728400

9. APPENDIX A – HAND SAMPLE DESCRIPTIONS

Sample MSZ-1

Sample number	Length along Drillhole	Descriptions
MSZ-1	**265.47**	This sample appears to be dominant in its magnetite and biotite (50%), apatite (25%) and calcite (25%) with trace amounts of pyrite and chalcopyrite. The apatite appears green in colour and found mainly on one side of the slab, past the large vein of biotite and often broken up another mineral. The thin section was cut to accommodate the highest concentration of apatites (see blue rectangle).

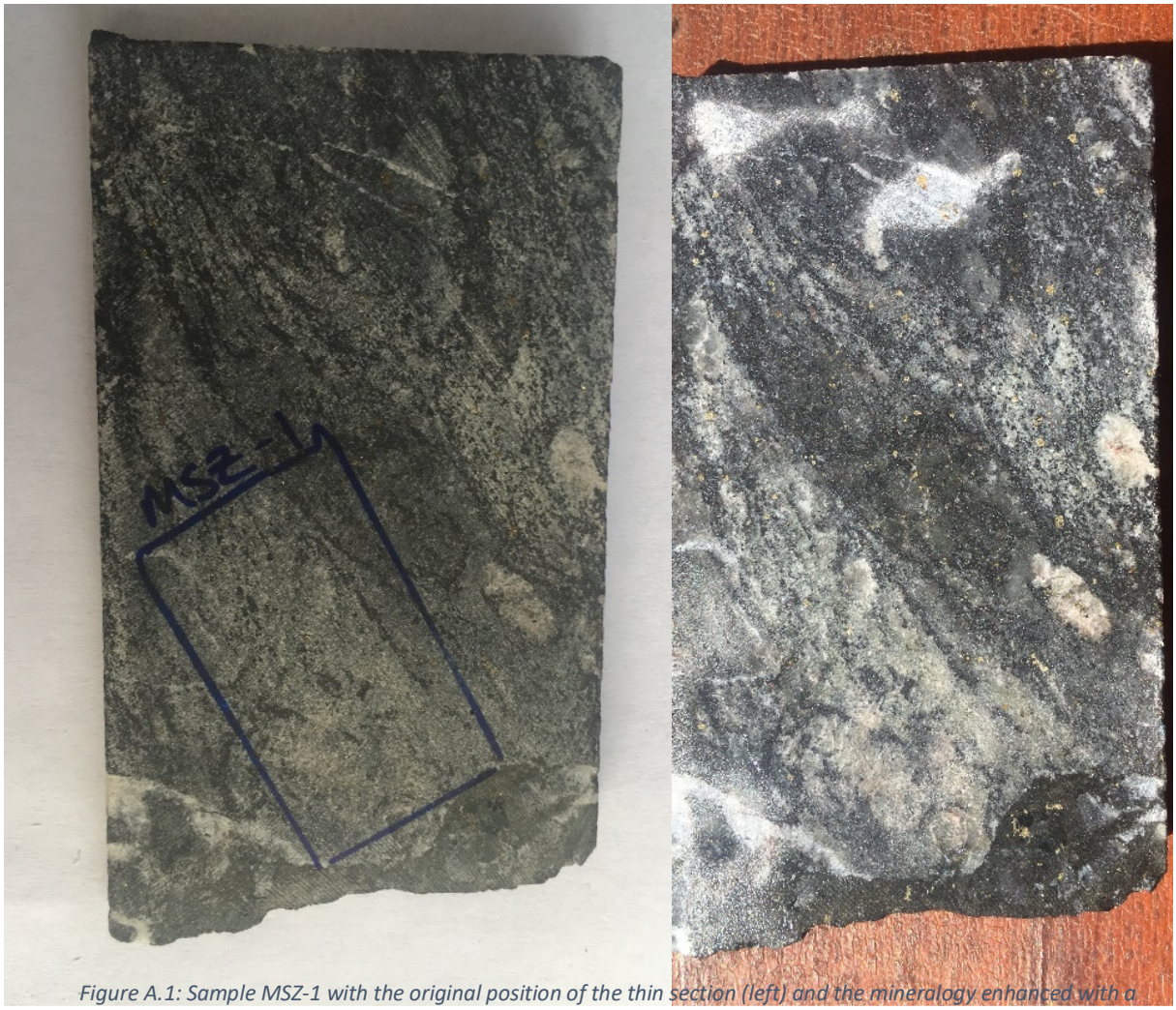

Figure A.1: Sample MSZ-1 with the original position of the thin section (left) and the mineralogy enhanced with a layer of water (right).

Sample MSZ-2

Sample number	Length along Drillhole	Descriptions
MSZ-2	**265.8m**	This sample is dominated by magnetite/biotite (60%), apatite (30%) and calcite (10%) with trace amounts of pyrite/chalcopyrite. The apatite is a faint green to a cloudy white colour, euhedral and concentrated on one side of the slab. No visible calcite veins. Magnetite/biotite appears to be separating the apatite grains. The best place to make the thin section from was in the large cluster of fine apatite grains in the bottom (see blue rectangle).

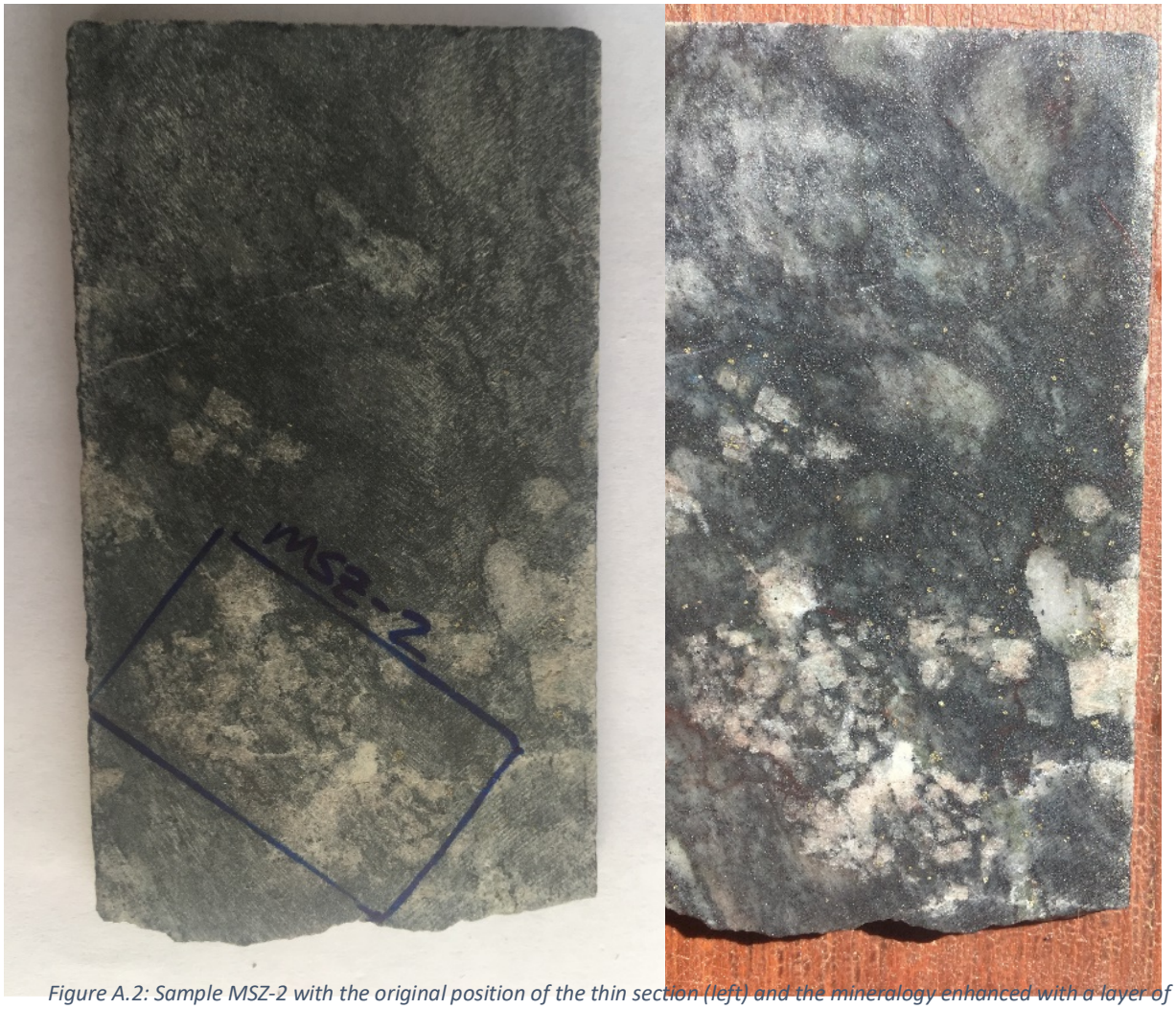

Figure A.2: Sample MSZ-2 with the original position of the thin section (left) and the mineralogy enhanced with a layer of water (right).

Sample MSZ-3

Sample number	Length along Drillhole	Descriptions
MSZ-3	**269.7m**	This sample is dominated by apatite (70%), biotite/magnetite (20%) and calcite (10%) with trace amounts of pyrite. Apatite grains range from 0.5 to 2 cm in width, green (edge) to red (core) in colour and found widely distributed throughout rock. The apatite is separated by veins comprising of magnetite, biotite and calcite, likely formed after the apatite. Two thin sections were made to investigate the coarser and multi-coloured apatites of this sample (see blue rectangles).

Figure A.3. Sample MSZ-3 with the original position of the thin section (left) and the mineralogy enhanced with a layer of water (right).

Sample MSZ-4

Sample number	Length along Drillhole	Descriptions
MSZ-4	**271.2m**	Comprised of apatite (70%), calcite (10%), magnetite/biotite (10%), quartz (10%) and trace amounts of pyrite. The apatite is 0.5-1.5cm in width, euhedral, closely compact (minimal veining separating grains) and again, green and red in colour. One large quartz vein can be seen in the bottom and minimal magnetite/biotite veining can be seen. The thin section location was picked as it had the highest abundance of apatite that additionally, had sufficient amounts of multicoloured apatite grains.

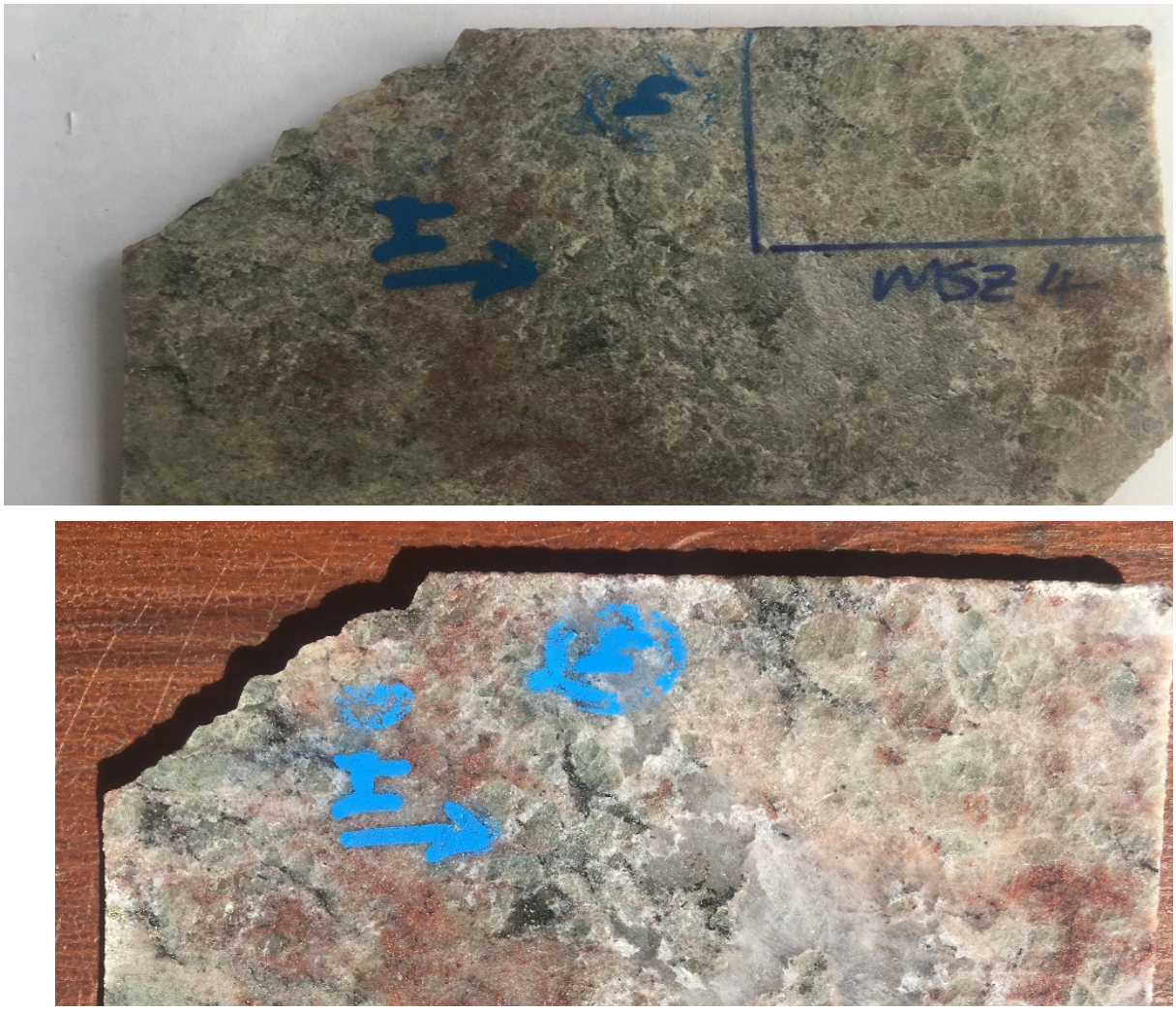

Figure A.4: Sample MSZ-4 with the original position of the thin section (left) and the mineralogy enhanced with a layer of water (right).

Sample MSZ-5

Sample number	Length along Drillhole	Descriptions
MSZ-5	**271.4m**	Comprised of apatite (70%), biotite/magnetite (15%), calcite (15%) and trace amounts of pyrite/chalcopyrite within the biotite/magnetite. Apatite grains are up to several cm in width, both red and green in colour, mostly euhedral and separated by magnetite/biotite veins. Two thin sections were produced in order to highlight the multicoloured, coarsed grains and sobserve how the biotite/magnetite vein interacts with the apatite on the left side of the image.

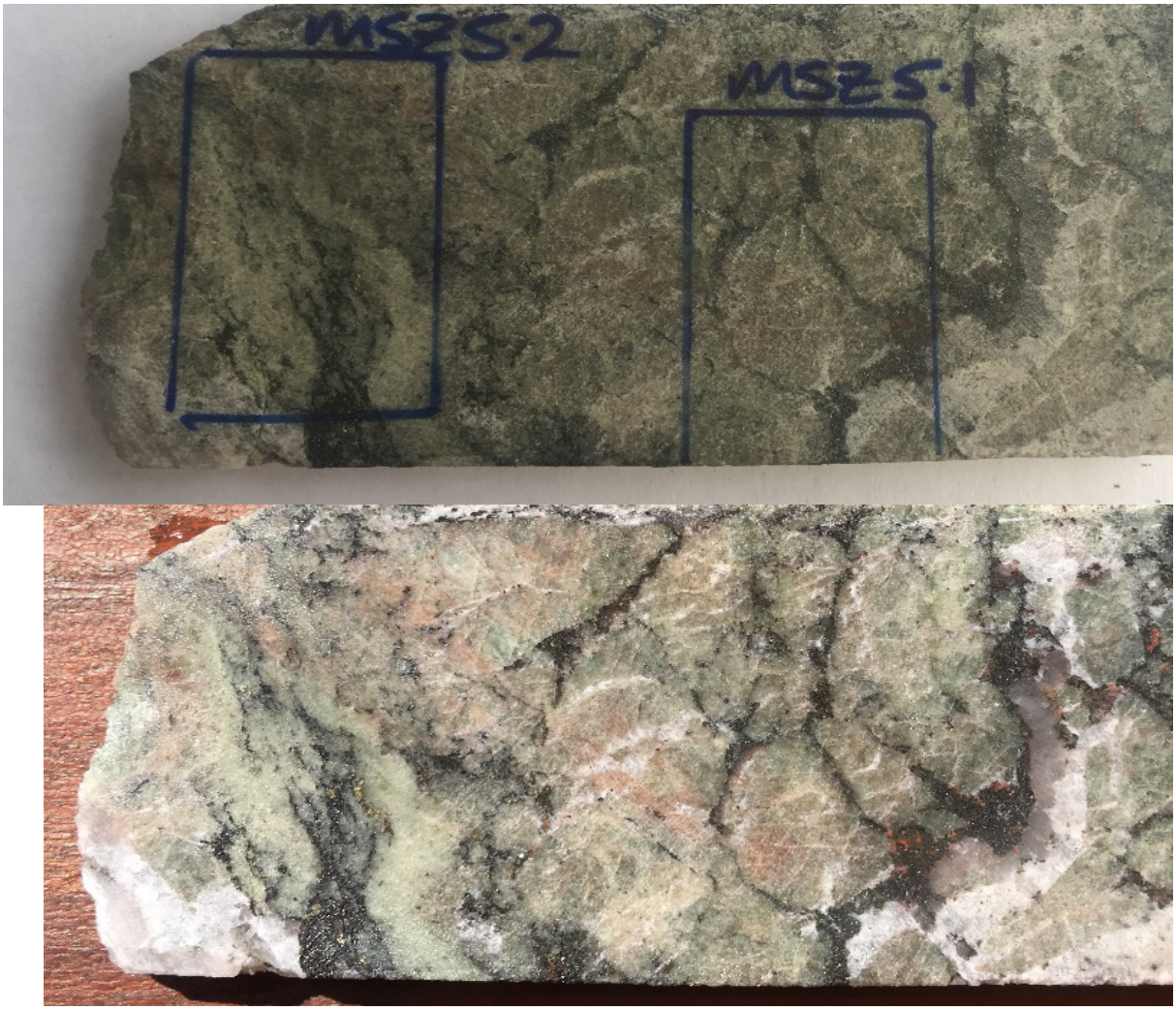

Figure A.5: Sample MSZ-5 with the original position of the thin section (left) and the mineralogy enhanced with a layer of water (right).

Sample MSZ-6

Sample number	Length along Drillhole	Descriptions
MSZ-6	**276.0m**	Comprised of apatite (40%), calcite (25%), magnetite/biotite (20%), quartz (10%), pyrite (5%) and trace amounts of chalcopyrite. The apatite grains are up to 1cm in width, mostly euhedral and occasionally fully green or red in colours opposed to red cores and green edges. Significant amounts of pyrite is seen on the edge of a large magnetite/biotite vein on the left. The thin section location was chosen based on the abundance ofmulticoloured apatite grains.

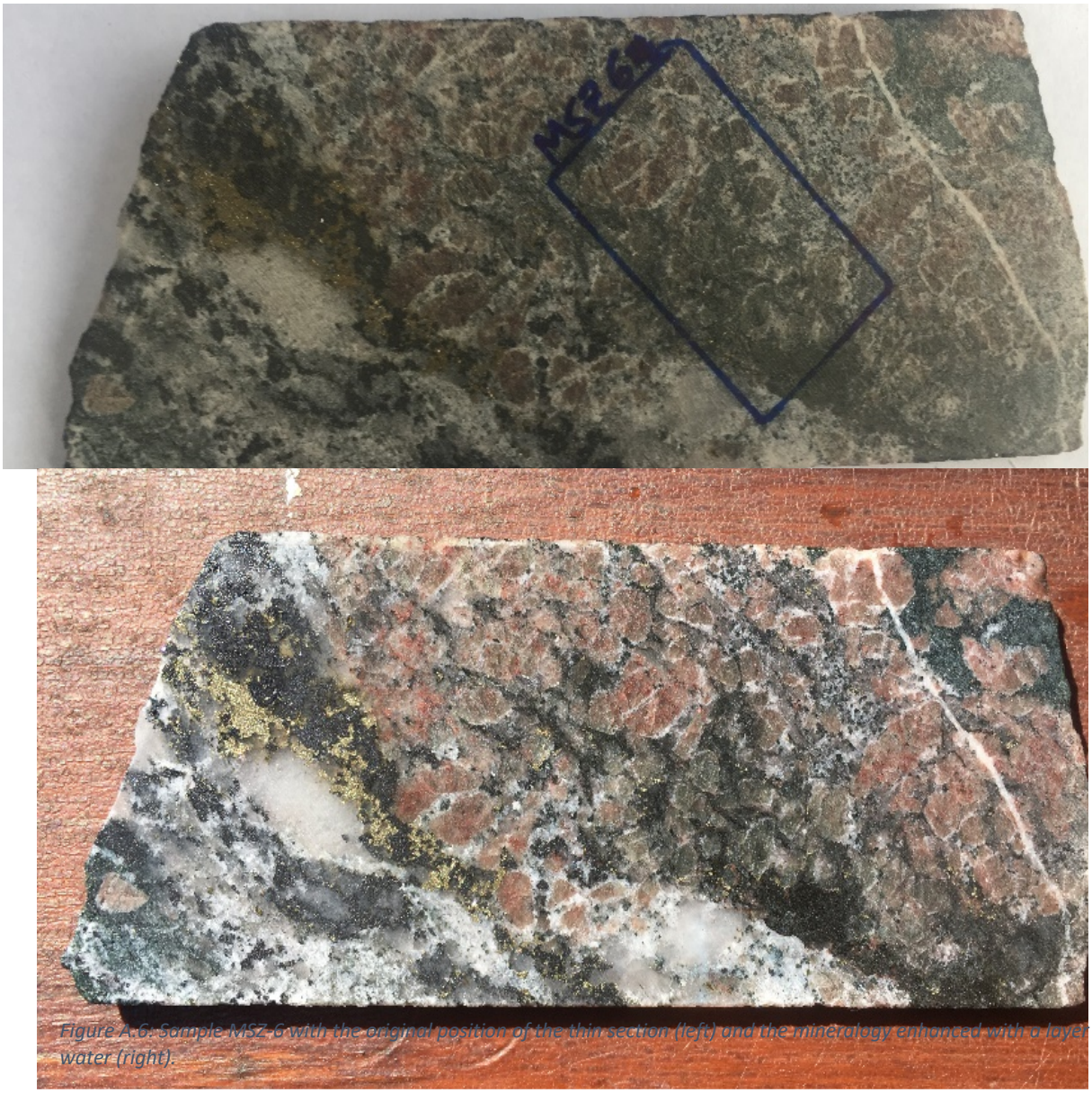

Figure A.6: Sample MSZ-6 with the original position of the thin section (left) and the mineralogy enhanced with a layer of water (right).

Sample MSZ-7

Sample number	Length along Drillhole	Descriptions
MSZ-7	**280.2m**	Comprised of magnetite/biotite (58%), calcite (15%), apatite (15%), quartz (10%) and pyrite (2%). Apatite grains are few in this sample with the only significant grain being elongated, colourless and cut in half. The majority of this sample comprises of fine-grained quartz and calcite and the biotite/magnetite shear that cuts across the rock. The sheared area contains a red mineral that appears to be garnet. The thin section was made to observe the elongated apatite grain and the shear zone to determine its history.

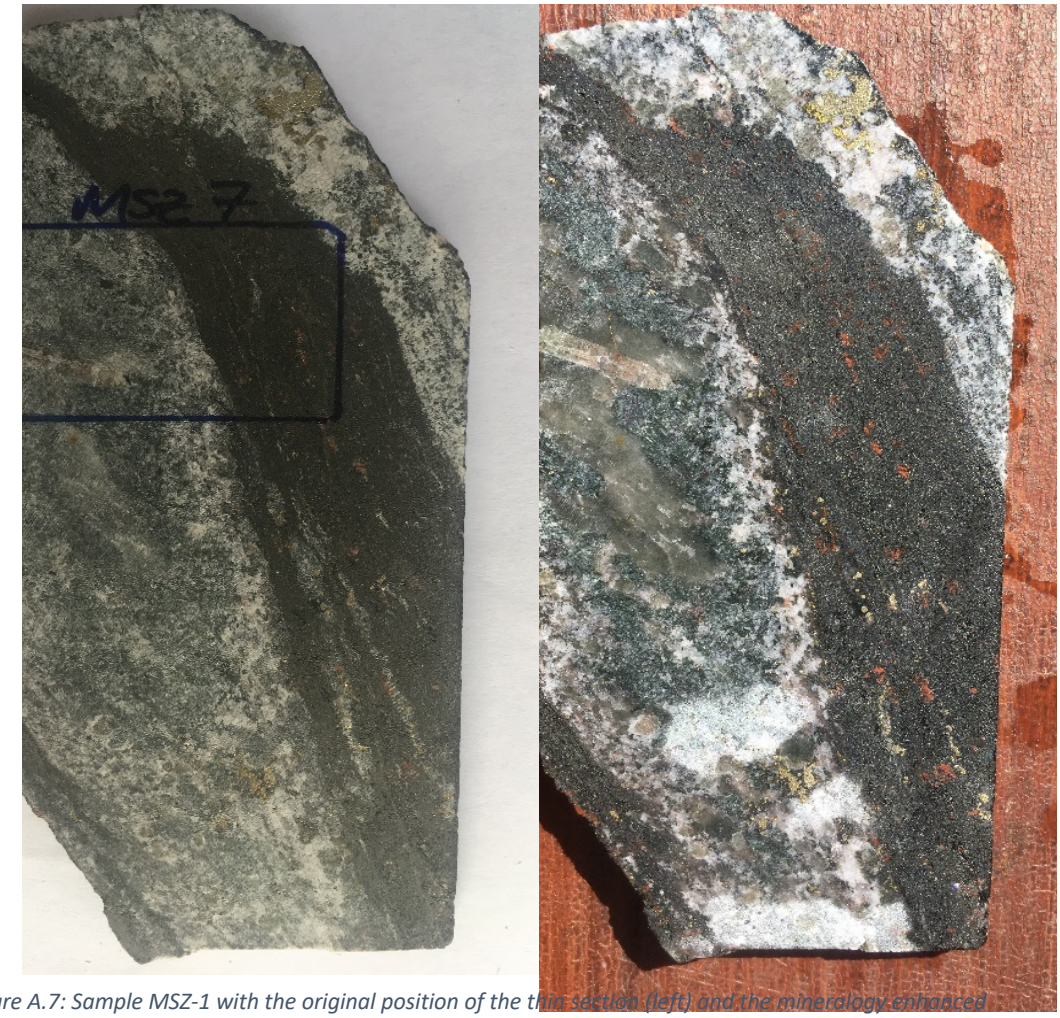

Figure A.7: Sample MSZ-1 with the original position of the thin section (left) and the mineralogy enhanced with a layer of water (right).

10. APPENDIX B – OPTICAL PETROGRAPHY DESCRIPTIONS

Sample MSZ-1

This sample is comprised of predominately fine-grained quartz, magnetite and calcite with coarser grained apatite, minor amounts of biotite and chlorite and trace amounts of euhedral pyrite and chalcopyrite. The apatite is concentrated on one side of the thin section with the other side being dominated by quartz and calcite. The majority of apatite grains are heavily brecciated by coarse calcite veining or intruded by finer calcite veining. The magnetite, biotite and chlorite appear to form proximal to each other but the magnetite can also be found within the calcite veins.

Figure B.1: A: Multiple brecciated apatite grains with visible coarse and fine-grained calcite veining. B: Magnetite, biotite and chlorite cluster. C: Euhedral chalcopyrite grain

This sample is again comprised of predominately fine-grained quartz, magnetite and calcite with coarser grained apatite and trace amounts of euhedral pyrite and chalcopyrite. However, some calcite grains do appear as coarse as the apatite grains. The apatite is more abundant, coarser and more intact in this sample. The distribution of minerals is more consistent throughout the sample.

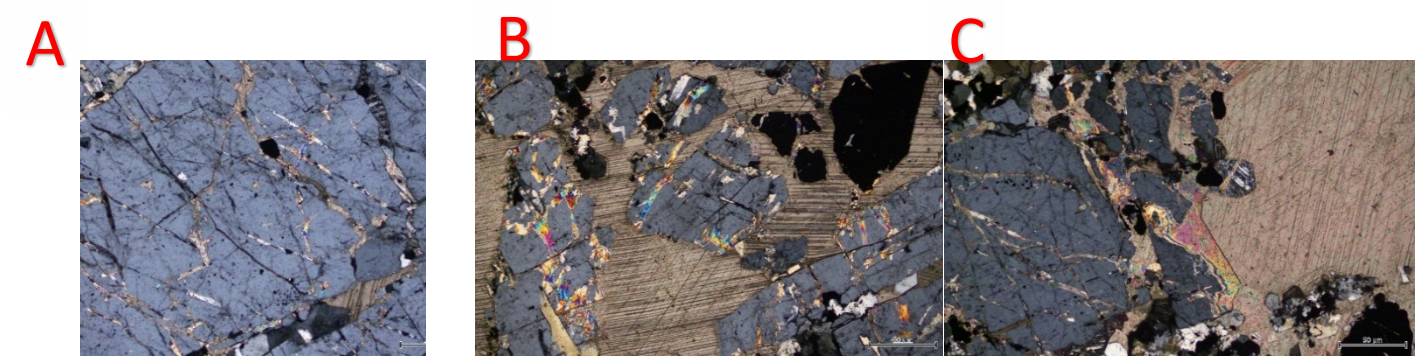

Figure B.2: A: Coarse-grained apatite grain with visible fine-grained clacite veining. B: brecciated apatite grains. C: Coarse calcite grain proximal to a coarse-grained apatite grain.

Sample MSZ-3.1

Coarse- to fine-grained apatite makes up most of the composition of this sample with minor amounts of fine-grained magnetite, biotite, quartz and calcite and trace amounts of euhedral pyrite and chalcopyrite. Apatite is widely spread throughout the sample with varying levels of brecciation but heavily dominated by fine-grained calcite veining. Sulphide grains are seen to have inclusions of biotite and follow the veins created by the coarse-grained calcite.

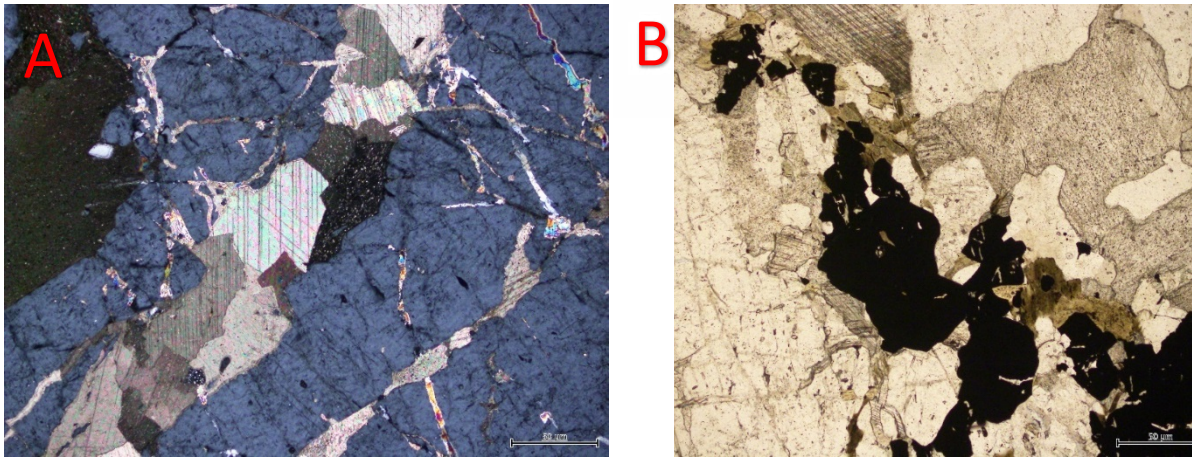

Figure B.3: Coarse-grained calcite vein cutting through apatite grains. B: Sulphide grains snaking along the calcite veins with fine-grained biotite inclusions.

Sample MSZ-3.2

This sample has a similar composition to MSZ-3.1 with the addition of trace amounts of biotite and chlorite found on the edges of one side of the sample. The grains of biotite and chlorite that aren't found on the edge snake their way through the veins created by coarse calcite. Apatite, calcite and quartz have the same qualities as those in MSZ-3.1 with the exception of a few medium- to coarse- grained quartz and calcite..

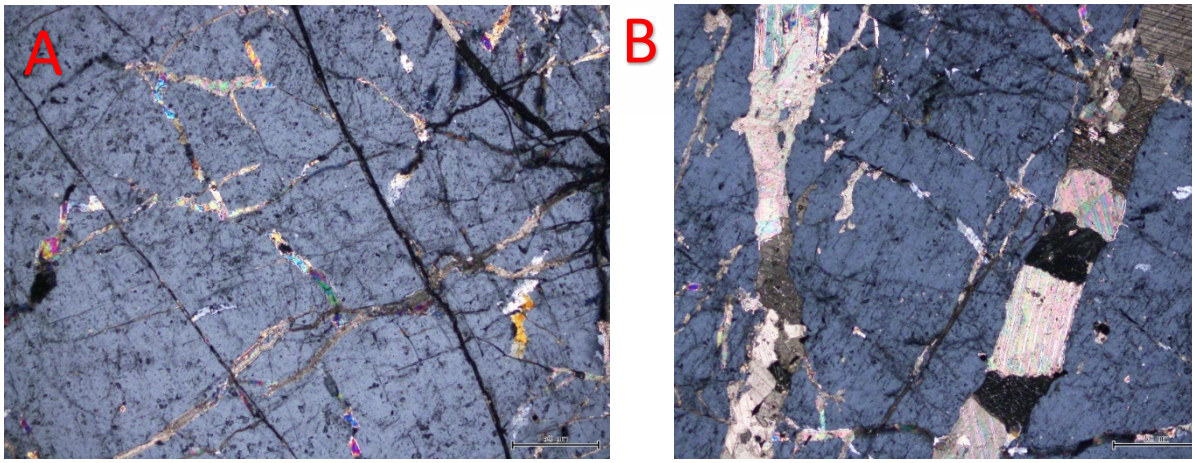

Figure B.4: A: Coarse-grained apatite showing fine-grained calcite veining. B: Two coarse-grained calcite veins cutting through multiple apatite grains.

Sample MSZ-4

Comprised of mostly apatite (green and red in hand sample) with minor amounts of fine-grained quartz, calcite and magnetite and trace amounts of euhedral pyrite and chalcopyrite. Apatite grains range from very coarse- to fine-grained. Coarse apatite is affected by both fine and coarse-grained calcite veins whereas finer grained apatite isn't and often found within said coarse-grained calcite veins. The origins of the finer grained apatites could be fragments of coarser grains broken off and entrained by coarse calcite veins or possibly a later stage of apatite. No visible difference between red and green apatites under a microscope. Calcite and magnetite are widely distributed throughout the sample whereas fine-grained quartz is concentrated in a single corner.

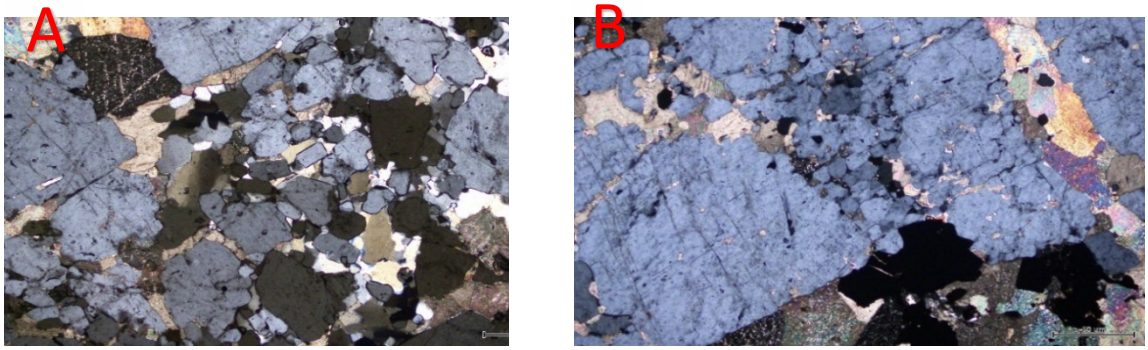

Figure B.5: A: A combination of fine and coarse apatite grains. B: Fine-grained apatites adjacent to coarse apatite grains and within a coarse-grained calcite vein.

Sample MSZ-5.1

Dominated by apatites (both green and red in hand sample) with minor amounts of quartz, calcite magnetite, biotite and chlorite and trace amounts of euhedral pyrite and chalcopyrite. Fine and coarse apatite grains present with varying levels of coarse and fine-grained calcite veining in the coarser apatites. The size of the apatites are easily defined by darker minerals highlighting the coarse calcite veins found in between apatite grains. Medium- to fine-grained quartz only found in two pockets in the sample. Medium- to coarse-grained calcite and fine magnetite, biotite and chlorite widely distributed and found in the veins between apatite grains.

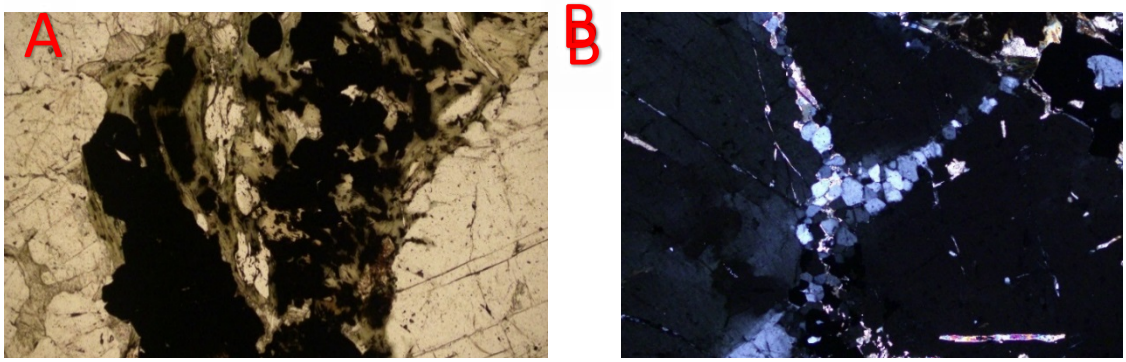

Figure B.6: A: Biotite, magnetite, chlorite & sulphides clustered together with the coarse-grained calcite vein. B: Coarse and fine-grained apatite.

Sample MSZ-5.2

This sample is dominated by coarse and fine-grained apatite with minor amounts of magnetite and calcite and trace amounts of biotite, chlorite and quartz. Coarse-grained apatite has varying levels of brecciation and intrusive calcite veins. As before, the fine-grained apatite appears mostly within coarse calcite veins however, is also seen as a large cluster in one section of the sample.

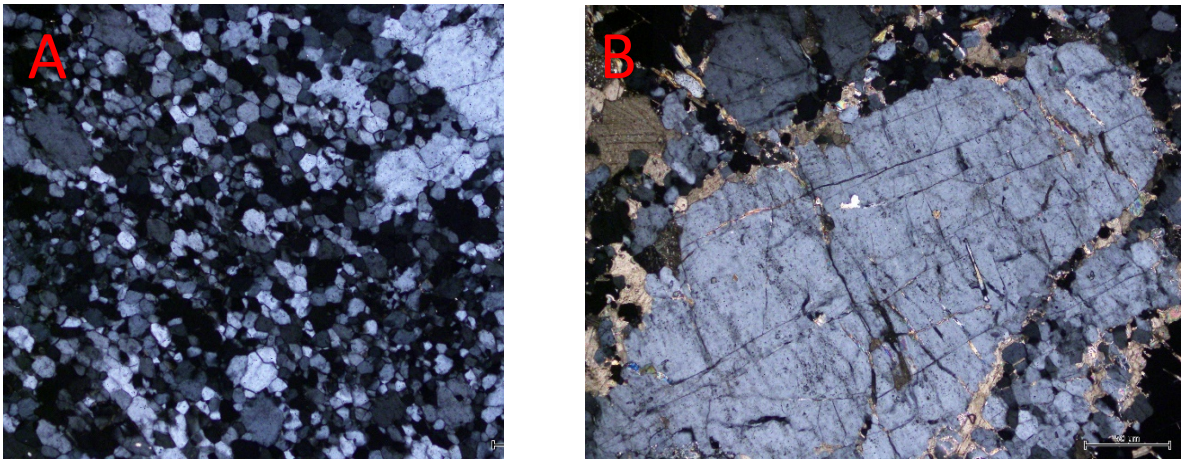

Figure B.7: A: Fine-grained apatite cluster with interlaid coarse-grained apatite. B: Fine-grained apatite adjacent to coarse-grained apatite.

Sample MSZ-6

Sample dominated by apatite (both red and green in hand sample) with minor amounts of calcite, quartz, chlorite, magnetite and biotite and euhedral copper sulphides. The apatite is again coarse- to fine-grained but not as coarse as seen previously. The apatite grains of different colours show no difference under this section. A large biotite vein with minor amounts of chlorite and sulphides runs through the centre of the sample and finishes in the middle point, moving around apatite grains in the process.

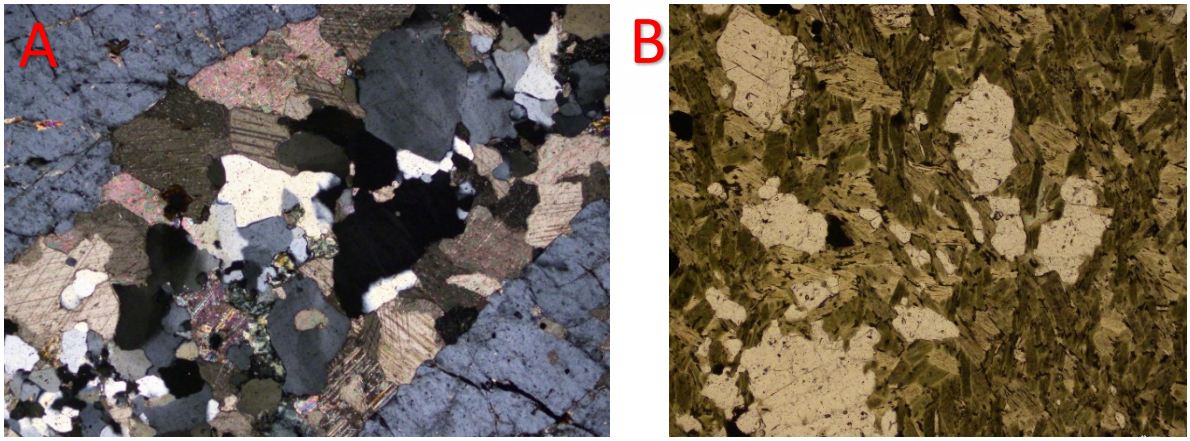

Figure B.8: A: Coarse calcite vein with quartz in the centre, calcite adjacent to the quartz and coarse calcite adjacent to the coarse calcite. B: Biotite vein moving around apatite grains.

Sample MSZ-7

This sample only contains 3-4 apatite grains and only one of sufficient size to analyse. The rest of the sample is dominated by a fine- to medium-grained calcite and quartz groundmass with several areas appearing to be altered and a shearing event comprised of biotite and unaltered magnetite that formed post shear. The sheared area covers just under half the thin section and contains no trace of apatites.

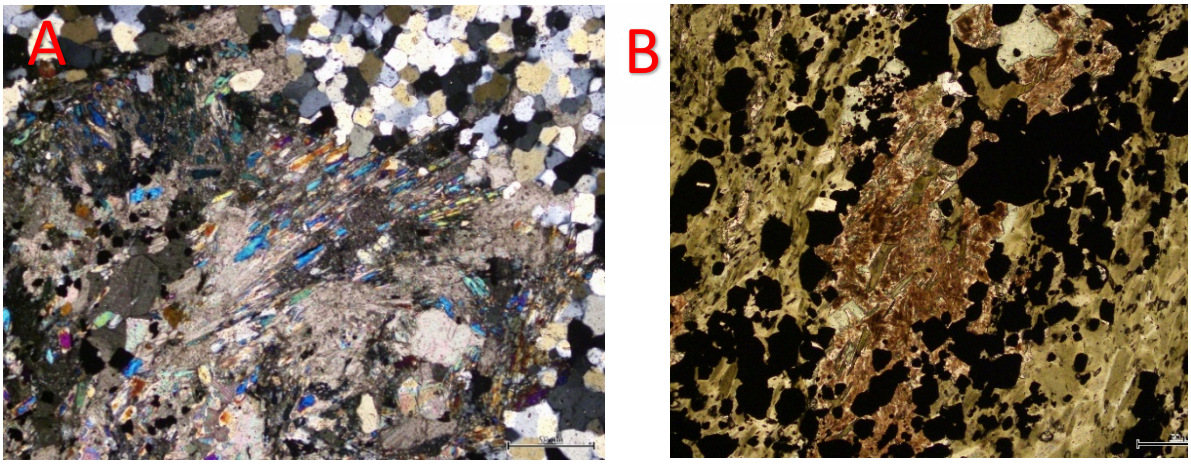

Figure 9.B: A: Altered calcite and chlorite with adjacent unaltered quartz. B: Biotite and unaltered magnetite within the shear zone.

Sample EMMD026-221.3 (E1-N)

The majority of this sample is magnetite, sulphides and apatite with minor amounts of quartz, calcite and biotite. Apatite is medium- to coarse-grained with minimal brecciation and intrusive fine-grained calcite veins and found throughout the sample. Calcite and quartz are fine to medium grain and found in between the sulphide, magnetite and apatite grains. The biotite is fine-grained, found adjacent to the magnetite and found as inclusions in the sulphide and magnetite grains. The magnetite and copper sulphide grains are fine to coarse-grained and found throughout the sample.

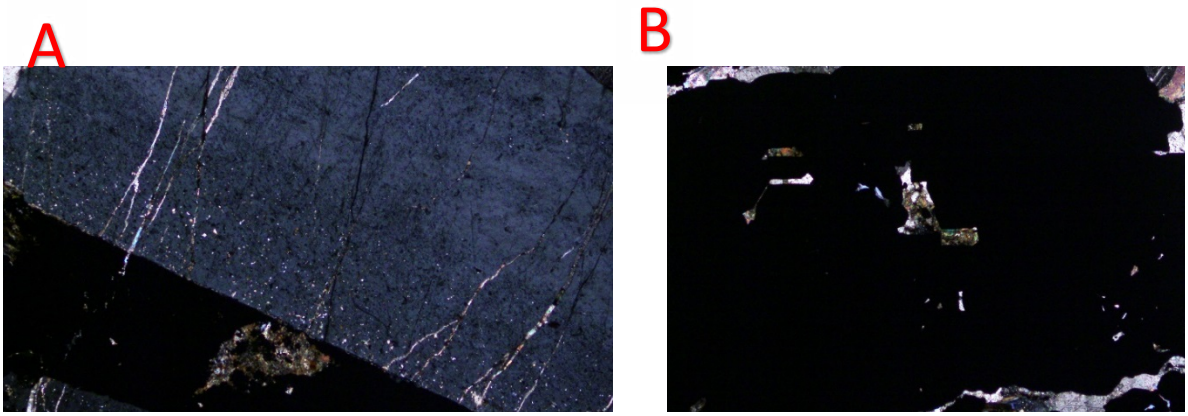

Figure B.10: A: Corse gained apatite with adjacent sulphide grains. B: Sulphide grain with biotite inclusions.

11. APPENDIX C – SPOT ABLATION DISTRIBUTION

Figure C.1: Thin section samples analysed during LA-ICP-MS studies with red boxes highlighting locations of apatite grains where ablation spots were taken. A: Sample MSZ-2. B: Sample MSZ-3.1. C: Sample MSZ-4. D: Sample MSZ-5.2. E: Sample MSZ-6. F: EMMD026-221.3 (E1-N).

MSZ-2	
Section	**Description**
1	7 spots taken from grain boundary to boundary in a single linear line across the centre of a single grain. 3 spots had potential contamination with a neighbouring mineral. 2 spots had potential contamination with a neighbouring mineral.
2	8 spots taken from grain boundary to boundary in a single linear line across the centre of three co-genetic grains. No spots had potential contamination with a neighbouring mineral.
3	17 spots taken from grain boundary to boundary in two linear lines across the centre and bottom of a single grain. 5 spots had potential contamination with a neighbouring mineral.
4	5 spots taken from grain boundary to boundary in a linear fashion over a single grain. 3 spots had potential contamination with a neighbouring mineral. 2 spots had potential contamination with a neighbouring mineral.
5	17 spots taken from grain boundary to boundary in a single linear line across the centre of three co-genetic grains. 5 spots had potential contamination with a neighbouring mineral.
6	17 spots taken from grain boundary to boundary in a single linear line across the centre of three co-genetic grains. 6 spots had potential contamination with a neighbouring mineral.
MSZ-3.1	
1	27 spots taken across 15 co-genetic grains that show a high reflectance core and a low reflectance rim. 13 spots were taken from the core and 14 from the rim. Hard to estimate potential contamination with a neighbouring mineral or zone due to size of rims and cores.
2	14 spots taken from grain boundary to boundary in a single linear line across the centre of three co-genetic grains. 1 spot had potential contamination with a neighbouring mineral.
3	11 spots taken across 8 co-genetic grains that show a high reflectance core and a low reflectance rim. 5 spots were taken from the core and 6 from the rim. Hard to estimate potential contamination with a neighbouring mineral or zone due to size of rims and cores.
4	4 spots taken from grain boundary to boundary in a single linear line across the centre of a single grain. 3 spots had potential contamination with a neighbouring mineral.
5	22 spots taken from grain boundary to boundary in a single linear line across the centre of a single grains. 4 spots had potential contamination with a neighbouring mineral.
MSZ-4	
Section	**Description**
1	24 spots taken across 16 co-genetic grains that show a high reflectance core and a low reflectance rim. 18 spots were taken from the core and 6 from the rim. Hard to estimate potential contamination with a neighbouring mineral or zone due to size of rims and cores.
2	26 spots taken across 13 grains. 9 spots over two grains were sampled boundary to boundary in a linear fashion and the remaining were sampled in the high reflective core or low reflective rim. 12 spots were taken from the core and 5 from the rim. Hard to estimate potential contamination with a neighbouring mineral or zone due to size of rims and cores.
3	13 spots taken from grain boundary to boundary in a single linear line across the centre of a single grain. No spots had potential contamination with a neighbouring mineral.
4	18 spots taken from grain boundary to boundary in a single linear line across the centre of a single grain. 1 spot had potential contamination with a neighbouring mineral.

MSZ-5.2	
Section	**Description**
1	16 spots taken across 7 grains. 7 spots over two grains were sampled boundary to centre in a linear fashion and the remaining were sampled in the high reflective core or low reflective rim. 5 spots were taken from the core and 4 from the rim. Hard to estimate potential contamination with a neighbouring mineral or zone due to size of rims and cores.
2	15 spots taken across 8 grains. 6 spots over two grains were sampled boundary to centre in a linear fashion and the remaining were sampled in the high reflective core or low reflective rim. 6 spots were taken from the core and 3 from the rim. Hard to estimate potential contamination with a neighbouring mineral or zone due to size of rims and cores.
3	12 spots taken across 8 co-genetic grains that show a high reflectance core and a low reflectance rim. 10 spots were taken from the core and 2 from the rim. Hard to estimate potential contamination with a neighbouring mineral or zone due to size of rims and cores.
MSZ-6	
Section	**Description**
1	4 spots taken from grain boundary to boundary in a single linear line across the centre of a single grain. No spots had potential contamination with a neighbouring mineral.
2	8 spots taken from grain boundary to boundary in a single linear line across the centre of a single grain. No spots had potential contamination with a neighbouring mineral.
3	5 spots taken from grain boundary to boundary in a single linear line across the centre of a single grain. 2 spots had potential contamination with a neighbouring mineral.
4	5 spots taken from grain boundary to boundary in a single linear line across the centre of a single grain. 1 spot had potential contamination with a neighbouring mineral.
5	11 spots taken from grain boundary to boundary in a single linear line across the centre of a single grain. No spots had potential contamination with a neighbouring mineral.
6	5 spots taken from grain boundary to boundary in a single linear line across the centre of a single grain. 1 spot had potential contamination with a neighbouring mineral.
7	12 spots taken from grain boundary to boundary in a single linear line across the centre of a single grain. No spots had potential contamination with a neighbouring mineral.
8	12 spots taken from grain boundary to boundary in a single linear line across the centre of a single grain. No spots had potential contamination with a neighbouring mineral.
EMMD026 (E1-N)	
Section	**Description**
1	10 spots taken from grain boundary to boundary in two linear lines across the top and bottom of a single grain. 4 spots had potential contamination with a neighbouring mineral.
2	9 spots taken from grain boundary to boundary in two linear lines across the top and bottom of a single grain. No spots had potential contamination with a neighbouring mineral.
3	19 spots taken from grain boundary to boundary in four linear lines across the top (x2) and bottom (x2) of a single grain. 2 spots had potential contamination with a neighbouring mineral.
4	12 spots taken across a single grain that shows a high reflectance core and a low reflectance rim. 7 spots were taken from the core and 5 from the rim. 6 spots had potential contamination with a neighbouring mineral.
5	8 spots taken from grain boundary to boundary in a single linear line across the centre of a single grain. 2 spots had potential contamination with a neighbouring mineral.
6	10 spots taken from grain boundary to boundary in a single linear line across the centre of a single grain. 1 spot had potential contamination with a neighbouring mineral.

12. APPENDIX D – ADDITIONAL TERA-WASSERBURG PLOTS

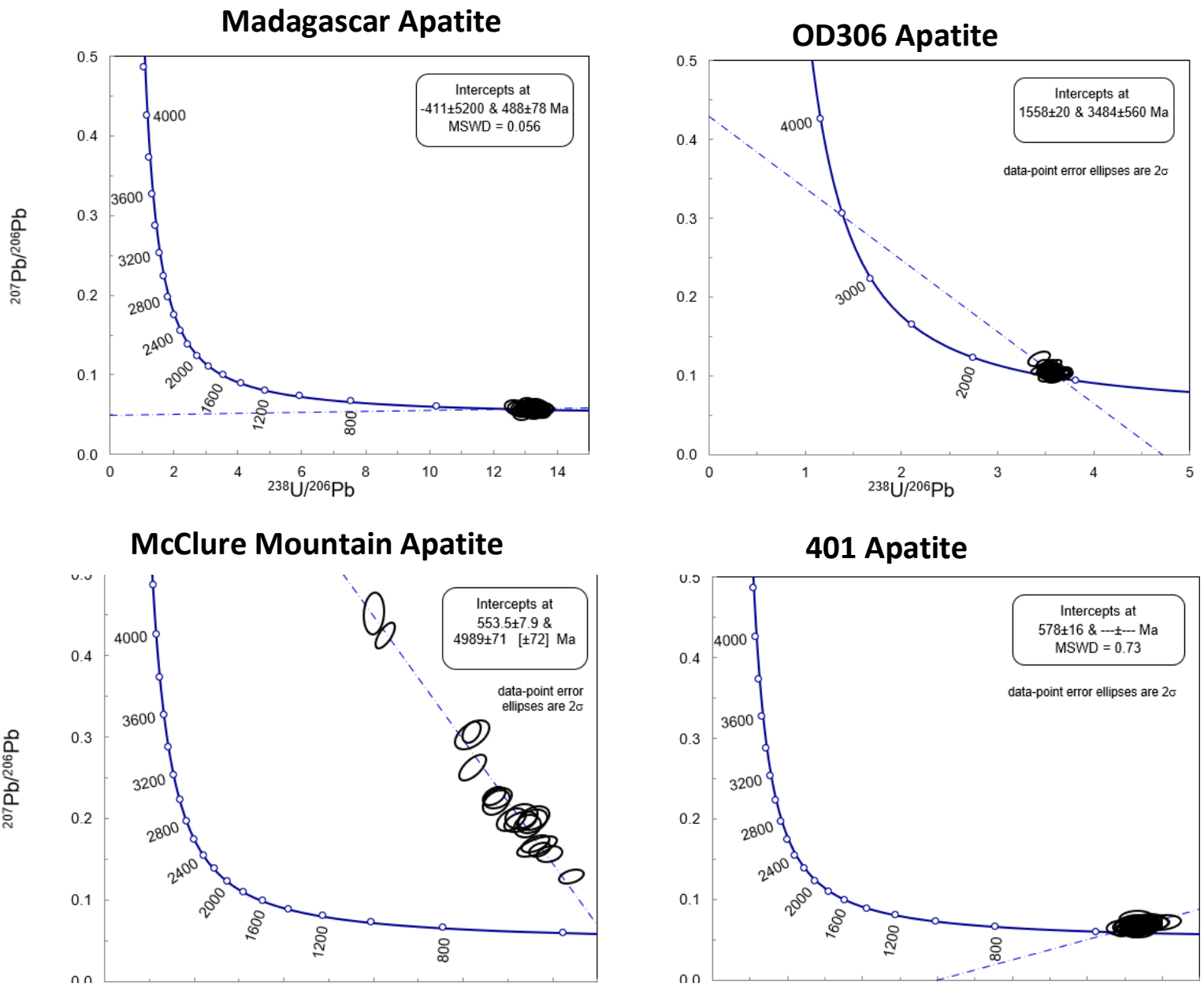

Figure D.1: Tera-Wasserburg plot ages for standards using Madagascar apatite as a primary standard. TW Concordia plot for A) Madagascar apatite primary standard. B) OD306 apatite secondary standard. C) McClure Mountain apatite secondary standard. D) 401 Apatite secondary standard. The 'n' value indicated the number of samples. The ellipses represent the 2σ error range for the $^{238}U/^{206}Pb$ and $^{207}Pb/^{206}Pb$ values of each data point. Black ellipses signify the sample points utilised in the creation of the common lead line.

MSZ-3.1 WG

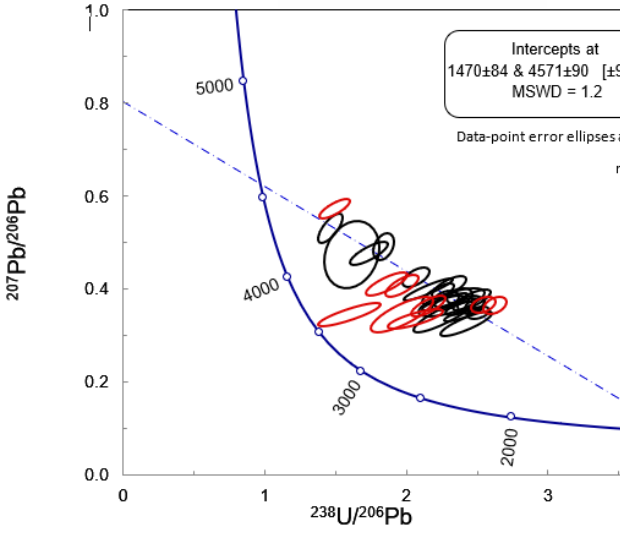

MSZ-3.1 Core

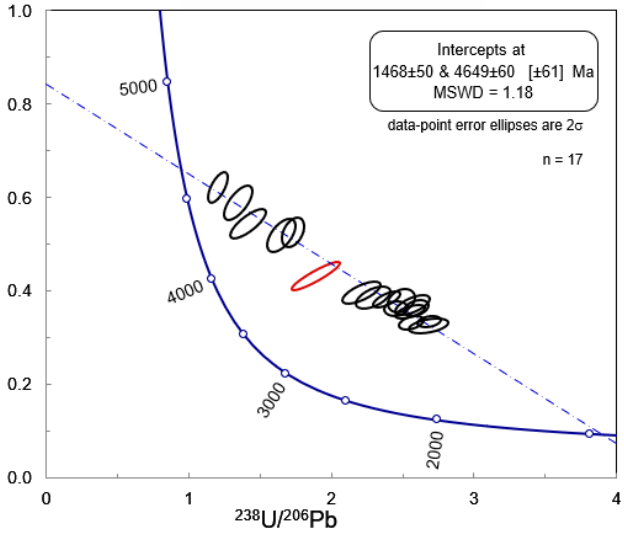

MSZ-3.1 Rim

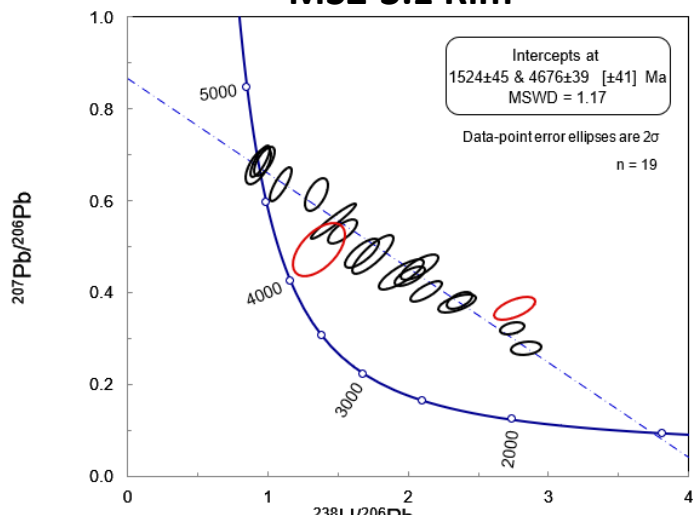

MSZ-4 WG

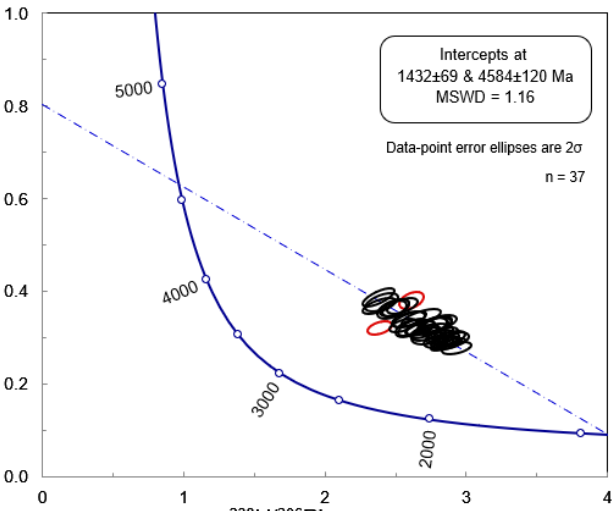

MSZ-4 Core

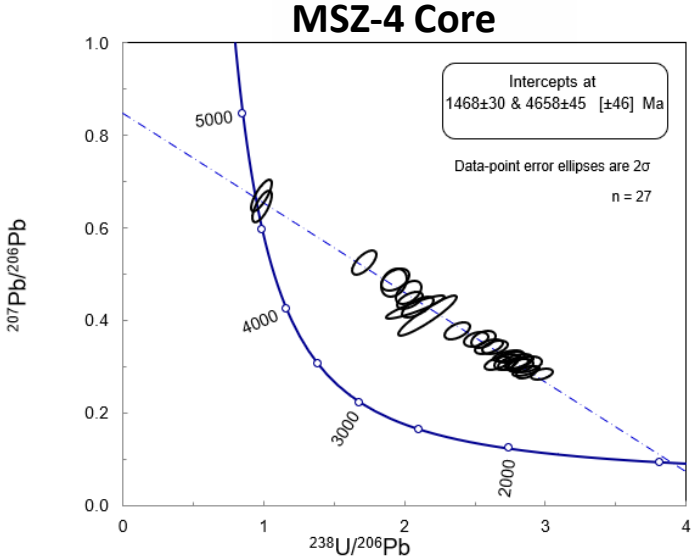

MSZ-4 Rim

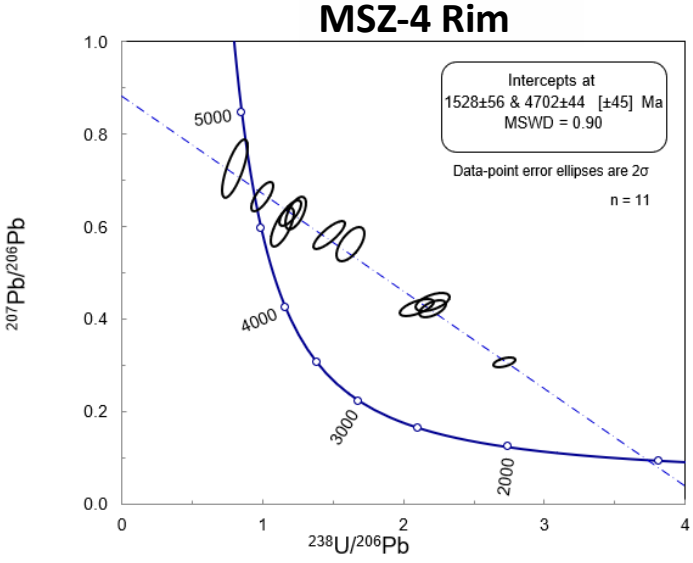

MSZ-5.2 WG

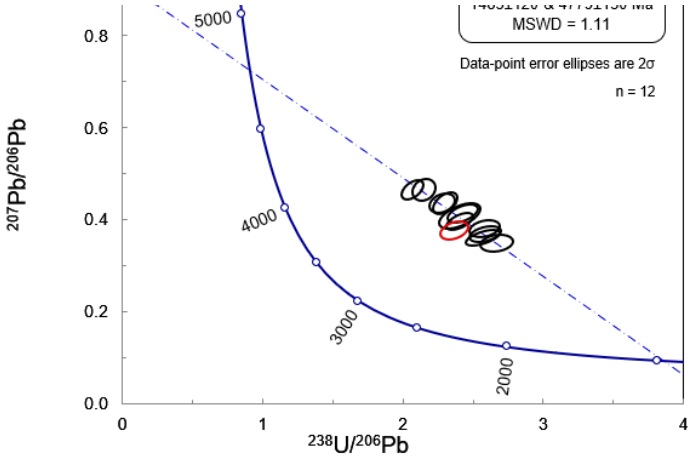

MSZ-5.2 Core

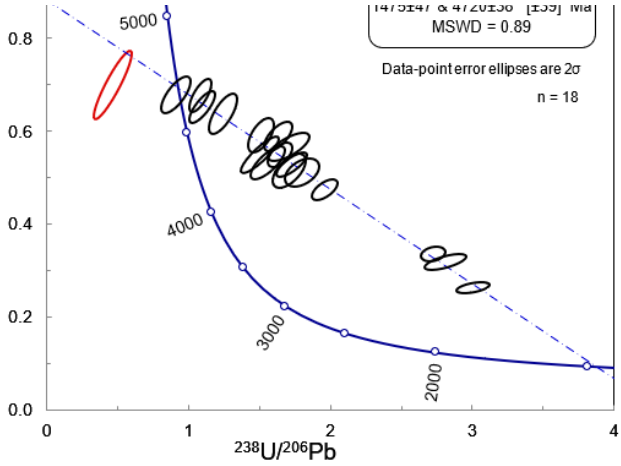

MSZ-5.2 Rim

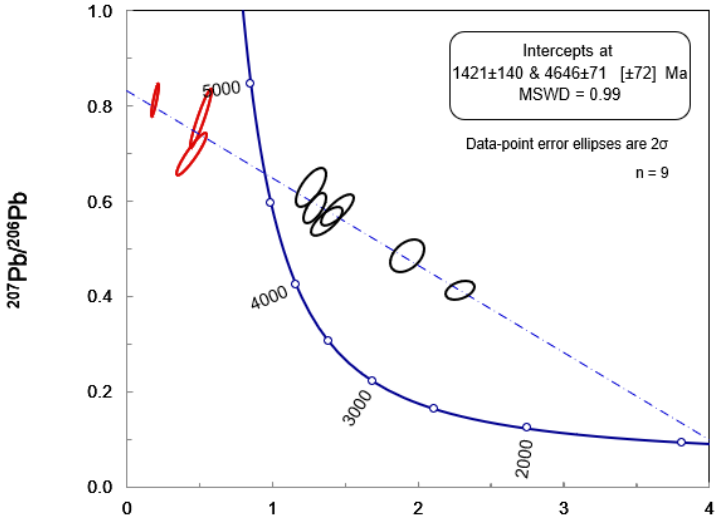

E1-N WG

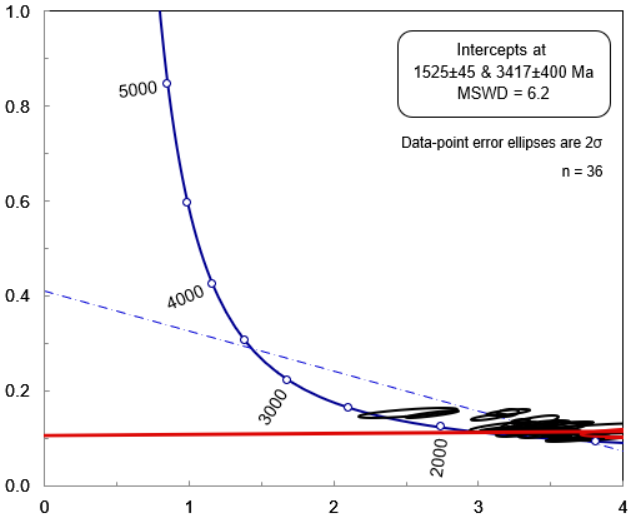

E1-N Core

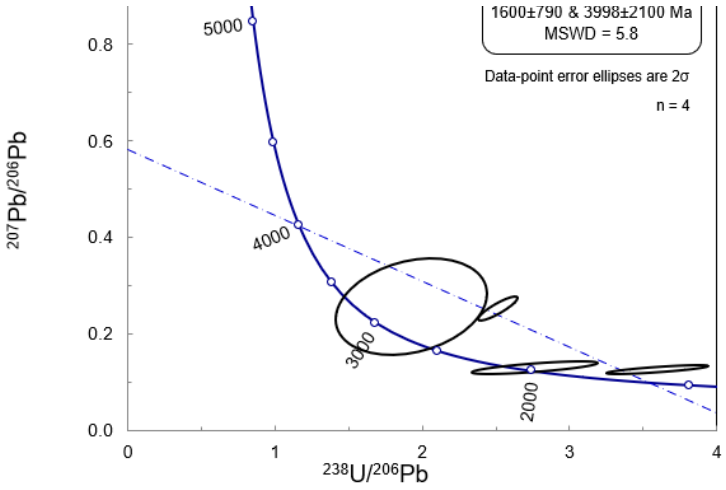

E1-N Rim

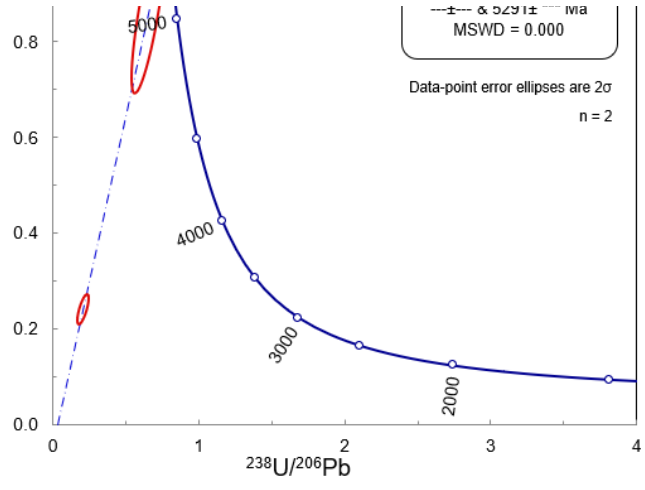

Figure D.2: Tera-Wasserburg plots for the MSZ and E1-N samples with data from cores, rims and entire grains within fine and coarse-grained apatite. Samples were combined to form a single Tera-Wasserburg plot as the uncertainty in ages overlapped and could therefore be considered as co-co-genetic. The 'n' value indicated the number of samples. The ellipses represent the 2σ error range for the $^{238}U/^{206}Pb$ and $^{207}Pb/^{206}Pb$ values of each data point. Black ellipses signify the sample points utilised in the creation of the common lead line whereas the red ellipses signify the sample points considered as outliers and were removed from further investigation. The lower intercept of the common lead line represents the point in which the apatite grains ceased common lead diffusion a ~350-550°C (Chew et al., 2015). Sample E1-N rim did not generate a sufficient number of suitable data points and was thus not included in further calculations.

13. APPENDIX E – GEOCHRONOLOGY DATA

MSZ-2							
Sample spot	Final U238/Pb 206	Final U238/Pb206 2σ	Final Pb207/Pb 206	Final Pb207/Pb206 2σ	Final Pb207 Age (Ma)	Final Pb 207 Age 2σ (Ma)	U238/Pb206 vs. Pb207/Pb206 Error Correlation
MSZ2- 44-45 - 1	2.590674	0.071	0.35	0.012	1501	62	0.34032
MSZ2- 44-45 - 2	2.572016	0.06	0.36	0.014	1481	57	0.23425
MSZ2- 44-45 - 3	2.666667	0.086	0.36	0.015	1441	71	0.34827
MSZ2- 44-45 - 4	2.55102	0.074	0.36	0.012	1503	61	0.33793
MSZ2- 44-45 - 5	2.604167	0.078	0.35	0.013	1504	70	0.20721
MSZ2- 44-45 - 6	2.65252	0.08	0.342	0.013	1492	57	0.40526
MSZ2- 44-45 - 7	2.610966	0.09	0.344	0.013	1504	68	0.61492
MSZ2- 44-45 - 8	2.710027	0.076	0.322	0.012	1514	64	0.26157
MSZ2- 44-45 - 9	2.898551	0.072	0.294	0.011	1494	51	0.31802
MSZ2- 44-45 - 10	2.853067	0.077	0.309	0.01	1474	51	0.21716
MSZ2- 44-45 - 11	2.857143	0.11	0.303	0.015	1487	72	0.42564
MSZ2- 44-45 - 12	2.762431	0.08	0.3111	0.0095	1511	55	0.477
MSZ2- 44-45 - 13	2.868617	0.075	0.2759	0.0085	1545	50	0.30825
MSZ2- 44-45 - 14	2.666667	0.074	0.348	0.016	1478	59	0.39488
MSZ2- 44-45 - 15	2.84576	0.082	0.327	0.013	1444	58	0.5435
MSZ2- 44-45 - 16	2.597403	0.15	0.358	0.022	1480	100	0.66391
MSZ2- 40-41 - 1	2.590674	0.086	0.347	0.013	1519	69	0.44897
MSZ2- 40-41 - 2	2.680965	0.078	0.333	0.013	1516	63	0.34054
MSZ2- 40-41 - 5	2.702703	0.072	0.343	0.014	1470	66	0.31767
MSZ2- 40-41 - 6	2.48139	0.066	0.367	0.013	1528	63	0.48969
MSZ2- 40-41 - 7*	2.427184	0.099	0.322	0.017	1690	100	0.34585
MSZ2- 40-41 - 8	2.65252	0.073	0.334	0.012	1515	57	0.44721
MSZ2- 40-41 - 9	1.550388	0.087	0.57	0.028	1500	180	0.71869
MSZ2- 40-41 - 10	2.469136	0.085	0.361	0.015	1555	77	0.36224
MSZ2- 40-41 - 11	2.659574	0.085	0.36	0.014	1435	63	0.33471
MSZ2- 40-41 - 12	2.624672	0.084	0.361	0.013	1460	61	0.49769
MSZ2- 40-41 - 13	2.604167	0.088	0.347	0.014	1515	71	0.36249
MSZ2- 40-41 - 14	2.905288	0.074	0.2871	0.009	1491	47	0.29244
MSZ2- 40-41 - 15	2.822467	0.077	0.317	0.01	1464	52	0.29585
MSZ2- 40-41 - 16	2.759382	0.069	0.3087	0.009	1516	50	0.46635
MSZ2- 40-41 - 17	2.873563	0.089	0.2947	0.0079	1498	52	0.45011
MSZ2- 38-39 - 1	2.570694	0.1	0.344	0.015	1530	66	0.50179

MSZ2- 38-39 - 2	2.506266	0.089	0.366	0.013	1519	74	0.54396
MSZ2- 38-39 - 3	2.463054	0.074	0.382	0.014	1495	65	0.51526
MSZ2- 38-39 - 4.d	2.589332	0.064	0.337	0.012	1559	65	0.30234
MSZ2- 38-39 - 5*	2.364066	0.093	0.352	0.014	1631	88	0.19513
MSZ2- 7-8 - 1	2.570694	0.11	0.343	0.013	1543	76	0.54289
MSZ2- 7-8 - 2	2.688172	0.07	0.334	0.012	1491	61	0.12631
MSZ2- 7-8 - 4	2.65252	0.075	0.33	0.013	1520	65	0.29785
MSZ2- 7-8 - 5	2.583979	0.13	0.358	0.014	1471	81	0.52241
MSZ2- 7-8 - 6	2.741228	0.06	0.321	0.013	1499	47	0.37763
MSZ2- 7-8 - 7	2.695418	0.076	0.3311	0.0097	1502	57	0.53666
MSZ2- 7-8 - 8	2.673797	0.078	0.335	0.013	1503	62	0.28862
MSZ2- 7-8 - 9	2.583979	0.084	0.38	0.017	1430	67	0.46725
MSZ2- 7-8 - 10	2.506266	0.082	0.361	0.015	1520	75	0.43736
MSZ2- 7-8 - 11	2.688172	0.064	0.361	0.014	1421	52	0.073358
MSZ2- 7-8 - 12	2.673797	0.087	0.337	0.013	1497	61	0.48948
MSZ2- 7-8 - 13	2.717391	0.081	0.309	0.011	1546	60	0.3508
MSZ2- 7-8 - 14	2.747253	0.095	0.301	0.011	1560	65	0.46595
MSZ2- 7-8 - 15	2.688172	0.08	0.329	0.012	1513	63	0.2317
MSZ2- 7-8 - 16	2.717391	0.082	0.322	0.011	1512	58	0.42532
MSZ2- 46-47- 1	2.820874	0.065	0.306	0.011	1495	51	0.32813
MSZ2- 46-47 - 3	2.57732	0.074	0.334	0.012	1560	61	0.50118
MSZ2- 46-47 - 4	2.736727	0.063	0.33	0.013	1482	53	0.3392
MSZ2- 46-47 - 5	2.604167	0.081	0.343	0.012	1520	64	0.48306
MSZ2- 46-47 - 6	2.73224	0.08	0.33	0.013	1484	52	0.54016
MSZ2- 50-51 - 1	2.785515	0.079	0.316	0.012	1494	61	0.19641
MSZ2- 50-51 - 2	2.557545	0.077	0.36	0.012	1494	64	0.50848
MSZ2- 50-51 - 3	2.820874	0.07	0.306	0.012	1497	53	0.27642
MSZ2- 50-51 - 4	2.617801	0.089	0.34	0.014	1523	68	0.18366
MSZ2- 50-51 - 5*	2.380952	0.089	0.364	0.014	1595	72	0.63709
MSZ2- 50-51 - 6	2.564103	0.081	0.343	0.014	1546	51	0.76927
MSZ2- 50-51 - 7	2.770083	0.097	0.322	0.013	1488	69	0.36752
MSZ2- 50-51 - 8	2.57732	0.086	0.351	0.012	1509	60	0.50342
MSZ-3.1 WG (Unzoned Grains)							
Sample spot	Final U238/Pb 206	Final U238/Pb206 2σ	Final Pb207/Pb 206	Final Pb207/Pb206 2σ	Final Pb207 Age (Ma)	Final Pb 207 Age 2σ (Ma)	U238/Pb206 vs. Pb207/Pb206 Error Correlation
MSZ3.1- 93-97 - 3	2.222222	0.092	0.391	0.018	1496	83	0.76985

MSZ3.1- 93-97 - 4*	2.155172	0.1	0.364	0.019	1661	91	0.75085
MSZ3.1- 93-97 - 5*	1.612903	0.16	0.474	0.059	1680	340	0.20066
MSZ3.1- 93-97 - 6	2.463054	0.11	0.377	0.019	1408	75	0.74197
MSZ3.1- 93-97 - 9	2.392344	0.1	0.345	0.012	1585	80	0.84115
MSZ3.1- 93-97 - 10	2.272727	0.13	0.374	0.015	1513	94	0.87772
MSZ3.1- 93-97 - 11*	2.061856	0.16	0.337	0.017	1830	150	0.784
MSZ3.1- 93-97 - 12*	1.964637	0.18	0.346	0.031	1770	150	0.77804
MSZ3.1- 93-97 - 14	2.304147	0.099	0.405	0.019	1421	84	0.70159
MSZ3.1- 93-97 - 15*	2.421308	0.15	0.325	0.022	1590	70	0.84571
MSZ3.1- 93-97 - 18	2.066116	0.077	0.425	0.017	1513	91	0.58644
MSZ3.1- 93-97 - 19	2.155172	0.14	0.399	0.019	1488	88	0.91171
MSZ3.1- 93-97 - 20*	1.862197	0.12	0.411	0.02	1650	160	0.79197
MSZ3.1- 93-97 - 21	1.736111	0.11	0.477	0.02	1530	130	0.79236
MSZ3.1- 93-97 - 22*	1.464129	0.068	0.531	0.025	1570	160	0.72031
MSZ3.1- 99-102 - 1	2.277904	0.076	0.379	0.015	1495	82	0.33151
MSZ3.1- 99-102 - 2	2.457002	0.076	0.366	0.016	1479	83	0.16383
MSZ3.1- 99-102 - 4	2.485089	0.057	0.367	0.012	1452	57	0.53401
MSZ3.1- 99-102 - 6	1.838235	0.062	0.491	0.024	1440	130	0.35018
MSZ3.1- 99-102 - 7	2.375297	0.074	0.385	0.014	1454	72	0.30802
MSZ3.1- 99-102 - 8	2.506266	0.065	0.349	0.011	1487	61	0.40607
MSZ3.1- 99-102 - 9	2.298851	0.094	0.37	0.013	1535	81	0.64432
MSZ3.1- 99-102 - 10	2.625361	0.065	0.365	0.015	1371	57	0.40508
MSZ3.1- 99-102 - 13	2.314815	0.19	0.372	0.025	1480	150	0.6845
MSZ3.1- 99-102 - 14	2.544529	0.071	0.367	0.014	1412	70	0.39707
MSZ3.1- 103-106 - 1*	2.380952	0.085	0.359	0.012	1516	78	0.66347
MSZ3.1- 103-106 - 2*	2.267574	0.18	0.345	0.03	1580	120	0.8688
MSZ3.1- 103-106 - 3*	1.972387	0.095	0.408	0.019	1617	99	0.72027
MSZ3.1- 103-106 - 4	1.494768	0.089	0.573	0.018	1310	120	0.78024
MSZ3.1- 103-106 - 5*	1.6	0.18	0.345	0.021	2050	160	0.86047

MSZ-3.1 Core

Sample spot	Final U238/Pb 206	Final U238/Pb206 2σ	Final Pb207/Pb 206	Final Pb207/Pb206 2σ	Final Pb207 Age (Ma)	Final Pb 207 Age 2σ (Ma)	U238/Pb206 vs. Pb207/Pb206 Error Correlation
MSZ3.1- 23-24_core - 1	2.597403	0.071	0.364	0.014	1419	66	0.34261
MSZ3.1- 23-24_core - 2	2.55102	0.087	0.355	0.012	1480	64	0.59055
MSZ3.1- 23-24_core - 4	2.293578	0.1	0.387	0.019	1530	100	0.55052

MSZ3.1- 23-24_core -5	2.686728	0.069	0.335	0.01	1451	52	0.30398
MSZ3.1- 23-24_core -6	2.45098	0.069	0.363	0.013	1507	72	0.089672
MSZ3.1- 23-24_core -7	2.570694	0.097	0.37	0.017	1410	71	0.626
MSZ3.1- 23-24_core -8	2.559509	0.068	0.332	0.011	1532	63	0.38949
MSZ3.1- 23-24_core -9	2.493766	0.078	0.379	0.021	1434	86	0.26852
MSZ3.1- 23-24_core -10	2.386635	0.077	0.382	0.013	1480	64	0.66974
MSZ3.1- 23-24_core -11	1.414427	0.1	0.544	0.026	1600	200	0.78222
MSZ3.1- 23-24_core -12	2.212389	0.11	0.397	0.02	1550	100	0.69553
MSZ3.1- 23-24_core -13	2.680965	0.11	0.326	0.013	1493	77	0.43455
MSZ3.1- 17-18_core -1*	1.890359	0.14	0.433	0.025	1583	93	0.91053
MSZ3.1- 17-18_core -2	1.344086	0.08	0.59	0.03	1310	160	0.67648
MSZ3.1- 17-18_core -3	1.204819	0.056	0.622	0.027	1440	200	0.6551
MSZ3.1- 17-18_core -4	1.647446	0.082	0.518	0.029	1530	170	0.57952
MSZ3.1- 17-18_core -5	1.730104	0.065	0.526	0.026	1410	140	0.4022
MSZ-3.1 Rim							
Sample spot	Final U238/Pb 206	Final U238/Pb206 2σ	Final Pb207/Pb 206	Final Pb207/Pb206 2σ	Final Pb207 Age (Ma)	Final Pb 207 Age 2σ (Ma)	U238/Pb206 vs. Pb207/Pb206 Error Correlation
MSZ3.1- 23-24_rim -1	2.347418	0.11	0.377	0.016	1531	91	0.61649
MSZ3.1- 23-24_rim -2	0.933706	0.076	0.676	0.032	1360	240	0.6389
MSZ3.1- 23-24_rim -3	2.364066	0.075	0.383	0.015	1511	64	0.55241
MSZ3.1- 23-24_rim -4	1.953125	0.13	0.44	0.026	1670	170	0.80381
MSZ3.1- 23-24_rim -5	1.531394	0.085	0.533	0.022	1570	130	0.71649
MSZ3.1- 23-24_rim -6	2.742732	0.068	0.323	0.011	1472	54	0.3823
MSZ3.1- 23-24_rim -7	2.840909	0.089	0.279	0.012	1527	61	0.22204
MSZ3.1- 23-24_rim -8*	2.762431	0.12	0.367	0.02	1346	84	0.59997
MSZ3.1- 23-24_rim -9	0.974658	0.058	0.687	0.026	1280	240	0.66752
MSZ3.1- 23-24_rim -10	0.946073	0.059	0.687	0.028	1430	250	0.79144
MSZ3.1- 23-24_rim -11	1.672241	0.099	0.486	0.026	1660	170	0.7566
MSZ3.1- 23-24_rim -12	1.748252	0.12	0.483	0.034	1610	170	0.83135
MSZ3.1- 23-24_rim -13	1.345895	0.068	0.615	0.029	1390	170	0.57097
MSZ3.1- 23-24_rim -14	2.079002	0.11	0.456	0.023	1460	120	0.74626
MSZ3.1- 17-18_rim -1	1.089325	0.064	0.637	0.03	1470	220	0.80961

MSZ3.1- 17-18_rim -2	2.12766	0.089	0.403	0.019	1606	92	0.76886
MSZ3.1- 17-18_rim -3	1.466276	0.13	0.556	0.032	1500	140	0.95785
MSZ3.1- 17-18_rim -4*	1.36612	0.15	0.495	0.047	1680	290	0.55427
MSZ3.1- 17-18_rim -6	2.012072	0.091	0.436	0.017	1590	110	0.67185
MSZ-4 WG (Unzoned Grains)							
Sample spot	Final U238/Pb 206	Final U238/Pb206 2σ	Final Pb207/Pb 206	Final Pb207/Pb206 2σ	Final Pb207 Age (Ma)	Final Pb 207 Age 2σ (Ma)	U238/Pb206 vs. Pb207/Pb206 Error Correlation
MSZ4- 144-149(2) - 1	2.55102	0.08	0.326	0.012	1507	65	0.55293
MSZ4- 144-149(2) - 2	2.873563	0.1	0.286	0.011	1439	56	0.74212
MSZ4- 144-149(2) - 4	2.812148	0.076	0.299	0.011	1452	58	0.27194
MSZ4- 144-149(2) - 5	2.380952	0.09	0.387	0.016	1414	73	0.71861
MSZ4- 144-149(2) - 6	2.86123	0.079	0.292	0.01	1447	59	0.29379
MSZ4- 144-149(2) - 7	2.780868	0.076	0.329	0.013	1382	62	0.30594
MSZ4- 144-149(2) - 8	2.673797	0.08	0.322	0.012	1440	58	0.60789
MSZ4- 144-149(2) - 9	2.80112	0.085	0.291	0.011	1473	66	0.25135
MSZ4- 144-149(2) - 10	2.770083	0.074	0.329	0.013	1384	57	0.39009
MSZ4- 144-149(2) - 11	2.832861	0.088	0.31	0.011	1410	63	0.5002
MSZ4- 144-149(2) - 13	2.73224	0.1	0.305	0.015	1476	77	0.36817
MSZ4- 144-149(2) -14*	2.610966	0.073	0.382	0.015	1311	67	0.42824
MSZ4- 144-149(2) - 15	2.487562	0.085	0.365	0.014	1420	80	0.48182
MSZ4- 144-149(2) - 16	2.5	0.075	0.365	0.015	1417	67	0.54925
MSZ4- 144-149(2) - 17	2.544529	0.088	0.37	0.014	1383	75	0.55808
MSZ4- 150-153 - 1	2.380952	0.095	0.368	0.014	1485	92	0.64186
MSZ4- 150-153 - 2	2.475248	0.083	0.36	0.016	1469	87	0.4763
MSZ4- 150-153 - 3	2.680965	0.11	0.344	0.015	1386	86	0.66279
MSZ4- 150-153 - 4	2.777778	0.1	0.326	0.016	1388	67	0.62835
MSZ4- 150-153 - 5	2.590674	0.098	0.339	0.014	1453	83	0.50789
MSZ4- 150-153 - 6	2.398082	0.096	0.376	0.016	1443	82	0.5564
MSZ4- 150-153 - 7	2.617801	0.079	0.322	0.015	1484	67	0.63921
MSZ4- 150-153 - 8	2.80112	0.088	0.316	0.013	1391	59	0.19362
MSZ4- 150-153 - 9	2.813731	0.076	0.305	0.011	1433	59	0.41811
MSZ4- 150-153 - 10	2.793296	0.082	0.328	0.012	1379	64	0.39636
MSZ4- 150-153 - 11	2.930832	0.073	0.298	0.011	1394	53	0.35812
MSZ4- 150-153 - 12	2.673797	0.084	0.321	0.014	1472	75	0.53704
MSZ4- 150-153 - 13	2.702703	0.084	0.313	0.012	1452	51	0.66008
MSZ4- 46 - 1	2.854696	0.076	0.298	0.011	1426	48	0.43009

MSZ4- 46 - 2	2.590674	0.072	0.321	0.015	1483	57	0.46148
MSZ4- 46 - 3*	2.386635	0.069	0.322	0.012	1626	59	0.45045
MSZ4- 46 - 4	2.597403	0.094	0.341	0.014	1450	74	0.65072
MSZ4- 46 - 5	2.793296	0.11	0.332	0.015	1363	73	0.58149
MSZ4- 46 - 6	2.857143	0.087	0.288	0.011	1454	62	0.36951
MSZ4- 46 - 7	2.891845	0.08	0.301	0.012	1412	56	0.50028
MSZ4- 46 - 8	2.932551	0.087	0.278	0.011	1444	53	0.48861
MSZ4- 46 - 9	2.710027	0.08	0.312	0.014	1466	65	0.4825
MSZ-4 Core							
Sample spot	Final U238/Pb 206	Final U238/Pb206 2σ	Final Pb207/Pb 206	Final Pb207/Pb206 2σ	Final Pb207 Age (Ma)	Final Pb 207 Age 2σ (Ma)	U238/Pb206 vs. Pb207/Pb206 Error Correlation
MSZ4- 49 _core - 1	2.557545	0.07	0.36	0.015	1469	65	0.38107
MSZ4- 49 _core - 2	2.754821	0.079	0.321	0.01	1471	58	0.46747
MSZ4- 49 _core - 4	2.375297	0.073	0.379	0.015	1516	65	0.52044
MSZ4- 49 _core - 5	2.506266	0.071	0.36	0.013	1489	71	0.35118
MSZ4- 49 _core - 6	2.727769	0.071	0.31	0.014	1511	58	0.44774
MSZ4- 49 _core - 7	1.926782	0.076	0.483	0.025	1490	130	0.26269
MSZ4- 49 _core - 9	2.096436	0.091	0.429	0.018	1545	96	0.65678
MSZ4- 49 _core - 10	1.712329	0.072	0.525	0.021	1460	110	0.66268
MSZ4- 49 _core - 11	1.937984	0.081	0.489	0.02	1450	110	0.42987
MSZ4- 49 _core - 12	2.028398	0.077	0.461	0.021	1480	100	0.4621
MSZ4- 49 _core - 14	0.9871668	0.055	0.647	0.027	1520	220	0.70934
MSZ4- 49 _core - 15	2.164502	0.17	0.411	0.035	1520	100	0.92486
MSZ4- 49 _core - 16	2.73224	0.084	0.3241	0.0098	1470	55	0.56185
MSZ4- 49 _core - 17	2.973536	0.064	0.284	0.01	1450	43	0.42021
MSZ4- 49 _core - 18	2.03666	0.074	0.444	0.016	1538	91	0.55746
MSZ4- 46_core - 1	0.982318	0.062	0.671	0.028	1370	230	0.77586
MSZ4- 46_core - 2	2.074689	0.17	0.43	0.02	1500	110	0.90116
MSZ4- 46_core - 3	2.645503	0.074	0.343	0.012	1453	56	0.39821
MSZ4- 46_core - 4	2.826456	0.075	0.31	0.011	1448	46	0.62683
MSZ4- 46_core - 5	2.822467	0.072	0.303	0.011	1474	59	0.33827
MSZ4- 46_core - 6	2.659574	0.073	0.309	0.012	1561	58	0.5526
MSZ4- 46_core - 7	2.874389	0.084	0.307	0.014	1455	64	0.36373
MSZ4- 46_core - 8	2.597403	0.083	0.343	0.013	1491	62	0.49689
MSZ4- 46_core - 9	2.785515	0.1	0.311	0.013	1476	70	0.55957
MSZ4- 46_core - 10	2.867795	0.062	0.288	0.011	1493	47	0.48047

MSZ4- 46_core - 11	2.860412	0.078	0.2911	0.0092	1489	49	0.64126
MSZ4- 46_core - 12	2.795639	0.068	0.307	0.011	1491	54	0.41144
MSZ4- 49 _core - 1	2.557545	0.07	0.36	0.015	1469	65	0.38107
MSZ4- 49 _core - 2	2.754821	0.079	0.321	0.01	1471	58	0.46747
MSZ4- 49 _core - 4	2.375297	0.073	0.379	0.015	1516	65	0.52044
MSZ4- 49 _core - 5	2.506266	0.071	0.36	0.013	1489	71	0.35118
MSZ4- 49 _core - 6	2.727769	0.071	0.31	0.014	1511	58	0.44774
MSZ4- 49 _core - 7	1.926782	0.076	0.483	0.025	1490	130	0.26269
MSZ4- 49 _core - 9	2.096436	0.091	0.429	0.018	1545	96	0.65678
MSZ4- 49 _core - 10	1.712329	0.072	0.525	0.021	1460	110	0.66268
MSZ4- 49 _core - 11	1.937984	0.081	0.489	0.02	1450	110	0.42987
MSZ4- 49 _core - 12	2.028398	0.077	0.461	0.021	1480	100	0.4621
MSZ4- 49 _core - 14	0.987166	0.055	0.647	0.027	1520	220	0.70934
MSZ4- 49 _core - 15	2.164502	0.17	0.411	0.035	1520	100	0.92486
MSZ4- 49 _core - 16	2.73224	0.084	0.3241	0.0098	1470	55	0.56185
MSZ4- 49 _core - 17	2.973536	0.064	0.284	0.01	1450	43	0.42021
MSZ4- 49 _core - 18	2.03666	0.074	0.444	0.016	1538	91	0.55746
MSZ4- 46_core - 1	0.982318	0.062	0.671	0.028	1370	230	0.77586
MSZ4- 46_core - 2	2.074689	0.17	0.43	0.02	1500	110	0.90116
MSZ4- 46_core - 3	2.645503	0.074	0.343	0.012	1453	56	0.39821
MSZ4- 46_core - 4	2.826456	0.075	0.31	0.011	1448	46	0.62683
MSZ4- 46_core - 5	2.822467	0.072	0.303	0.011	1474	59	0.33827
MSZ4- 46_core - 6	2.659574	0.073	0.309	0.012	1561	58	0.5526
MSZ4- 46_core - 7	2.874389	0.084	0.307	0.014	1455	64	0.36373
MSZ4- 46_core - 8	2.597403	0.083	0.343	0.013	1491	62	0.49689
MSZ4- 46_core - 9	2.785515	0.1	0.311	0.013	1476	70	0.55957
MSZ4- 46_core - 10	2.867795	0.062	0.288	0.011	1493	47	0.48047
MSZ4- 46_core - 11	2.860412	0.078	0.2911	0.0092	1489	49	0.64126
MSZ4- 46_core - 12	2.795639	0.068	0.307	0.011	1491	54	0.41144
MSZ-4 Rim							
Sample spot	Final U238/Pb 206	Final U238/Pb206 2σ	Final Pb207/Pb 206	Final Pb207/Pb206 2σ	Final Pb207 Age (Ma)	Final Pb 207 Age 2σ (Ma)	U238/Pb206 vs. Pb207/Pb206 Error Correlation
MSZ4- 49 _rim - 1	0.806451	0.074	0.726	0.051	1340	440	0.74835
MSZ4- 49 _rim - 2	1.623377	0.078	0.562	0.03	1480	150	0.6237
MSZ4- 49 _rim - 3	0.997009	0.065	0.666	0.026	1480	210	0.73937
MSZ4- 49 _rim - 4	2.714441	0.062	0.3069	0.0093	1546	44	0.51654

MSZ4- 49 _rim - 5	2.202643	0.078	0.424	0.015	1531	85	0.55089
MSZ4- 49 _rim - 1	1.194743	0.065	0.629	0.023	1530	170	0.71941
MSZ4- 46_rim - 1	1.140251	0.068	0.599	0.035	1790	260	0.70938
MSZ4- 46_rim - 2	2.09205	0.097	0.425	0.015	1615	98	0.63797
MSZ4- 46_rim - 3	1.237624	0.06	0.63	0.029	1500	180	0.60458
MSZ4- 46_rim - 4	2.207506	0.099	0.437	0.016	1489	95	0.54744
MSZ4- 46_rim - 5	1.472754	0.093	0.582	0.025	1550	180	0.82212
MSZ-5.2 WG (Unzoned Grains)							
Sample spot	Final U238/Pb 206	Final U238/Pb206 2σ	Final Pb207/Pb 206	Final Pb207/Pb206 2σ	Final Pb207 Age (Ma)	Final Pb 207 Age 2σ (Ma)	U238/Pb206 vs. Pb207/Pb206 Error Correlation
MSZ5.2- 72-73 - 1	2.583979	0.091	0.37	0.014	1473	72	0.40108
MSZ5.2- 72-73 - 3	2.570694	0.1	0.361	0.014	1515	84	0.61807
MSZ5.2- 72-73 - 4	2.427184	0.087	0.414	0.016	1454	75	0.51451
MSZ5.2- 72-73 - 5	2.283105	0.074	0.437	0.017	1478	84	0.29901
MSZ5.2- 72-73 - 6	2.298851	0.07	0.437	0.019	1461	79	0.50059
MSZ5.2- 68-69 - 1	2.150538	0.069	0.466	0.019	1461	95	0.19736
MSZ5.2- 68-69 - 2	2.066116	0.063	0.465	0.017	1529	73	0.50304
MSZ5.2- 68-69 - 3	2.364066	0.08	0.377	0.017	1574	73	0.37805
MSZ5.2- 68-69 - 4	2.403846	0.076	0.397	0.015	1507	60	0.58682
MSZ5.2- 68-69 - 5	2.403846	0.12	0.409	0.023	1460	110	0.56432
MSZ5.2- 68-69 - 6	2.583979	0.088	0.381	0.015	1454	75	0.28978
MSZ5.2- 68-69 - 7	2.666667	0.095	0.35	0.015	1483	71	0.21391
MSZ-5.2 Core							
Sample spot	Final U238/Pb 206	Final U238/Pb206 2σ	Final Pb207/Pb 206	Final Pb207/Pb206 2σ	Final Pb207 Age (Ma)	Final Pb 207 Age 2σ (Ma)	U238/Pb206 vs. Pb207/Pb206 Error Correlation
MSZ5.2- 66-67_core - 1	2.725538	0.071	0.336	0.012	1485	58	0.27067
MSZ5.2- 66-67_core - 2	2.808989	0.12	0.319	0.013	1468	68	0.66884
MSZ5.2- 66-67_core - 3	1.801802	0.097	0.511	0.024	1480	130	0.43417
MSZ5.2- 66-67_core - 4	1.956947	0.074	0.474	0.018	1544	94	0.62146
MSZ5.2- 66-67_core- 5*	0.467289	0.11	0.699	0.06	1020	640	0.90893
MSZ5.2- 66-67_core - 6	1.703578	0.12	0.566	0.024	1370	130	0.71043
MSZ5.2- 66-67_core - 7	1.712329	0.096	0.514	0.03	1600	150	0.5926
MSZ5.2- 66-67_core - 8	3.003905	0.096	0.264	0.01	1516	62	0.51419
MSZ5.2- 66-67_core- 10	1.560062	0.1	0.531	0.029	1640	170	0.7533

MSZ5.2- 72-73_core-1*	0.908265	0.086	0.678	0.032	1630	340	0.72493
MSZ5.2- 72-73_core - 2	1.084599	0.065	0.677	0.029	1370	200	0.72233
MSZ5.2- 72-73_core - 3	1.501502	0.11	0.55	0.032	1550	150	0.87181
MSZ5.2- 72-73_core - 4	1.508296	0.074	0.591	0.03	1410	150	0.59221
MSZ5.2- 72-73_core - 6	1.642036	0.071	0.55	0.022	1500	120	0.55244
MSZ5.2- 68-69_core - 1	1.628664	0.081	0.589	0.026	1360	140	0.65761
MSZ5.2- 68-69_core-2*	1.098901	0.075	0.653	0.028	1510	210	0.77978
MSZ5.2- 68-69_core - 3	1.240695	0.081	0.637	0.035	1460	220	0.71634
MSZ5.2- 68-69_core - 4	1.724138	0.089	0.528	0.021	1520	120	0.77658
MSZ-5.2 Rim							
Sample spot	Final U238/Pb 206	Final U238/Pb206 2σ	Final Pb207/Pb 206	Final Pb207/Pb206 2σ	Final Pb207 Age (Ma)	Final Pb 207 Age 2σ (Ma)	U238/Pb206 vs. Pb207/Pb206 Error Correlation
MSZ5.2- 66-67_rim -1	1.440922	0.093	0.582	0.026	1350	150	0.77288
MSZ5.2- 66-67_rim -2	1.261034	0.082	0.63	0.033	1290	230	0.68624
MSZ5.2- 72-73_rim -1*	1.367989	0.087	0.559	0.024	1530	170	0.72321
MSZ5.2- 72-73_rim -2*	1.290323	0.063	0.587	0.026	1510	170	0.68
MSZ5.2- 72-73_rim -3*	0.442477	0.086	0.7	0.037	1230	430	0.91652
MSZ5.2- 68-69_rim -1	1.923077	0.093	0.486	0.027	1350	120	0.41741
MSZ5.2- 68-69_rim-2*	0.194552	0.022	0.812	0.028	-200	1300	0.88259
MSZ5.2- 68-69_rim -3	2.28833	0.08	0.414	0.016	1450	95	0.38127
MSZ5.2- 68-69_rim -4*	0.510204	0.061	0.774	0.051	440	540	0.94029
MSZ-6							
Sample spot	Final U238/Pb 206	Final U238/Pb206 2σ	Final Pb207/Pb 206	Final Pb207/Pb206 2σ	Final Pb207 Age (Ma)	Final Pb 207 Age 2σ (Ma)	U238/Pb206 vs. Pb207/Pb206 Error Correlation
MSZ6- 52-54 - 1.d	2.364066	0.14	0.369	0.018	1537	97	0.80681
MSZ6- 52-54 - 2.d*	2.645503	0.71	0.248	0.027	1480	210	0.72871
MSZ6- 52-54 - 3	1.569859	0.08	0.552	0.026	1480	190	0.45241
MSZ6- 52-54 - 4	1.736111	0.081	0.499	0.022	1530	130	0.74618
MSZ6- 52-54 - 5	2.024291	0.1	0.46	0.019	1432	97	0.69789
MSZ6- 52-54 - 6	2.48139	0.13	0.353	0.02	1515	92	0.7372
MSZ6- 52-54 - 7	2.375297	0.19	0.356	0.02	1540	120	0.80962
MSZ6- 52-54 - 8	2.597403	0.13	0.322	0.014	1560	110	0.83861
MSZ6- 52-54 - 9	2.118644	0.1	0.416	0.018	1520	95	0.73632
MSZ6- 52-54 - 11	1.785714	0.089	0.521	0.022	1370	160	0.62629

MSZ6- 52-54 - 12	2.380952	0.081	0.379	0.013	1495	68	0.73066
MSZ6- 56-59 - 1	2.506266	0.13	0.361	0.016	1458	90	0.71912
MSZ6- 56-59 - 3*	1.620746	0.095	0.513	0.018	1480	100	0.81772
MSZ6- 56-59 - 6	2.074689	0.085	0.449	0.018	1470	110	0.60872
MSZ6- 56-59 - 9	2.087683	0.092	0.428	0.02	1510	110	0.55644
MSZ6- 56-59 - 10	1.148106	0.085	0.613	0.032	1590	270	0.82111
MSZ6- 56-59 - 12	2.5	0.15	0.353	0.019	1476	77	0.9135
MSZ6- 62-69(2) - 1	2.415459	0.09	0.375	0.014	1498	70	0.77725
MSZ6- 62-69(2) - 3*	2.132196	0.11	0.383	0.02	1660	130	0.61943
MSZ6- 62-69(2) - 4	2.202643	0.098	0.408	0.016	1527	99	0.69179
MSZ6- 62-69(2) - 6*	2.109705	0.13	0.378	0.025	1670	180	0.43959
MSZ6- 62-69(2) - 7	2.227171	0.096	0.461	0.028	1350	100	0.90016
MSZ6- 62-69(2) - 8	2.386635	0.086	0.394	0.018	1444	76	0.67483
MSZ6- 62-69(2) - 10	2.624672	0.089	0.337	0.015	1478	70	0.56027
MSZ6- 62-69(2) - 11	2.09205	0.074	0.447	0.021	1440	110	0.57597
MSZ6- 68-71(2) - 2	2.159827	0.11	0.458	0.025	1420	140	0.44516
MSZ6- 68-71(2) - 4	2.283105	0.14	0.384	0.014	1525	94	0.87663
MSZ6- 68-71(2) - 5	1.941748	0.074	0.479	0.019	1470	110	0.54813
MSZ6- 68-71(2) - 6	2.659574	0.098	0.347	0.023	1435	89	0.42087
MSZ6- 66-67(2) - 1	2.277904	0.095	0.417	0.024	1420	100	0.55945
MSZ6- 66-67(2) - 2	2.659574	0.11	0.341	0.014	1465	79	0.47223
MSZ6- 66-67(2) - 3	2.770083	0.13	0.319	0.012	1453	75	0.76871
MSZ6- 66-67(2) - 4	2.73224	0.073	0.322	0.011	1458	71	0.46181
MSZ6- 66-67(2) - 5	2.857143	0.096	0.2632	0.0098	1554	60	0.66966
MSZ6- 60-61(2) - 1	2.487562	0.071	0.369	0.014	1466	67	0.42845
MSZ6- 60-61(2) - 2	2.65252	0.1	0.33	0.015	1506	84	0.68869
MSZ6- 60-61(2) - 3	2.65252	0.11	0.334	0.013	1479	85	0.60432
MSZ6- 60-61(2) - 4	2.631579	0.088	0.333	0.012	1485	61	0.67657
MSZ6- 60-61(2) - 5*	2.702703	0.1	0.355	0.016	1394	79	0.50686
MSZ6- 87-88(2) - 1	3.069368	0.089	0.258	0.011	1457	49	0.61232
MSZ6- 87-88(2) - 2	2.80112	0.095	0.2916	0.0093	1510	63	0.7174
MSZ6- 87-88(2) - 3	2.525253	0.072	0.383	0.013	1401	61	0.52918
MSZ6- 87-88(2) - 4	1.811594	0.078	0.484	0.026	1520	130	0.66072
MSZ6- 89-92(2) - 1	1.890359	0.095	0.457	0.023	1580	140	0.67279
MSZ6- 89-92(2) - 2	1.215067	0.066	0.59	0.033	1570	240	0.59496
MSZ6- 89-92(2) - 4	2.469136	0.093	0.37	0.017	1473	81	0.54057

MSZ6- 89-92(2) - 5	2.415459	0.12	0.331	0.018	1599	96	0.7938
MSZ6- 89-92(2) - 6	2.469136	0.066	0.377	0.016	1452	69	0.35114
MSZ6- 89-92(2) - 7	2.7571	0.065	0.337	0.01	1407	41	0.68383
MSZ6- 89-92(2) - 8	2.824859	0.09	0.3048	0.0081	1472	54	0.81237
E1-N WG (Unzoned Grains)							
Sample spot	Final U238/Pb 206	Final U238/Pb206 2σ	Final Pb207/Pb 206	Final Pb207/Pb206 2σ	Final Pb207 Age (Ma)	Final Pb 207 Age 2σ (Ma)	U238/Pb206 vs. Pb207/Pb206 Error Correlation
E1- 76-77 - 3*	3.134796	0.12	0.1176	0.0042	1698	77	0.75924
E1- 76-77 - 7*	2.680965	0.15	0.1514	0.0067	1770	120	0.86296
E1- 76-77 - 8*	3.419973	0.051	0.112	0.0034	1585	36	0.45522
E1- 76-77 - 10*	3.067485	0.1	0.145	0.0058	1582	65	0.76021
E1- 78-79 _core - 1	3.203075	0.063	0.1553	0.0062	1459	56	0.29826
E1- 78-79 _core - 4*	2.50000	2.9	0.1115	0.0068	1380	310	0.98725
E1- 78-79 _core - 5*	4.1841	0.39	0.1151	0.009	1280	130	0.57155
E1- 78-79 _core - 7*	3.327787	0.09	0.12	0.0049	1608	73	0.60929
E1- 78-79 _core - 8	3.401361	0.32	0.1255	0.0079	1500	160	0.86147
E1- 78-79 _core - 9*	3.397893	0.096	0.1071	0.0053	1643	63	0.52609
E1- 86-88 _core - 2	3.663004	0.16	0.0991	0.0038	1529	89	0.72291
E1- 86-88 _core - 3*	3.952569	0.42	0.1217	0.0089	1310	150	0.53048
E1- 86-88 _core - 4	3.355705	0.16	0.134	0.012	1492	76	0.78495
E1- 86-88 _core - 5*	2.512563	0.28	0.1556	0.0085	1810	230	0.71706
E1- 86-88 _core - 6	3.357958	0.094	0.119	0.0035	1564	61	0.73911
E1- 86-88 _core - 7*	3.246753	0.1	0.1107	0.0056	1717	84	0.50942
E1- 86-88 _core - 8*	3.610108	0.11	0.1255	0.0074	1430	55	0.57111
E1- 86-88 _core - 10	3.289474	0.05	0.1351	0.0042	1531	38	0.33276
E1- 82-83 - 1	3.648304	0.12	0.1058	0.0055	1521	71	0.13745
E1- 82-83 - 2*	8.0000	0.81	0.1013	0.0065	685	76	0.82904
E1- 82-83 - 4	3.642987	0.045	0.1062	0.0029	1517	31	-0.19448
E1- 82-83 - 5	3.749531	0.13	0.1017	0.0042	1493	67	0.62776
E1- 82-83 - 6*	4.56621	0.3	0.1228	0.007	1129	83	0.5283
E1- 82-83 - 7*	3.174603	0.19	0.1244	0.0085	1590	100	0.76185
E1- 84-85 - 1*	3.483107	0.049	0.1307	0.0026	1458	25	0.43367
E1- 84-85 - 2	3.571429	0.055	0.1064	0.0033	1549	32	0.094786
E1- 84-85 - 3	3.518649	0.067	0.1102	0.003	1555	38	0.26036
E1- 84-85 - 4	3.519887	0.06	0.107	0.0031	1571	31	0.47381
E1- 84-85 - 5	3.566334	0.06	0.1038	0.0028	1558	34	0.32728

E1- 84-85 - 6*	3.636364	0.057	0.1152	0.0032	1473	36	-0.24259
E1- 84-85 - 8*	3.843198	0.12	0.1012	0.0031	1455	55	0.76782
E1- 74-75 - 1	3.448276	0.15	0.1311	0.006	1478	89	0.65222
E1- 74-75 - 2*	3.205128	0.12	0.1562	0.006	1419	45	0.71508
E1- 74-75 - 4	3.424658	0.19	0.1166	0.0052	1590	99	0.69217
E1- 74-75 - 5*	5.102041	1	0.1064	0.0043	1060	120	0.9486
E1- 74-75 – 6	3.311258	0.31	0.1208	0.0059	1550	120	0.88353
E1-N Core							
Sample spot	Final U238/Pb 206	Final U238/Pb206 2σ	Final Pb207/Pb 206	Final Pb207/Pb206 2σ	Final Pb207 Age (Ma)	Final Pb 207 Age 2σ (Ma)	U238/Pb206 vs. Pb207/Pb206 Error Correlation
E1- 80-81 _core - 1*	2.512563	0.11	0.253	0.02	1505	76	0.87844
E1- 80-81 _core - 3*	2.762431	0.35	0.13	0.011	1610	210	0.74105
E1- 80-81 _core - 4*	1.923077	0.42	0.257	0.082	1060	420	0.26555
E1- 80-81 _core - 7	3.597122	0.28	0.1276	0.0075	1490	110	0.79933
E1-N Rim							
Sample spot	Final U238/Pb 206	Final U238/Pb206 2σ	Final Pb207/Pb 206	Final Pb207/Pb206 2σ	Final Pb207 Age (Ma)	Final Pb 207 Age 2σ (Ma)	U238/Pb206 vs. Pb207/Pb206 Error Correlation
E1- 80-81 _rim1 - 1*	0.657	0.097	0.862069	0.14	4590	250	0.80792
E1- 80-81 _rim1 - 3*	0.205	0.03	0.240963	0.025	4560	240	0.73014
OD306							
Sample spot	Final U238/Pb 206	Final U238/Pb206 2σ	Final Pb207/Pb 206	Final Pb207/Pb206 2σ	Final Pb207 Age (Ma)	Final Pb 207 Age 2σ (Ma)	U238/Pb206 vs. Pb207/Pb206 Error Correlation
OD306 – 1	3.52982	0.067	0.1027	0.0043	1590	41	0.31346
OD306 – 2	3.43288	0.093	0.1217	0.0073	1563	54	0.49025
OD306 – 3	3.61663	0.068	0.0988	0.0048	1576	36	0.36024
OD306 – 4	3.54107	0.068	0.1139	0.006	1546	48	0.33531
OD306 – 5	3.50877	0.074	0.1088	0.0049	1573	45	0.50165
OD306 – 6	3.58937	0.07	0.1056	0.0047	1549	35	0.45127
OD306 – 7	3.58680	0.066	0.0964	0.0042	1599	39	0.29279
OD306 – 8	3.59324	0.067	0.0998	0.0044	1577	41	0.17822
OD306 – 9	3.56252	0.08	0.1142	0.0052	1542	52	0.58964
OD306 - 10.	3.55366	0.072	0.1083	0.0053	1560	41	0.41666
OD306 - 11	3.59325	0.063	0.1101	0.0038	1532	37	0.3171
OD306 - 12	3.57781	0.053	0.0998	0.0045	1577	37	0.2452
OD306 - 13	3.60490	0.054	0.1027	0.0041	1547	25	0.581
OD306 - 14	3.63504	0.063	0.0985	0.0036	1562	35	0.46569
OD306 - 15	3.69822	0.061	0.1033	0.0043	1537	36	0.35871

OD306 - 16	3.67376	0.084	0.1052	0.0049	1528	45	0.33773
OD306 - 17	3.62713	0.054	0.1068	0.0041	1527	32	0.37994
OD306 - 18	3.59582	0.064	0.106	0.0038	1536	35	0.33815
OD306 - 19	3.53107	0.065	0.1017	0.004	1595	39	0.16627
OD306 – 20	3.71609	0.059	0.1014	0.0045	1505	34	0.4691
OD306 – 21	3.58422	0.075	0.1047	0.0044	1551	39	0.42359
OD306 – 22	3.50267	0.079	0.1063	0.0059	1589	45	0.40721
OD306 – 23	3.58808	0.072	0.1024	0.005	1577	41	0.42275
OD306 – 24	3.58808	0.075	0.1016	0.0035	1585	43	0.44196
OD306 – 25	3.54107	0.073	0.1041	0.0044	1580	40	0.48868
OD306 – 26	3.58294	0.065	0.1018	0.0045	1568	33	0.27638
OD306 – 27	3.55366	0.062	0.1021	0.0037	1593	40	0.17836
OD306 - 28	3.48062	0.06	0.1136	0.0053	1588	45	0.1387
OD306 - 29	3.43997	0.073	0.108	0.0043	1596	42	0.43387
OD306 - 30	3.51741	0.063	0.102	0.004	1582	41	0.21702
OD306 - 31	3.54484	0.068	0.1034	0.0043	1585	42	0.29822
OD306 - 32	3.52236	0.07	0.1111	0.0057	1568	46	0.45964
OD306 - 33	3.53356	0.067	0.107	0.0044	1583	41	0.54231
OD306 - 34	3.59453	0.082	0.1052	0.0041	1566	44	0.33982
OD306 - 35	3.51988	0.08	0.0995	0.0052	1607	48	0.36687
OD306 - 36	3.56125	0.062	0.1048	0.0048	1567	42	0.30683
OD306 - 37	3.54484	0.071	0.1014	0.0049	1598	43	0.30859
OD306 - 38	3.56633	0.065	0.1074	0.0044	1566	38	0.5009
OD306 - 39	3.64965	0.076	0.1036	0.0045	1556	44	0.32176
OD306 - 40	3.55239	0.069	0.1012	0.0045	1602	40	0.34066
OD306 - 41	3.49528	0.067	0.1105	0.0061	1581	42	0.59562
OD306 - 42	3.54107	0.079	0.1083	0.0052	1555	44	0.3288
S401							
Sample spot	Final U238/Pb 206	Final U238/Pb206 2σ	Final Pb207/Pb 206	Final Pb207/Pb206 2σ	Final Pb207 Age (Ma)	Final Pb 207 Age 2σ (Ma)	U238/Pb206 vs. Pb207/Pb206 Error Correlation
401 - 1	11.3250	0.27	0.068	0.0062	571	21	0.11363
401 - 2	11.3122	0.3	0.0714	0.0074	588	22	-0.064087
401 - 3	11.4810	0.41	0.0705	0.0069	569	19	-0.074308
401 - 4	11.1358	0.36	0.0685	0.0073	580	24	0.3135
401 - 5	11.3636	0.35	0.0624	0.0057	555	22	0.32212
401 - 6	11.5340	0.31	0.0715	0.0066	570	22	0.26533

401 - 7	11.4678	0.26	0.0687	0.0068	566	19	0.15738
401 - 8	11.3636	0.35	0.0631	0.0074	564	22	-0.037893
401 - 9	11.3250	0.37	0.0716	0.0074	577	22	0.011061
401 - 10	11.3507	0.4	0.0689	0.0088	566	25	-0.006054
401 - 11	11.4810	0.29	0.0678	0.0086	559	22	-0.035085
401 - 12	11.709	0.36	0.0723	0.0079	567	23	-0.063933
401 - 13	11.2359	0.29	0.0719	0.007	586	22	0.16383
401 - 14	11.4810	0.41	0.0679	0.006	565	25	0.45281
401 - 15	12.0192	0.39	0.0719	0.0076	562	25	0.21664
401 - 16	11.7508	0.36	0.0704	0.0063	565	21	0.22425
401 - 17	11.2359	0.3	0.0647	0.0066	562	22	0.16807
401 - 18	11.1358	0.36	0.0689	0.0074	584	29	0.41045
401 - 19	11.2359	0.26	0.0707	0.0072	583	20	-0.039891
401 - 20	11.4025	0.33	0.0718	0.0063	577	23	0.12163
401 - 21	11.5740	0.32	0.0696	0.0085	560	23	-0.021077
401 - 22	11.2359	0.29	0.0651	0.0063	559	20	0.36023
401 - 23	11.2612	0.32	0.0638	0.0065	565	19	-0.010427
401 - 24	11.5874	0.32	0.0731	0.0068	579	22	0.16395
401 - 25	11.4810	0.35	0.0672	0.0066	559	20	0.087164
401 - 26	11.2739	0.28	0.0629	0.0071	557	21	0.095934
401 - 27	11.5074	0.37	0.0711	0.0063	573	19	0.2134
401 - 28	11.4547	0.33	0.0664	0.0063	564	19	0.12693
401 - 29	11.2107	0.35	0.0648	0.0072	564	25	0.23663
401 - 30	10.9051	0.33	0.0649	0.0076	573	23	0.071638
401 - 31	11.2359	0.29	0.0678	0.0067	575	25	0.42935
401 - 32	11.3250	0.33	0.0723	0.0072	576	20	0.12034
401 - 33	11.2612	0.27	0.0653	0.0071	564	23	0.23078
401 - 34	11.3122	0.37	0.0767	0.0076	595	22	0.069048
401 - 35	11.1982	0.38	0.0694	0.0082	576	23	0.090558
401 - 36	11.3378	0.35	0.0679	0.0065	567	20	0.15317
401 - 37	11.1731	0.36	0.0662	0.0062	574	23	0.30335
401 - 38	11.3636	0.3	0.0683	0.0067	572	24	0.21929
401 - 39	11.6414	0.28	0.0701	0.0062	565	17	-0.034427
401 - 40	11.1856	0.27	0.0679	0.0058	580	19	0.25839
401 – 41	11.0132	0.24	0.0627	0.0067	566	23	0.35526
401 - 42	11.261	0.23	0.0618	0.0064	552	18	-0.024782

McClure Mountain							
Sample spot	Final U238/Pb 206	Final U238/Pb206 2σ	Final Pb207/Pb 206	Final Pb207/Pb206 2σ	Final Pb207 Age (Ma)	Final Pb 207 Age 2σ (Ma)	U238/Pb206 vs. Pb207/Pb206 Error Correlation
MC - 1	8.69565	0.2	0.2283	0.0089	564	17	0.42356
MC - 2	9.43396	0.24	0.191	0.011	551	18	0.19433
MC - 3	9.70873	0.19	0.162	0.0066	554	13	0.39779
MC - 4	9.93048	0.23	0.1568	0.0084	553	18	0.24863
MC - 5	9.64320	0.36	0.166	0.01	552	21	0.6197
MC - 6	10.4166	0.22	0.1296	0.007	539	13	0.39705
MC - 7	9.57854	0.28	0.201	0.012	540	21	0.34185
MC - 8	8.20344	0.31	0.303	0.015	537	25	0.50341
MC - 9	8.18330	0.17	0.306	0.011	526	16	0.38876
MC - 10	9.08265	0.26	0.199	0.011	563	20	0.42221
MC - 11	9.61538	0.26	0.1698	0.0087	552	16	0.52542
MC - 12	6.01322	0.18	0.452	0.021	547	36	0.11067
MC - 13	8.7719	0.25	0.225	0.01	557	21	0.32715
MC - 14	9.30232	0.29	0.203	0.012	553	23	0.20765
MC - 15	8.74125	0.24	0.22	0.012	561	20	0.37277
MC - 16	6.26174	0.18	0.425	0.013	548	24	0.68172
MC - 17	8.21018	0.25	0.263	0.013	566	21	0.63265
MC - 18	9.54198	0.28	0.197	0.012	537	21	0.33708
MC - 19	9.27643	0.3	0.196	0.01	557	20	0.40418

14. APPENDIX F – TRACE ELEMENT DATA

MSZ-2																		
Sample Spot	La (ppm)	Ce (ppm)	Pr (ppm)	Nd (ppm)	Sm (ppm)	Eu (ppm)	Gd (ppm)	Dy (ppm)	Ho (ppm)	Er (ppm)	Tm (ppm)	Yb (ppm)	Lu (ppm)	Y (ppm)	Mn (ppm)	Sr (ppm)	Th (ppm)	U (ppm)
MSZ2- 44-45 - 1	200.9	392.4	41.3	181.3	36.6	8.89	44.2	5.99	37.35	7.47	19.35	2.62	16.31	3.3	217	2223	303.3	15.06
MSZ2- 44-45 - 2	331	542.3	52	218.9	39.6	9.73	48.7	6.49	41.01	8.08	21.61	2.78	18.08	3.72	233.8	2391	320.5	20.42
MSZ2- 44-45 - 3	297.2	503.7	49.41	207.4	37.6	9.57	44.3	5.94	38	7.6	19.99	2.515	16.66	3.47	217.2	2388	320.3	17.61
MSZ2- 44-45 - 4	227.5	437.5	45.41	197.2	36.98	9.3	45	6.2	37.8	7.35	20.85	2.63	16.32	3.41	220.4	2311	305.2	16.02
MSZ2- 44-45 - 5	205.5	397.1	41.46	184.4	34.7	8.46	42.6	5.43	35.4	6.72	17.84	2.27	14.93	2.98	200	2197	305.9	11.42
MSZ2- 44-45 - 6	256.6	473.2	48.27	207.7	37.9	9.56	45.7	6.04	37.5	7.42	19.49	2.5	16.2	3.23	215.5	2198	298.3	18.17
MSZ2- 44-45 - 7	251.7	468.4	47.38	204.3	36.7	9.44	45.8	6.08	36.93	7.44	19.6	2.7	16.11	3.3	214.9	2331	305	16.63
MSZ2- 44-45 - 8	192.3	393	42.25	186.2	35.5	8.43	44.7	5.69	36.45	7.34	19.12	2.48	16.38	3.32	214.2	2213	323.5	13.55
MSZ2- 44-45 - 9	355	616	61.4	261.2	50.3	12.19	61.5	8.04	49.8	10.08	27.32	3.51	21.86	4.48	293.4	2425	314.8	43.19
MSZ2- 44-45- 10	246.2	485.6	51.37	231.9	45.1	11.32	54.7	7.2	44.1	8.74	23.99	3.07	18.85	3.93	257.4	2233	297.3	26.43
MSZ2- 44-45- 11	214.6	427.5	46.2	204.6	40.3	10.17	48.7	6.52	38.7	7.85	20.44	2.71	16.74	3.46	229	2268	297.9	24.2
MSZ2- 44-45- 12	265.6	529.2	54.42	231.7	46.6	11.66	54.4	7.41	46.5	9.45	24.84	3.2	20.41	4.14	270.2	2354	305.1	30.92
MSZ2- 44-45- 13	298	578	59.1	245.1	49.6	11.92	56.5	7.8	49.8	9.6	26.41	3.4	21.92	4.47	287	2317	302.9	33.97
MSZ2- 44-45- 14	231.1	461	47.82	199.4	40.8	9.69	46.3	6.39	39.9	7.7	22.18	2.73	17.5	3.64	233.1	2314	297	23.15

MSZ2- 44-45-15	207.3	434.7	45.88	196.6	40.3	10.09	46.8	6.58	41.7	8.18	22.67	2.73	18.24	3.8	241.5	2142	307.3	21.88
MSZ2- 40-41 - 1	328.4	561.2	52.07	204.2	41.7	9.94	43.6	6	39.1	7.64	20.47	2.59	17.39	3.6	226.1	2375	322.6	18.81
MSZ2- 40-41 - 2	337	572	52.78	203.3	39.8	9.46	41.7	5.84	37.6	7.26	20.72	2.76	17.34	3.5	222.6	2304	322.2	19.66
MSZ2- 40-41 - 3	252.9	489.9	48.89	194.4	38.3	9.17	41.3	5.83	37.75	7.29	20.29	2.52	16.94	3.3	216.6	2310	307.6	16.38
MSZ2- 40-41 - 4	233.1	443	43.5	174.8	35.6	8.54	38.4	5.34	34.2	6.6	17.6	2.34	14.79	2.89	196.3	2123	296.1	13.22
MSZ2- 40-41 - 5	228.9	453	44.79	185.1	37.1	9.15	41	5.85	37.6	7.29	20.4	2.58	16.79	3.39	216.5	2253	307.9	15.74
MSZ2- 40-41 - 6	388.5	650.3	59.21	222.4	42.6	10.29	45	6.33	41.6	7.85	21.69	2.85	18.37	3.75	235.6	2371	322.4	30.95
MSZ2- 40-41 - 7	684	861	64.9	217.6	34.6	7.99	34.1	4.57	30.4	5.92	16.47	2.22	13.82	2.84	181.7	2387	397	19.03
MSZ2- 40-41 - 8	284	516	48.62	191.6	37.3	8.94	40.7	5.59	37.36	7.11	19.4	2.57	16.6	3.13	207.9	2299	314.2	17.57
MSZ2- 40-41 - 9	113.7	234.3	23.93	98.4	20.6	5.58	23.9	3.34	21.4	4.11	11.41	1.387	8.83	1.73	124.8	2640	310.8	1.04
MSZ2- 40-41-10	321.7	558	50.3	191.7	36.5	8.75	38.2	5.04	33.6	6.29	18.08	2.28	14.91	2.92	194.1	2277	307.1	15.49
MSZ2- 40-41-11	225.6	456.4	44.37	179.1	36	8.53	38.9	5.29	34.14	6.41	18.46	2.31	15.11	3.02	195.5	2314	304.7	13.79
MSZ2- 40-41-12	318.2	580.9	53.38	202.5	37.6	9.2	40.4	5.48	35.7	6.76	19.35	2.46	16.85	3.26	207.3	2369	315.7	18.68
MSZ2- 40-41-13	261	504.1	48.54	195	39.7	9.76	44.2	6.01	39.67	7.44	21.53	2.65	17.01	3.36	222.2	2346	305.1	17.17
MSZ2- 40-41-14	494	728	61.68	231.6	43.6	10.41	49.1	6.73	44.3	8.35	23.82	2.96	20.01	4.17	259.2	2423	341	30.74
MSZ2- 40-41-15	270.4	541.7	52.77	215	44.2	10.44	49.6	6.7	43.63	8.49	23.09	2.864	18.34	3.75	244.7	2272	297.1	24.45
MSZ2- 40-41-16	450	709	65.5	254.8	47	11.28	51	6.98	43.4	8.99	24.66	3.36	21.87	4.41	266.8	2410	317.4	37.18

MSZ2- 40-41-17	368.6	631.9	61.31	243.7	46.3	10.64	50.6	6.72	42.26	8.93	23.51	3.12	21.26	4.05	260.9	2357	317.1	31.68
MSZ2- 38-39 - 1	232.8	440.5	45.9	193.8	37.9	9.3	44.5	5.94	35.81	7.39	19.51	2.64	16.41	3.42	216.9	2227	298.1	16.67
MSZ2- 38-39 - 2	257	474	48.4	200.5	36.4	8.59	39.3	5.31	32.71	6.86	17.81	2.43	15.63	3	199.5	2267	322.8	16.52
MSZ2- 38-39 - 3	429	645	59.41	230.3	38.2	9.04	40.5	5.38	32.3	6.9	18.25	2.58	16.14	3.17	206.8	2390	336.2	21.23
MSZ2- 38-39 - 4	324.7	553.5	54.36	222.1	40.4	9.42	44.2	5.67	35.25	7.32	19.28	2.55	18.09	3.38	215.2	2326	309.5	19.77
MSZ2- 38-39 - 5	163.8	322.5	35.89	160.4	33.9	7.91	37.6	5.13	31.28	6.15	16.2	2.08	12.9	2.53	183.8	1900	285.7	9.19
MSZ2- 7-8 - 1	161.5	316.1	34.5	151.6	31.1	7.88	39.5	5.35	33.07	6.83	18.08	2.222	15.32	2.86	205.2	2150	304.4	14.13
MSZ2- 7-8 - 2	317.6	557.7	55.8	234.3	43.9	10.46	47.5	6.68	38.4	8.16	21.46	2.84	18.25	3.51	235.7	2313	317.6	23.13
MSZ2- 7-8 - 4	249.9	472.6	48.76	209	40.8	9.55	45.7	5.96	36.84	7.78	20.46	2.5	16.4	3.32	220.1	2279	302.8	22.65
MSZ2- 7-8 - 5	224.8	429.4	45.09	195.4	37.1	9.17	42	5.75	34.9	7.22	18.81	2.5	16.11	3.06	209.1	2246	303.8	19.72
MSZ2- 7-8 - 6	330.4	574.7	57.45	236.9	41.3	10.08	44.3	6.08	37.69	7.7	20.38	2.74	17.55	3.51	231.1	2332	310.3	28.66
MSZ2- 7-8 - 7	566.4	750.2	62.27	237.6	36.6	8.76	39.8	5.35	31.55	6.7	17.95	2.45	16.28	3.14	208.9	2373	344.4	27.63
MSZ2- 7-8 - 8	256.8	481.4	50.23	216.1	41.1	9.87	45.6	6.17	37.85	7.92	20.47	2.734	17.95	3.53	228.2	2313	300.3	24.45
MSZ2- 7-8 - 9	169	324	34	153.2	31.4	7.73	36.7	5.02	29.7	6.25	16.65	2.2	13.37	2.55	187.7	2035	338.8	10.04
MSZ2- 7-8 - 10	231.1	423.1	42.95	185.9	36.8	9.05	41.6	5.69	34.08	6.86	18.36	2.34	15.93	2.96	203.6	2273	308.4	12.99
MSZ2- 7-8 - 11	317.3	528.4	50.71	212.2	38.1	9.22	43.3	6.01	36.14	7.37	19.44	2.62	16.44	3.31	215.8	2416	318.9	16.64
MSZ2- 7-8 - 12	233.4	447.1	46.58	198.2	38	9.44	44.6	5.99	36.3	7.51	19.44	2.66	16.96	3.17	219.3	2278	304.6	17.25
MSZ2- 7-8 - 13	212.6	430.8	45.1	197.8	37.9	9.42	43.5	6.33	37.6	7.96	19.77	2.55	17.6	3.39	225	2315	300.3	15.75
MSZ2- 7-8 - 14	475	707	62.9	236.1	44	10.4	46.5	6.22	38.8	7.79	21.03	2.84	19.43	3.76	237.8	2329	327.9	31.91
MSZ2- 7-8 - 15	360.3	605.8	57.11	220.2	41	9.94	45.4	5.98	37.55	7.51	20.69	2.7	18.1	3.65	227.7	2600	313.5	28.03

MSZ2- 7-8 - 16	464.6	686.1	61.35	231.4	42.8	10.09	46.6	6.32	40.6	7.83	22.26	2.96	18.47	3.9	245.2	2408	334.9	29.3
MSZ2- 7-8 - 17	210.2	420.9	45.57	189.5	42.3	10.16	48.1	6.42	41.6	8.07	21.65	2.77	18.6	3.66	240.4	2131	295.1	19.56
MSZ2- 46-47 - 1	236.5	465.7	48.67	205.8	43.7	10.88	49.3	6.66	42.9	8.53	22.2	2.73	19.64	3.69	243.7	2235	306.5	26.06
MSZ2- 46-47 - 3	289.6	540.4	54.94	217.2	45.7	10.69	49.6	6.85	42.1	8.43	22.71	3.05	19.07	3.9	246.5	2352	305.7	22.45
MSZ2- 46-47 - 4	409	663	61.2	230.4	44.5	10.46	47.8	6.03	39.1	7.59	20.81	2.82	17.49	3.58	233.9	2334	313.1	24.05
MSZ2- 46-47 - 5	434.6	644.5	57.29	207.9	38.1	8.74	39.9	5.43	35.4	6.82	18.7	2.43	15.46	3.31	210.7	2342	343.1	17.17
MSZ2- 46-47 - 6	250.3	455.1	46.57	187.1	39.2	9.8	46.1	6.13	38.9	7.69	20.36	2.7	16.63	3.52	229	2258	353	16.45
MSZ2- 46-47 - 7	198.7	383	41.12	169.6	38.3	9.6	46.4	6.1	39.9	7.7	20.23	2.72	17.03	3.27	232.5	2121	318.5	16.81
MSZ2- 50-51 - 1	443.5	667.9	61.17	230.2	45.7	10.76	49.7	6.55	42.7	8.48	21.76	2.91	19.95	4.03	256.1	2400	333.3	27.42
MSZ2- 50-51 - 2	221.2	431.1	45.8	189.5	41.3	10.2	47.6	6.28	40.3	7.93	20.75	2.63	17.88	3.77	231.4	2254	307.6	16.18
MSZ2- 50-51 - 3	322.6	562	56.43	220.1	47.7	10.98	52.9	7.01	45.2	8.83	23.28	2.96	19.14	4.05	259.4	2317	301.6	28.31
MSZ2- 50-51 - 4	264.1	482	49.7	203.2	42.5	10.19	50.1	6.65	42.05	8.14	21.61	2.83	18.48	3.79	244.4	2339	303.8	23.96
MSZ2- 50-51 - 5	652.1	835.4	68.7	236.9	42.1	9.34	45.3	5.95	38.74	7.48	19.55	2.71	18.64	3.59	230.2	2467	358.9	28.83
MSZ2- 50-51 - 6	482	727	66.6	247.5	47.9	11.29	53.1	7.12	44.5	8.94	23.35	3.09	20.01	4.22	266.9	2399	324.9	33.97
MSZ2- 50-51 - 7	237.9	458.2	47.96	200.2	42.2	10.37	49.3	6.51	41.46	8.2	21.74	2.83	17.88	3.88	243.7	2250	304.8	17.56
MSZ2- 50-51 - 8	447.6	675	61.7	232.2	45.1	9.98	49.9	6.53	41	8.26	21.78	2.87	18.85	3.82	246.6	2433	334.1	28.59
MSZ-3.1 WG (Unzoned Grain)																		
Sample Spot	La (ppm)	Ce (ppm)	Pr (ppm)	Nd (ppm)	Sm (ppm)	Eu (ppm)	Gd (ppm)	Dy (ppm)	Ho (ppm)	Er (ppm)	Tm (ppm)	Yb (ppm)	Lu (ppm)	Y (ppm)	Mn (ppm)	Sr (ppm)	Th (ppm)	U (ppm)

MSZ3.1- 93-97-1	69	126	13	52	12.2	2.2	8.9	1.36	10	1.96	5.8	0.54	4.8	0.72	67	368	241	9.4
MSZ3.1- 93-97 - 3	318.5	529	50	200.9	36.3	7.53	43	5.46	34.2	6.95	19.57	2.71	17.42	3.03	215.5	984	301.4	22.6
MSZ3.1- 93-97 - 4	357	594	55.4	219	37.9	7.42	44.8	5.81	35.9	7.12	21.7	2.86	18.1	3.04	223.7	975	303.2	27.3
MSZ3.1- 93-97 - 5	300.6	501	47	186.5	33.9	6.6	37.7	4.61	29.5	6.04	17.13	2.33	14.77	2.69	187.2	967	309	17.59
MSZ3.1- 93-97 - 6	396.2	642	57.79	222.5	35.3	6.49	38.4	4.48	28.4	5.82	16.61	2.28	13.78	2.33	181	995	294.3	18.27
MSZ3.1- 93-97 - 9	501	796	68.9	254.1	41	7.27	44.3	5.62	33.5	6.79	20.07	2.77	17.69	3	214.4	1026	299.7	24.42
MSZ3.1- 93-9 - 10	635	945	79.2	287.7	43.3	7.86	46.5	5.53	34.9	7.42	21.52	2.92	18.32	3.11	226	1028	298.7	31.99
MSZ3.1- 93-97-11	399	660	58.6	220	35.6	6.12	39	4.68	30	6.05	17.66	2.5	15.02	2.52	188.1	912	296.1	15.84
MSZ3.1- 93-97-13	467.8	696	56.77	200.9	31.6	5.71	33.6	3.95	25.8	5.45	15.96	2.24	13	2.33	168.8	999	302	13.98
MSZ3.1- 93-97-14	663	977	80	278.6	43.8	7.71	47.1	5.71	34.6	7.58	22.03	2.94	20	3.28	230.3	1056	308.3	29.98
MSZ3.1- 93-97-15	2100	2130	140	402	43.9	7.76	41.8	4.75	29.4	6.36	18.45	2.16	15.42	2.6	191.5	1050	312.7	45
MSZ3.1- 93-97-16	503.9	772	63.6	221.6	32.8	5.98	35.7	4.37	28.7	5.92	17.65	2.44	13.96	2.5	188.4	1490	315.5	16.87
MSZ3.1- 93-97-18	396	670	58.3	213.1	30.2	5.2	31.9	4.14	25.13	5.31	15.41	2	12.06	2.2	166.1	969	295.8	12.2
MSZ3.1- 93-97-20	255	450	42.3	165.8	28.6	5.53	31.8	4.16	26.7	5.41	15.74	1.97	12.89	2.09	168.2	987	289.8	8.87
MSZ3.1- 93-97-21	182.2	321.2	30.7	126	22.4	4.64	26.6	3.64	23.1	4.63	14.13	1.8	10.75	1.831	148	1064	296.2	9.9
MSZ3.1- 93-97-22	120	216.5	21.53	87.9	16.85	3.8	22.1	2.84	18.54	3.78	10.92	1.357	8.59	1.475	121.9	931	299.6	1.175
MSZ3.1- 99-102-1	200	353.6	34.96	143.8	28.5	6.46	32.2	4.49	27.4	5.8	16.39	2.13	13.02	2.35	181.6	955	296	7.28

MSZ3.1- 99-102-2	444	721.6	61.8	213.6	28.6	5.87	30.5	3.91	23.45	4.92	14.03	1.94	12.19	2.11	158	1027	305.1	20.59
MSZ3.1- 99-102-3	762	1064	80.2	258.7	32.6	6.48	33.6	4.21	26.17	5.49	15.51	2.11	12.6	2.24	168.1	1055	320.8	28.45
MSZ3.1- 99-102-4	941	1208	89.6	280.4	37.4	6.84	37.3	4.85	29.3	6.2	18.07	2.48	14.57	2.66	192.3	1065	324.5	32.16
MSZ3.1- 99-102-5	820	1109	83.6	267.8	36.1	7.17	38.8	4.8	29.9	6.26	18.11	2.4	15.4	2.83	198.3	1071	323.7	31.44
MSZ3.1- 99-102-6	402	629	51.6	172.7	24.39	5.12	26.2	3.46	20.94	4.37	12.39	1.58	9.64	1.78	139.3	1015	298.8	9.92
MSZ3.1- 99-102-7	603	915	73.3	245	35.1	7.3	38.4	4.73	29.9	6.15	17.66	2.24	14.17	2.54	194.1	1015	307.5	22.94
MSZ3.1- 99-102-8	730	1082	85.5	283.5	40.5	7.77	42.1	5.48	32.79	6.96	20.34	2.85	16.67	2.96	217.5	1079	330.9	33.54
MSZ3.1- 99-102-9	735	1040	81.6	272.9	38.7	7.42	41.1	5.18	31.97	6.6	20.16	2.52	16.24	2.72	211.2	965	304	31.9
MSZ3.1- 99-102-10	833	1150	91	297.7	40.2	7.95	43.6	5.53	33.86	7.27	21.24	2.71	17.39	2.96	225.4	1064	327.3	34.36
MSZ3.1- 99-102 -11	1620	1900	144	430	51.3	9.11	49.1	5.89	35.3	7.42	21.55	2.88	17.28	3	231.6	1070	312.8	46.1
MSZ3.1- 99-102 - 13	494.1	794	69.6	259.2	42.6	7.83	43.9	5.6	33.98	7.21	20.2	2.67	17.05	2.85	222.8	1044	307.4	35.7
MSZ3.1- 99-102 - 14	373.5	591.1	53.94	211	39.1	8.38	45.2	6.02	37.9	7.88	22.45	3.02	19.39	2.98	245.2	1039	299.3	32.66
MSZ3.1- 103-106 - 1	213.1	373.5	37.46	154.6	33.6	6.83	38.2	5.09	32.45	6.79	19.2	2.67	16.8	2.66	210.5	994	306.9	15.14
MSZ3.1- 103-106 - 3	236.8	411	39.8	163.9	32.6	6.22	35.6	4.54	28.8	6.04	17.32	2.3	14.19	2.38	186.9	951	311	12.2
MSZ-3.1 Core																		
Sample Spot	La (ppm)	Ce (ppm)	Pr (ppm)	Nd (ppm)	Sm (ppm)	Eu (ppm)	Gd (ppm)	Dy (ppm)	Ho (ppm)	Er (ppm)	Tm (ppm)	Yb (ppm)	Lu (ppm)	Y (ppm)	Mn (ppm)	Sr (ppm)	Th (ppm)	U (ppm)
MSZ3.1- 23-24_core - 1	332.3	521.6	47.85	190.4	38.9	8.19	48	6.24	40.5	8.59	24.3	3.17	20.19	3.16	261.4	1013	305.7	20.86

MSZ3.1- 23-24_core - 2	253.2	434.7	42.09	173.7	35.4	7.56	43.9	5.89	38.73	7.77	22.96	2.9	18.22	2.9	242.9	914	295	14.77
MSZ3.1- 23-24_core - 3	209	338	31.1	126.4	24.3	5.38	30.1	4.1	24.6	5.42	14.7	1.93	12.27	2.07	168.1	989	295.3	5.4
MSZ3.1- 23-24_core - 4	212.2	360	34.8	143.7	28.9	6.18	34.8	4.76	30.6	6.23	17.99	2.47	14.55	2.41	199.2	929	292	10.22
MSZ3.1- 23-24_core - 5	409.1	633.5	57.18	232.8	45.1	9.52	53.3	7.5	45.8	10.03	28.01	3.73	23.42	3.77	305.3	1004	306	37.64
MSZ3.1- 23-24_core - 6	290.7	480.5	45.33	186.4	36.8	7.84	46.1	6.16	37.9	8.22	23.57	3.18	19.13	3.11	250.2	971	292.6	18.47
MSZ3.1- 23-24_core - 8	338.9	535.9	49.43	200	38.4	8.34	47	6.42	39.8	8.59	24.64	3.17	20.13	3.34	267.8	1000	301.9	21.54
MSZ3.1- 23-24_core - 9	210.2	355.8	34.59	139.4	29.6	6.29	36.2	5.09	31.2	6.94	19.36	2.61	15.61	2.51	212.9	1028	317.9	9.46
MSZ3.1- 23-24_core - 10	205.4	348.6	33.28	142.3	29.4	6.66	36	5.06	30.49	6.64	19.02	2.5	14.24	2.36	204.3	1126	342.5	9.33
MSZ3.1- 23-24_core - 11	107.8	180.1	18.17	79.8	19.1	4.38	21.3	3.02	17.8	3.88	10.34	1.29	8.15	1.23	124.3	2380	307.2	1.72
MSZ3.1- 23-24_core - 13	226.1	370	34.83	144.7	30.8	6.84	40.2	5.32	34.8	7.31	20.05	2.72	15.88	2.53	225.6	1186	397.4	14.31
MSZ3.1- 17-18_core - 1	165.4	278.8	27.31	111.6	24.1	4.91	28.6	3.78	24.9	5.33	14.91	1.98	11.78	1.82	157.9	925	280.1	1.075
MSZ3.1- 17-18_core - 2	113.2	187	18.01	75.9	16.48	3.34	19.23	2.62	16.73	3.57	9.61	1.17	7.36	1.184	111.1	1039	294.4	0.091
MSZ3.1- 17-18_core - 3	109	174	16.58	67.7	13.54	3.17	18.4	2.35	13.86	2.87	7.82	1.1	6.73	1.066	91.5	1047	298.6	0.431
MSZ3.1- 17-18_core - 5	115.7	199.2	20.06	83.8	17.9	3.86	21.89	2.85	19.72	3.97	11.29	1.367	8.78	1.55	125	958	293.2	0.4
MSZ-3.1 Rim																		
Sample Spot	La (ppm)	Ce (ppm)	Pr (ppm)	Nd (ppm)	Sm (ppm)	Eu (ppm)	Gd (ppm)	Dy (ppm)	Ho (ppm)	Er (ppm)	Tm (ppm)	Yb (ppm)	Lu (ppm)	Y (ppm)	Mn (ppm)	Sr (ppm)	Th (ppm)	U (ppm)
MSZ3.1- 23-24_rim1 - 1	239.3	403	39	162.8	34	7.54	44	5.87	34.8	7.4	20.6	2.71	16.1	2.61	229.5	949	305.4	13.45

MSZ3.1- 23-24_rim1 - 2	125.2	195.4	17.66	74.3	15.12	3.15	19.02	2.39	14.68	3.11	8.75	1.04	6.39	1.036	97.7	1398	288.3	0.234
MSZ3.1- 23-24_rim1 - 3	221.3	374.4	35.42	145.8	29.4	6.42	35.1	4.88	30.66	6.66	18.7	2.3	14.35	2.5	201.4	971	299	11.3
MSZ3.1- 23-24_rim1 - 4	114.6	191.9	18.73	78.9	19	4.09	24.6	3.27	20.4	4.48	12.38	1.488	8.45	1.35	139.8	4370	296.7	0.425
MSZ3.1- 23-24_rim1 - 5	163.7	262.9	24.19	100.5	19.69	4.4	24	3.34	20.39	4.33	12.4	1.608	9.63	1.62	136.3	1006	300.7	4.22
MSZ3.1- 23-24_rim1 - 6	371.3	585.1	53.13	218.5	43.4	9.23	53.1	7.13	44.5	9.31	27.15	3.37	22.3	3.51	289.1	1031	329.4	33.95
MSZ3.1- 23-24_rim1 - 7	247.3	425.6	41	171.1	34.7	7.55	44.1	6.2	38.1	8.35	24.5	3.15	19.3	3.1	261.3	1083	330.3	17.98
MSZ3.1- 23-24_rim1 - 8	177.8	304.6	29.39	125	25.8	5.71	32.3	4.43	28.3	6.25	16.8	2.29	13.7	2.19	192.9	1066	317.9	7.75
MSZ3.1- 23-24_rim1 - 9	137.7	214.7	19.08	78.2	15.58	3.14	18.32	2.409	14.75	3.14	8.46	1.131	6.47	1.097	96.6	1021	300.2	0.086
MSZ3.1- 23-24_rim1 - 10	136.3	214.4	19.85	81.2	15.89	3.47	19.59	2.54	15.26	3.33	9.22	1.141	6.74	1.125	101.8	982	299.1	0.131
MSZ3.1- 23-24_rim1 - 11	144.9	244	24	100.4	21	4.7	24.5	3.25	20.7	4.16	11.31	1.35	8.5	1.37	129.1	2009	261.7	1
MSZ3.1- 23-24_rim1 - 12	133	220.5	21.32	88.6	18.42	4.3	26	3.4	21.23	4.51	11.87	1.64	9.64	1.52	141.2	991	284	1.45
MSZ3.1- 23-24_rim1 - 13	152.4	245.6	23.03	93.9	18.55	4.04	22.2	2.95	18.6	3.87	11.09	1.398	8.26	1.372	119.7	965	287.5	0.53
MSZ3.1- 23-24_rim1 - 14	216.8	356	33.6	141.1	28.3	5.62	33.3	4.61	28.8	6.14	16.82	2.32	14.1	2.19	187.3	993	294.8	8.5
MSZ3.1- 17-18_rim1 - 1	118.1	188.2	17.86	72.7	15.72	3.13	17.9	2.34	14.78	2.96	8.06	1.046	6.97	1.08	93.6	1005	292.8	0.067
MSZ3.1- 17-18_rim1 - 2	204.4	330.1	31.46	130.8	27.5	6.2	33.3	4.29	27.8	5.7	14.89	2.11	12.4	2.05	170.8	1293	281.9	1.03
MSZ3.1- 17-18_rim1 - 3	162.2	261	25.1	108.4	21.1	4.92	25.8	3.32	21.6	4.72	12.6	1.68	11	1.96	139.3	1040	299.2	0.269
MSZ3.1- 17-18_rim1 - 4	61.5	97	9.7	39.4	9.2	1.89	11	1.58	11.1	2.28	6.64	0.93	5.52	0.86	77.4	5760	227	1.42

MSZ3.1- 17-18_rim1 - 5	137.2	239.1	23.73	101.3	20.5	4.51	25.2	3.57	21.4	4.46	12.26	1.55	9.56	1.58	137.3	932	298.4	2.25
MSZ3.1- 17-18_rim1 - 6	183.2	308.2	29.56	121.9	26	5.67	31.9	4.31	26.7	5.59	15.4	1.83	13.21	2.2	170.5	992	280.1	0.914
MSZ-4 WG (Unzoned Grains)																		
Sample Spot	La (ppm)	Ce (ppm)	Pr (ppm)	Nd (ppm)	Sm (ppm)	Eu (ppm)	Gd (ppm)	Dy (ppm)	Ho (ppm)	Er (ppm)	Tm (ppm)	Yb (ppm)	Lu (ppm)	Y (ppm)	Mn (ppm)	Sr (ppm)	Th (ppm)	U (ppm)
MSZ4- 144-149(2) - 1.d	365.9	553.8	47.79	179.3	31.2	6.44	34.7	4.69	28.81	6.2	17.65	2.44	14.62	2.57	195.2	901	351.2	20.28
MSZ4- 144-149(2) - 2.d	545.8	796	66.1	241	38	7.66	41.9	5.82	35.7	7.72	22	3.02	20.23	3.25	245.3	1016	353.9	38.5
MSZ4- 144-149(2) - 3.d	611	892	71.5	257.6	38.1	7.37	37.9	5.14	30.7	6.64	18.55	2.58	16	2.88	206.5	984	348.8	39.1
MSZ4- 144-149(2) - 4.d	619.4	909.5	75.6	268	39.1	7.21	39.2	5.04	31.72	6.93	19.38	2.73	16.71	2.93	211.7	1036	355.3	38.95
MSZ4- 144-149(2) - 5.d	379.1	565	47.4	171.4	26.8	5.27	29.7	3.73	23.6	4.95	14.25	1.86	12.18	2.12	157.1	1013	358.6	14.3
MSZ4- 144-149(2) - 6.d	543.6	810.6	67.39	247.9	38.5	7.73	40.9	5.43	33.3	7.27	20.82	2.74	18.69	3.17	227.9	1020	351.2	34.36
MSZ4- 144-149(2) - 7.d	456.2	679.8	56.8	203.4	33.46	6.6	35.1	4.72	29.21	6.37	17.92	2.43	15.66	2.67	196	1002	354.5	26.17
MSZ4- 144-149(2) - 8.d	485	720	60.4	218.7	35.5	6.93	38.9	4.99	31.7	6.75	19.48	2.72	16.8	2.97	213	1000	360.8	28.39
MSZ4- 144-149(2) - 9.d	495.9	729.9	60.8	223.7	36.6	7.45	41	5.21	33.4	7.12	20.96	2.64	17.76	3.08	222.8	1007	354.6	31.41
MSZ4- 144-149(2) - 10.d	501.9	723	59.9	223.2	37.7	7.44	41.8	5.39	33.8	7.01	20.83	2.72	18.22	3.18	224.4	1026	353.8	33.71
MSZ4- 144-149(2) - 11.d	469.6	701.4	59.55	219.2	36.2	7.39	41.6	5.27	33.18	7.59	20.95	2.8	17.94	3.04	227.9	1008	351.7	30.63
MSZ4- 144-149-12	106	158	14.1	53	8.3	1.47	8.2	1.25	6.8	1.34	3.6	0.63	3.55	0.45	48	413	277	7.43
MSZ4- 144-149-13	405.4	609.6	52.6	195.4	34.85	7	38.6	4.87	31.74	6.76	19.74	2.67	16.05	2.88	213.4	1009	362.5	20.78

MSZ4-144-149-14	416.3	577.1	47.83	175.5	28.7	5.86	32.4	4.23	25.44	5.61	16.19	2.1	13.2	2.51	176	1005	357.2	12.28
MSZ4-144-149-15	373.2	544.2	45.7	171	29.1	5.62	32.7	4.27	25.62	5.69	15.65	2.195	13.6	2.32	173.7	986	356.3	13.63
MSZ4-144-149-16	358.3	530.8	45.8	171.7	28.7	6.05	33.8	4.24	26.47	5.8	15.94	2.19	13.71	2.5	177.5	937	351.2	14.52
MSZ4-144-149-17	452.8	644	53.13	200.6	33	6.78	38.3	4.73	30	6.57	18.12	2.42	15.64	2.728	199.5	1015	361.2	19.17
MSZ4-144-149-18	380.5	553	46.8	173.5	30	6.16	34.2	4.26	27	5.53	16.66	2.15	13.72	2.32	177.8	993	363.3	14.77
MSZ4-150-153-1	251.6	389.3	35.17	134.4	25.6	5.22	29.7	3.71	24.14	5.2	14.67	1.98	12.85	2.11	162.5	932	352.7	10.08
MSZ4-150-153-2	247.2	385.5	34.21	135.7	24.8	5.32	30	3.95	24.41	5.25	14.95	1.896	12.5	2.04	163.8	857	349	10.62
MSZ4-150-153-3	321.2	492.5	42.59	165.8	30.6	6.15	34.8	4.59	28.44	5.97	17.7	2.34	14.88	2.6	189	968	349.3	15.76
MSZ4-150-153-4	324.1	491.1	44	172.8	31	6.36	35.6	4.5	28.5	6.02	17.03	2.23	15.03	2.56	188.1	966	355	27.5
MSZ4-150-153-5	342.8	512.8	44.82	174.2	30.3	6.27	38.7	4.8	30	6.54	18.59	2.29	15.4	2.74	199.9	976	350.8	16.4
MSZ4-150-153-6	263.5	397.4	34.71	134.9	24.07	5.19	29.2	3.63	24.15	5.12	14.6	1.93	11.92	2.05	158	963	351.6	9.61
MSZ4-150-153-7	348.2	528.8	46.32	179	32	6.61	40.2	5.17	32.1	6.8	19.91	2.47	16.1	2.6	211.5	981	349.4	25
MSZ4-150-153-8	409.7	612.4	53.21	204.5	36.6	8.07	45	5.88	36.5	7.89	22.79	2.96	19.12	3.27	244.3	1006	347.7	33.59
MSZ4-150-153-9	335.1	519.3	45.93	181.3	32.5	7.12	40.1	5.19	31.49	6.91	19.72	2.61	16.9	2.74	214.8	972	349.2	24.27
MSZ4-150-153-10	259.7	408.6	36.5	145	27.58	5.75	31.8	4.11	26.58	5.64	16.4	2.14	13	2.22	179	963	363.4	11.75
MSZ4-150-153-11	364.1	556.7	48.9	191.8	34.4	7.24	40.6	5.33	33.6	7.36	20.7	2.71	17.53	3.05	224.7	996	350.3	28.5
MSZ4-150-153-12	303.4	471.4	42.13	162.6	31.2	6.63	34.9	4.7	29.58	6.25	17.8	2.45	15.36	2.63	195.8	983	344.7	18.71

MSZ4- 150-153- 13	298.3	467.2	42.11	165.9	32.3	6.82	37	4.86	30.42	6.47	18.59	2.54	16.16	2.82	203.9	965	346.2	21.65
MSZ4- 46 - 1	316.9	492.3	44.64	171.9	33.4	7.12	39.4	5.29	31.53	6.97	19.74	2.7	17.05	3.05	220.4	1007	358.2	25.93
MSZ4- 46 - 2	338	520.8	46.51	180.2	35.61	7.05	39.6	5.09	32.09	7.01	19.8	2.62	17.85	3.07	217.4	989	365.3	27.86
MSZ4- 46 - 3	324	492.4	43.52	174.7	32.7	6.88	36.5	4.88	30.3	6.5	18.59	2.4	14.98	2.59	200.7	995	349.2	24.57
MSZ4- 46 - 4	339.9	520.4	46.1	177	33	7.07	36.9	4.79	29.1	6.39	18.2	2.48	15.87	2.63	199.1	951	352.3	24.56
MSZ4- 46 - 5	336.5	504.3	44.56	170.9	31.8	6.69	37	4.7	28.3	6.17	17.78	2.38	16.49	2.69	200	1011	354.1	25.69
MSZ4- 46 - 6	311.3	495.4	44.91	176.2	34.9	7.15	39.7	5.49	34.1	7.74	21.58	2.86	18.64	3.14	235.6	975	350.9	23.52
MSZ4- 46 - 7	233.9	378.3	35.59	139.2	27.9	5.94	33	4.47	27.74	6.2	17.52	2.45	14.28	2.63	191.4	972	355.6	11.56
MSZ4- 46 - 8	267.8	430	39.36	155.4	30.6	6.5	35.9	4.93	30.9	6.49	18.81	2.55	16.2	2.67	206.9	998	364.1	18.31
MSZ4- 46 - 9	269.1	424.3	38.45	147.8	29.9	6.38	34.4	4.6	28.7	6.27	17.86	2.38	15.59	2.63	199	906	343.4	18.15
MSZ-4 Core																		
Sample Spot	La (ppm)	Ce (ppm)	Pr (ppm)	Nd (ppm)	Sm (ppm)	Eu (ppm)	Gd (ppm)	Dy (ppm)	Ho (ppm)	Er (ppm)	Tm (ppm)	Yb (ppm)	Lu (ppm)	Y (ppm)	Mn (ppm)	Sr (ppm)	Th (ppm)	U (ppm)
MSZ4- 49 _core-1	345	476.3	40.23	150.7	26.36	5.55	29.5	3.72	24.34	5.36	15.97	2.12	12.95	2.31	169	1006	360	12.44
MSZ4- 49 _core-2	365	529.9	45.32	174	29.8	6.66	35.5	4.75	29.24	6.4	19.18	2.51	16.29	2.77	203.2	1012	351.3	23.13
MSZ4- 49 _core-3	272.6	397.6	33.93	129.1	22.6	4.81	26.6	3.68	22.63	4.83	14.28	1.86	11.71	2.02	152.3	980	345.2	10.13
MSZ4- 49 _core-4	269.4	408.3	34.85	137.6	24.7	5.27	28.2	3.84	24.29	5.25	14.94	1.97	13.12	2.22	162.9	945	346.6	9.58
MSZ4- 49 _core-5	431.1	554.8	44.34	162.5	26.5	5.63	28.6	4.1	24.5	5.29	15.36	2.12	13.29	2.34	172.6	1026	371	16.21
MSZ4- 49 _core-6	377	546	45.8	175.1	31.2	6.58	35.7	4.79	29.2	6.53	18.48	2.53	15.59	2.76	203.4	1005	351	27.5
MSZ4- 49 _core-7	284.6	413.3	35.2	133.3	22.9	4.9	26.1	3.59	22.09	4.68	14.07	1.87	11.92	1.93	152.1	999	354.1	8.01

MSZ4- 49 _core-8	202.3	280	23.42	88.3	15.2	3.3	18.3	2.45	14.4	3.07	8.85	1.178	7.37	1.31	100.3	1044	350.3	2.03
MSZ4- 49 _core-9	405	522	41.69	153	25.9	4.75	26.6	3.67	22.69	5.01	14.73	1.99	12.2	2.14	162.1	1018	363.8	11.02
MSZ4- 49 core-10	296.2	425.2	36.24	137.5	24.43	5.13	27.23	3.61	23.49	4.98	14.68	1.88	12.63	2.14	161.3	1017	336.5	10.81
MSZ4- 49 core-11	258.2	383	33.1	127.6	23.4	4.84	26.1	3.54	22.1	4.78	13.55	1.76	11.35	1.95	150	987	354.7	14.7
MSZ4- 49 core-12	255.7	379.3	32.86	126	23.5	4.66	26.97	3.42	21.73	4.68	13.48	1.804	11.06	1.94	150	1008	373.4	5.14
MSZ4- 49 core-13	166.8	235.4	19.9	73.8	12.95	2.87	14.38	1.974	11.91	2.6	6.53	0.967	5.83	1.012	82.2	994	351.9	0.276
MSZ4- 49 core-14	168.9	241.5	20.57	74.4	13.88	2.92	15.65	2.01	12.54	2.69	7.34	0.925	6.3	0.992	84.2	979	356.8	0.397
MSZ4- 49 core-16	270.1	419.5	37.71	142.8	27.7	5.67	32.4	4.28	26.85	5.66	16.08	2.19	13.51	2.36	183.1	946	367.3	7.6
MSZ4- 49 core-17	339.9	523.1	46.16	176.2	33.1	7.01	38.2	5.2	33.6	7.02	20.34	2.85	17.68	2.88	222.3	990	366.1	25.26
MSZ4- 49 core-18	218.5	319.5	27.66	103.7	19.47	4.07	21.6	2.98	17.65	3.84	10.85	1.476	8.87	1.541	121.2	1013	364.3	1.708
MSZ4- 46_core- 1	141.9	204.7	18.06	69.3	13.29	2.86	15.05	2.03	12.39	2.58	7.21	0.936	5.92	0.976	83.9	988	345	0.121
MSZ4- 46_core- 2	187	275	24.3	94.7	17.8	3.97	20.9	2.68	17	3.72	10.19	1.37	8.61	1.52	117	999	349.7	5.8
MSZ4- 46_core- 3	293.2	454.8	40.73	154	30	6.38	34.9	4.65	29.55	6.36	17.92	2.53	15.79	2.59	199.1	978	346.9	19.32
MSZ4- 46_core- 4	340.6	532	47.7	184.6	35.6	7.65	41.5	5.66	35.1	7.66	22.14	2.92	18.52	3.1	237.7	975	347.8	26.77
MSZ4- 46_core- 5	302	473.7	42.73	164	33.1	7.03	37.7	5.01	31.26	6.9	19.41	2.57	16.29	2.77	214.8	985	371.5	20.48
MSZ4- 46_core- 6	313.1	479.1	42.41	161.1	31.2	6.33	36	4.77	29.74	6.42	18.41	2.54	15.34	2.6	204.1	991	349.1	22.07
MSZ4- 46_core- 7	306.5	474	42.5	162.7	31.1	6.65	36.8	4.71	30.2	6.63	18.44	2.61	16.41	2.83	207.1	1004	358.6	22.2

MSZ4-46_core-8	257.8	397.4	35.08	135.3	26.4	5.7	29.97	4	25.01	5.54	15.88	1.99	12.99	2.37	174	990	353.1	16.23
MSZ4-46_core-9	288.6	447	40.5	157	29.3	6.19	35.8	4.76	30.1	6.44	18.52	2.46	15.49	2.6	202.4	980	358.1	21.3
MSZ4-46_core-10	339.2	519.3	46.86	183.9	34.7	7.53	40.5	5.55	33.95	7.33	21.19	2.82	18.08	3.02	230.2	1002	353.8	30.17
MSZ4-46_core-11	284.5	447.2	40.92	164	31.8	6.89	37.1	5.04	31.69	6.68	19.41	2.66	16.42	2.87	212.9	964	354	23.71
MSZ4-46_core-12	338.3	515	46.79	179.5	32.7	7.26	38.8	5.25	34.21	7.2	21	2.85	17.44	3.04	223.6	1013	358.5	27.93
MSZ-4 Rim																		
Sample Spot	La (ppm)	Ce (ppm)	Pr (ppm)	Nd (ppm)	Sm (ppm)	Eu (ppm)	Gd (ppm)	Dy (ppm)	Ho (ppm)	Er (ppm)	Tm (ppm)	Yb (ppm)	Lu (ppm)	Y (ppm)	Mn (ppm)	Sr (ppm)	Th (ppm)	U (ppm)
MSZ4-49_rim-1	178.2	246.2	21.1	78.5	14.2	3.04	15.5	2.08	12.92	2.74	7.77	1.021	6.57	1.084	89.1	1027	341	1.17
MSZ4-49_rim-2	183.3	261.9	22.36	83	13.81	3.14	18.03	2.33	14.22	3.14	8.32	1.084	7	1.166	95.7	1002	368.1	0.728
MSZ4-49_rim-3	162.7	227.9	19.09	72.6	12.86	2.69	14.47	1.85	11.68	2.43	6.98	0.805	5.75	0.942	80.8	1006	347.6	0.179
MSZ4-49_rim-4	368.4	550.3	47.92	180	34.1	7.05	37.8	5.2	32.1	7.08	19.87	2.72	17.26	3.13	220.2	1013	357.1	24.58
MSZ4-49_rim-5	258.8	374.6	32.23	120.3	22.3	4.72	24.8	3.34	20.54	4.3	13.24	1.622	10.72	1.94	140.8	1060	357	0.94
MSZ4-49_rim-1	151.7	217.9	18.57	67.7	12.55	2.57	14.39	1.86	11.29	2.29	6.57	0.884	5.72	0.942	78.4	978	350.7	0.159
MSZ4-46_rim-1	152.3	220.4	19.38	74.8	13.55	3.1	16.44	2.21	13.34	2.81	8.05	1.073	6.38	1.07	89.8	1007	353.8	0.268
MSZ4-46_rim-2	230.8	335.9	29.41	110.3	20.15	4.41	23.8	3.04	20.42	4.28	12.4	1.53	10.68	1.71	133.2	1047	347.4	0.822
MSZ4-46_rim-3	145.5	212.4	18.85	72.4	13.34	2.88	14.68	1.99	12.3	2.61	7.45	1.004	5.96	1.047	85	986	355.6	0.186
MSZ4-46_rim-4	232	338.9	30.01	113.1	20.28	4.39	25.1	3.13	20.79	4.43	11.82	1.707	10.41	1.83	135.7	1023	352.2	1.461

MSZ4- 46_rim - 5	141	198	17.6	65.8	12.19	2.68	15.6	2.02	13.1	2.65	7.17	1.009	6.1	0.99	83.2	1024	343	0.5
MSZ-5.2 WG (Unzoned Grains)																		
Sample Spot	La (ppm)	Ce (ppm)	Pr (ppm)	Nd (ppm)	Sm (ppm)	Eu (ppm)	Gd (ppm)	Dy (ppm)	Ho (ppm)	Er (ppm)	Tm (ppm)	Yb (ppm)	Lu (ppm)	Y (ppm)	Mn (ppm)	Sr (ppm)	Th (ppm)	U (ppm)
MSZ5.2- 72-73 - 1	173.5	276.9	26.37	110.9	25.79	5.56	33.6	4.82	31.27	6.87	19.75	2.61	16.32	2.58	210.1	1021	343.6	11.14
MSZ5.2- 72-73 - 2	121	191.9	17.94	77	17.2	4.11	24.4	3.47	22.3	4.79	13.87	1.77	11.29	1.91	152.8	2180	356.6	4.66
MSZ5.2- 72-73 - 3	141.3	227.9	21.75	92.8	20.8	4.93	28.3	3.99	25.8	5.66	16.03	2.15	13.61	2.16	176.8	1018	358.5	5.99
MSZ5.2- 72-73 - 4	146.2	235.1	22.14	90.6	19.87	4.83	28.6	3.84	25.56	5.36	15.76	2.14	12.77	2.03	171	1017	351.2	7.02
MSZ5.2- 72-73 - 5	138.9	217.1	20.56	83.9	18.26	4.37	25.9	3.49	22.87	5.15	14.6	1.955	11.38	1.97	157.6	1008	350.2	4.75
MSZ5.2- 72-73 - 6	133.3	208.8	19.61	83.1	18.07	4.22	24.6	3.5	22.28	4.87	14.38	1.9	11.68	1.826	153.4	1008	351.2	3.6
MSZ5.2- 68-69 - 1	160.6	244.4	22.61	92.9	17.63	4.28	24.31	3.47	21.1	4.77	13.94	1.761	10.55	1.861	145.2	1029	340.1	1.522
MSZ5.2- 68-69 - 2	157	245.4	23.01	95	18.73	4.13	25.16	3.56	21.57	4.59	14.17	1.843	11.13	1.794	148.5	1012	353.4	1.691
MSZ5.2- 68-69 - 3	168.2	273.6	26.08	107.7	20.7	5.02	29.9	4.07	26	5.73	16.75	2.13	13.11	2.22	173.8	1080	343.4	9.53
MSZ5.2- 68-69 - 4	153.6	249.7	23.59	99.7	19.3	4.52	26.7	3.71	23.09	5.18	15.79	1.9	12.16	1.98	159.9	999	344.6	5.54
MSZ5.2- 68-69 - 5	132.7	219.6	20.89	88.5	18.39	4.25	26.1	3.56	22.7	4.83	15.19	1.85	11	1.93	153.2	1018	363.7	2.73
MSZ5.2- 68-69 - 6	176.1	284.3	27.16	113.1	21.89	5	31.1	4.26	26.68	6.03	17.84	2.268	14.01	2.35	186.4	977	346.5	9.18
MSZ5.2- 68-69 - 7	193.8	316.4	30	124.7	25.32	5.73	34.3	4.73	30.67	6.65	19.8	2.49	15.41	2.57	205.3	973	347.5	12.29
MSZ-5.2 Core																		
Sample Spot	La (ppm)	Ce (ppm)	Pr (ppm)	Nd (ppm)	Sm (ppm)	Eu (ppm)	Gd (ppm)	Dy (ppm)	Ho (ppm)	Er (ppm)	Tm (ppm)	Yb (ppm)	Lu (ppm)	Y (ppm)	Mn (ppm)	Sr (ppm)	Th (ppm)	U (ppm)

MSZ5.2- 66-67_core - 1	269.3	444.4	43.02	185.7	42.1	9.25	55.7	7.75	49.2	10.93	31.49	4.01	26.48	4.37	341.1	1111	345.6	29.18
MSZ5.2- 66-67_core - 2	232.7	412.6	41.26	184.6	43.6	9.75	56.2	8.16	53.2	11.58	33.8	4.34	27.11	4.49	355.5	1074	338.5	41.31
MSZ5.2- 66-67_core - 3	75.3	120	11.76	52.7	12.82	3.01	17.83	2.396	15.43	3.37	9.09	1.196	6.75	1.238	102.6	1283	347.7	0.159
MSZ5.2- 66-67_core - 4	101	163.2	15.78	68.7	15.74	3.35	21.22	2.78	18.43	3.83	11.05	1.337	8.91	1.461	120.3	1059	334.6	0.255
MSZ5.2- 66-67_core - 5	50.5	87	8.64	36.6	7.7	2.1	8.5	1.23	8.3	1.8	4.27	0.64	3.91	0.48	53	1610	261	4.35
MSZ5.2- 66-67_core - 6	84.3	143	13.63	62	13.43	2.89	19	2.52	16.18	3.41	10.22	1.3	7.21	1.139	107.1	1093	346	0.159
MSZ5.2- 66-67_core - 7	72.4	124.9	12.69	58.7	14.37	3.23	20.4	2.68	17.5	3.6	9.72	1.247	7.62	1.21	112.2	1082	326.5	1.53
MSZ5.2- 66-67_core - 8	167.9	311.3	31.48	148.3	35.6	8.36	51	7.04	47	9.81	29.2	3.75	23.82	3.77	310.6	1192	403.6	28.04
MSZ5.2- 66-67_core - 10	95.7	153.9	15.14	67.1	15.97	3.18	19.8	2.68	16.41	3.5	10.08	1.27	7.18	1.28	114.2	1144	357.7	0.629
MSZ5.2- 72-73_core - 1	100.9	151.3	13.44	57.9	13.21	2.73	16.7	2.22	14.22	3.04	8.63	1.048	7.28	1.154	97.2	1014	340.7	0.181
MSZ5.2- 72-73_core - 2	93.4	142.9	13.09	55.2	12.08	2.6	16.46	2.08	13.62	2.94	8.26	1.032	6.56	1.087	94.4	1032	341.3	0.18
MSZ5.2- 72-73_core - 3	122.8	188.4	17.01	70.7	15.82	3.32	20.9	2.75	16.98	3.63	10.17	1.361	7.76	1.278	115.5	1399	339	0.576
MSZ5.2- 72-73_core - 4	100.9	152.8	13.5	58.6	13.38	2.87	17.63	2.34	15.39	3.13	8.82	1.139	7.22	1.156	102.4	1185	342.8	0.323
MSZ5.2- 72-73_core - 5	109.8	167.9	15.35	64.4	14.73	3.17	19.72	2.55	17.59	3.59	10.17	1.362	8.02	1.343	114.9	1063	336.7	0.455
MSZ5.2- 72-73_core - 6	118.9	179.2	16.44	67.7	13.92	3.24	19.84	2.61	17.74	3.8	11.2	1.383	8.84	1.331	118.9	1005	341.1	1.06
MSZ5.2- 68-69_core - 1	104.7	163.3	15.61	63.9	12.87	3.12	18.5	2.69	16.51	3.72	10.46	1.303	8.82	1.427	113	1065	389.8	0.514
MSZ5.2- 68-69_core - 2	74.2	117.1	11.19	47	9.93	2.36	13.45	2.016	12.44	2.58	7.54	0.911	5.1	0.983	78.8	928	339	0.062

MSZ5.2- 68-69_core - 3	97.8	152.7	14.39	60.2	11.74	2.84	16.91	2.347	15.5	3.16	9.56	1.16	6.97	1.221	101.7	944	342.4	0.535
MSZ5.2- 68-69_core - 4	230	287	21.9	80	13.67	3.32	19.1	2.54	15.69	3.49	10.18	1.305	8.03	1.311	110	2300	322	1.102
MSZ5.2- 68-69_core - 5	7.83	14	1.39	5.34	1.26	0.347	1.68	0.299	1.83	0.61	2.17	0.4	3.72	0.8	21.4	12350	304	1.27
MSZ-5.2 Rim																		
Sample Spot	La (ppm)	Ce (ppm)	Pr (ppm)	Nd (ppm)	Sm (ppm)	Eu (ppm)	Gd (ppm)	Dy (ppm)	Ho (ppm)	Er (ppm)	Tm (ppm)	Yb (ppm)	Lu (ppm)	Y (ppm)	Mn (ppm)	Sr (ppm)	Th (ppm)	U (ppm)
MSZ5.2- 66-67_rim1 - 1	74.6	118.1	11.35	48.7	11.68	2.48	15.05	2	13.33	2.73	8.16	1.027	6.19	1.099	92.7	1081	354.2	0.063
MSZ5.2- 66-67_rim1 - 2	74.1	125.1	12.06	56.3	12.81	2.8	16.94	2.36	15.17	3.31	8.92	1.171	7.61	1.128	101.7	1137	351.1	0.87
MSZ5.2- 72-73_rim1 - 1	97.2	150.8	13.87	60.3	14.07	3.11	19.65	2.54	17.5	3.57	10.05	1.326	8.07	1.308	115.8	1341	367.1	0.604
MSZ5.2- 72-73_rim1 - 2	94.4	144.5	13.46	56.9	12.42	2.62	17.01	2.21	14.74	3.13	9.27	1.161	7.77	1.429	101.2	4810	329.1	0.46
MSZ5.2- 72-73_rim1 - 3	73.7	95.1	7.59	26.5	5.47	1.13	7.4	0.95	6.12	1.45	4.13	0.648	5.03	1.14	46.3	13720	285.5	0.176
MSZ5.2- 68-69_rim1 - 1	41.5	70.8	7.35	33.8	8.23	2.15	13.53	1.9	11.95	2.623	7.51	0.924	5.68	0.96	79.4	818	322.8	0.061
MSZ5.2- 68-69_rim1 - 2	39.7	50.4	4.03	15.1	2.64	0.648	3.25	0.522	3.31	0.9	3.02	0.447	3.84	0.924	28.8	14260	259	0.104
MSZ5.2- 68-69_rim1 - 3	161.4	243	22.87	91.7	18.2	4.19	24.5	3.32	21.36	4.92	13.7	1.76	10.69	1.77	146.4	1041	343.5	1.58
MSZ5.2- 68-69_rim1 - 4	69.7	107.8	10.33	42.5	7.4	1.6	9.2	1.33	8.6	1.77	5.64	0.63	4.4	0.64	55	1730	282.2	3.19
MSZ-6																		
Sample Spot	La (ppm)	Ce (ppm)	Pr (ppm)	Nd (ppm)	Sm (ppm)	Eu (ppm)	Gd (ppm)	Dy (ppm)	Ho (ppm)	Er (ppm)	Tm (ppm)	Yb (ppm)	Lu (ppm)	Y (ppm)	Mn (ppm)	Sr (ppm)	Th (ppm)	U (ppm)
MSZ6- 52-54 - 1	183.3	320.3	32.5	131.7	25.1	4.72	28.3	3.8	24.4	5.03	14.09	1.74	11.9	1.91	153.7	1002	275.1	3.54
MSZ6- 52-54 - 2	159.7	313	32.56	135.6	24.5	4.19	26.1	3.28	20.44	4.05	11.42	1.44	9.55	1.59	127.6	560	264.9	134

MSZ6- 52-54 - 3	268.5	450.1	42.49	165.2	26.5	4.4	28	3.56	21.47	4.62	13.14	1.647	10.36	1.625	140.3	1095	264.5	7.33
MSZ6- 52-54 - 4	393.4	640	57.86	216.8	34.3	5.18	34.5	4.14	25.18	5.45	14.79	1.914	11.32	1.92	159.3	983	251.2	10.52
MSZ6- 52-54 - 5	421	671	57.7	209.9	32.5	5.15	33.3	4.07	25.3	5.28	14.79	1.93	11.76	2.05	162.2	1170	257.5	12.6
MSZ6- 52-54 - 6	533.3	874	75.2	276.8	43.5	7.1	45.5	5.77	35.4	7.38	21.56	3	17.32	2.97	234.7	1195	268.1	21.87
MSZ6- 52-54 - 8	432.1	731	64.8	239	37.8	6.12	40.5	5.04	30.5	6.71	19.26	2.51	15.14	2.69	206.8	1153	262.3	12.22
MSZ6- 52-54 - 9	521	816	68.6	243	35.8	6.34	38.4	4.68	30.1	6.31	18.82	2.43	14.94	2.5	195.3	1204	262.9	20.1
MSZ6- 52-54 - 10	440	673	58	201.2	28.9	4.91	30.5	3.84	23.8	5.08	14	1.69	11	1.89	155.7	1235	264.6	10.4
MSZ6- 52-54 - 11	320.8	511	45.98	176	28.7	5.38	31.1	4.07	24.78	5.35	15.19	2	12.04	2.03	162.7	1162	264.9	9.28
MSZ6- 52-54 - 12	316.9	542.6	52.31	206.1	35.5	7.74	43.9	5.91	37.6	8.3	23.5	2.92	17.47	2.9	244.4	1151	269	22.49
MSZ6- 56-59 - 1	187.5	322.7	32.22	132.2	24.84	5.46	31.1	4.16	27.37	5.79	16.22	2.18	12.74	2.07	180.4	1005	271.7	6.5
MSZ6- 56-59 - 3	238	393	37	148.4	24.6	4.99	28.9	3.76	24.1	5.04	14.66	1.7	10.87	1.76	152	1177	261.4	6.03
MSZ6- 56-59 - 4	339.9	570	52.9	201.6	30	5.42	32.9	3.99	25.6	5.3	14.84	2.06	11.88	2.09	164.7	1189	263.6	9.28
MSZ6- 56-59 - 6	280.3	478.1	45.39	175.3	29.82	5.94	35.2	4.73	29.17	6.24	17.43	2.22	13.47	2.28	185.8	1198	267.3	14.74
MSZ6- 56-59 - 9	288.1	499.6	49.41	193.5	34.1	7.48	41.2	5.42	35.1	7.79	21.2	2.71	17.28	2.69	224.4	1166	278.6	21.54
MSZ6- 56-59 - 10	156.3	258.6	25.46	99.3	17.5	4.32	23.5	3.14	18.78	3.95	10.67	1.42	8.62	1.43	123.6	1175	263.7	4.12
MSZ6- 56-59 - 12	219.1	384	38.4	166.1	35.2	7.66	41.3	5.76	37.9	8.16	22.1	2.81	17.2	2.99	235	1079	304.9	22.1
MSZ6- 62-69 - 1	280.9	490.4	49.1	214.7	43	9.07	49	6.85	44	9.55	25.52	3.54	21.3	3.58	274.5	1157	267.2	27.42

MSZ6- 62-69 - 2	219.4	365.5	35.13	146.9	27	5.07	28.5	3.78	23.05	4.98	13.29	1.78	11	1.78	147.7	1139	276.7	7.02
MSZ6- 62-69 - 4	415.7	711	65.77	261.2	44.8	7.7	43.8	5.75	35.58	7.31	20.99	2.84	17.01	2.82	225.8	1165	273.1	24.6
MSZ6- 62-69 - 5	302	494	45.1	178.2	28.9	4.74	28.7	3.44	22	4.72	12.39	1.74	10.64	1.76	144.8	1173	275.3	9.5
MSZ6- 62-69 - 6	287	498	47.1	196.9	34.9	6.44	37.7	4.81	32	6.41	17.67	2.27	14.77	2.41	199.1	1079	277.2	12.76
MSZ6- 62-69 - 7	320.7	554.8	52.43	217.7	40.2	7.16	40.8	5.37	35.3	7.32	19.96	2.67	16.11	2.8	221.3	1060	260.9	16.03
MSZ6- 62-69 - 8	308.3	532.3	52.1	215	40.7	7.63	40.8	5.39	33.9	7.27	19.41	2.73	16.78	2.66	222.8	1214	263.9	15.5
MSZ6- 62-69 - 9	5730	5250	305.2	815	80.5	12.79	57.4	6.91	41.8	8.02	21.72	2.98	19.1	3.14	250.2	1955	331.7	390.6
MSZ6- 62-69 - 10	254.7	443.4	43.9	190.6	38.9	7.7	43.5	5.68	37.6	7.88	20.71	2.88	17.91	2.76	234.8	1090	268.5	18.35
MSZ6- 62-69 - 11	208.1	348.2	34.7	151	30	6.57	34.7	4.78	31.3	6.19	17.1	2.34	13.82	2.49	190.4	1111	258.9	10.08
MSZ6- 68-71 - 1	82.4	135.8	13.62	63	14.2	3.41	19.72	2.8	19.38	4.02	11.21	1.34	7.91	1.27	128.8	1470	298.7	1.62
MSZ6- 68-71 - 2	99.7	168.2	16.82	74.4	15.61	3.59	19.26	2.76	19.29	4.15	10.74	1.382	8.45	1.351	126.2	1079	315	0.883
MSZ6- 68-71 - 3	139.9	239	23.9	108.3	23.7	5.45	30.7	4.38	31.5	6.51	18.4	2.31	14.8	2.44	206	1119	316.5	16.6
MSZ6- 68-71 - 4	151.2	257.2	26.53	115.2	24.5	5.49	29.9	4.13	27.5	5.9	15.3	2.117	13.21	2.14	181.8	1106	338.2	7.24
MSZ6- 68-71 - 5	121.1	205.3	20.67	92.2	19.84	4.48	24.19	3.36	21.7	4.49	12.37	1.605	9.88	1.698	137.4	1048	279.5	1.76
MSZ6- 68-71 - 6	108.8	185	18.9	84.4	18.5	4.68	24.8	3.74	27.2	5.64	16.06	2.05	12.04	1.96	179	1007	315.4	7.1
MSZ6- 66-67 - 1	167.9	304	31.2	137.1	29	6.28	33.1	4.68	30.8	6.33	17.16	2.38	13.92	2.54	192.9	1173	283.7	13.3
MSZ6- 66-67 - 2	297.9	537.2	54.52	226.6	47.4	10.71	57.1	8.09	52.15	10.97	31.55	4.05	25.89	4.28	323.8	1061	279.2	35.84

MSZ6- 66-67 - 3	725	730	58.5	220.7	38.7	8.19	44.9	5.99	38.2	8.33	23.2	2.7	17.5	3.07	242.4	1997	260.8	15.64
MSZ6- 66-67 - 4	294.7	541.7	54.02	223.7	46.9	10.9	58.7	8.16	53.9	11.23	31.94	4.04	26.1	4.37	333.9	1074	274.3	40.1
MSZ6- 66-67 - 5	172.2	336.9	35.77	156.9	35.9	7.9	45.7	6.46	42.8	9.28	26.46	3.29	20.55	3.56	269.6	1025	275.1	24.67
MSZ6- 60-61 - 1	251	453.2	45.3	191.7	42.3	10.06	53	7.29	47.3	10.01	28	3.68	22.02	3.68	293	1095	266.6	19.89
MSZ6- 60-61 - 2	167.3	301	30.3	127.6	28.4	6.59	34.9	5.02	32.6	6.7	19.47	2.36	14.17	2.38	201.1	1036	269.1	6.28
MSZ6- 60-61 - 3	181.4	316.7	31.97	132.5	28.5	6.87	35.8	5.12	31.86	6.9	19.07	2.46	15.11	2.6	200.9	1245	276.5	5.55
MSZ6- 60-61 - 4	207.1	377.2	38.17	163.7	36.8	8.33	46	6.44	39.7	8.55	23.75	3.04	19.02	3.18	249.9	1067	269.7	15.83
MSZ6- 60-61 - 5	122.4	227.7	23.68	103.4	23.16	5.61	30	4.23	26.95	5.8	16.23	2.03	12.48	2.08	175.9	1182	276.6	3.77
MSZ6- 87-88 - 1	82.8	176.9	20.35	93.4	21.7	6.02	30.9	4.41	30.07	6.74	19.15	2.49	15.45	2.57	200.6	883	278.4	8.26
MSZ6- 87-88 - 2	232.5	440.6	44.76	191.7	42.45	11.33	56.5	8.2	51	11.28	31.5	4.14	25.87	4.57	327.6	1006	260.4	40.5
MSZ6- 87-88 - 3	259.3	461.1	46.09	190.1	40.7	9.92	49.1	6.7	42.27	9.24	27.15	3.57	22.6	3.85	275.6	1049	269.5	40.36
MSZ6- 87-88 - 4	57.6	110.6	11.9	54.1	12.79	3.4	18.22	2.5	16.68	3.77	10.8	1.33	8.62	1.43	114.9	924	265.3	0.72
MSZ6- 89-92 - 1	89.5	170.6	17.85	76.9	16.55	4.48	23.2	3.15	19.49	4.21	12.19	1.49	9.15	1.63	130.1	957	267	4.9
MSZ6- 89-92 - 2	229.8	401.8	38.53	151.1	26.9	5.01	28.7	3.72	22.3	4.58	13.21	1.64	10.35	1.8	143.7	1016	282.7	5.1
MSZ6- 89-92 - 4	261.6	494.8	48.09	185.6	32.3	5.8	36.4	4.57	28	6.11	17.3	2.33	14.33	2.38	184.7	1060	272.7	24.1
MSZ6- 89-92 - 5	274.3	501	48	189.5	35.4	7.28	39.6	4.93	31.4	6.76	18.97	2.44	15.84	2.6	208.2	999	275.7	27
MSZ6- 89-92 - 6	341	593.5	55.7	210.9	38	7.4	39.9	5.07	31.53	6.83	19.12	2.67	16.42	2.87	210.5	1089	264	30.87

MSZ6- 89-92 - 7	319.4	579.4	56.1	222.9	40.4	9.13	45.1	6.03	37.9	7.95	22.89	3.18	19.89	3.6	248.8	1061	262.4	40.9
MSZ6- 89-92 - 8	259.9	491	50.8	213.5	42.3	10.79	53.2	7.07	47.4	10.22	28.61	3.82	23.86	4.17	301.8	1043	265.8	36.4
E1-N WG (Unzoned Grains)																		
Sample Spot	La (ppm)	Ce (ppm)	Pr (ppm)	Nd (ppm)	Sm (ppm)	Eu (ppm)	Gd (ppm)	Dy (ppm)	Ho (ppm)	Er (ppm)	Tm (ppm)	Yb (ppm)	Lu (ppm)	Y (ppm)	Mn (ppm)	Sr (ppm)	Th (ppm)	U (ppm)
E1- 76-77 - 3	4750	7.20E+03	633	2260	353	34.1	308	40	237.5	47.76	124.7	15.54	78.9	8.53	1355	196	428.8	296
E1- 76-77 - 4	520	1170	134	628	167.8	20.3	196.9	29.3	183.5	38.4	102.4	12.84	63.9	6.51	1087	88.6	381.9	14.4
E1- 76-77 - 6	870	1840	210	923	199	22.5	200.7	28.92	178.9	35.8	97	12.3	63.4	6.66	1041	191.4	415.8	43.2
E1- 76-77 - 7	3680	5680	514	1880	294	29.6	258.8	35.04	202.9	39.82	106.4	12.72	63.2	6.74	1139	181.7	450.6	222
E1- 76-77 - 8	4325	6620	591.8	2139	327.4	32.16	281.8	37.03	218.2	43.06	114.5	13.7	70.1	7.53	1230	211.9	478.9	295.4
E1- 76-77 - 10	4200	6480	577	2075	319.6	32.47	281	36.65	217.5	43.65	117	13.9	71.5	7.56	1241	274	504.4	320
E1- 78-79 core - 1	3270	5060	455	1588	253.4	23.7	214.1	27.81	168.1	34.1	92.7	11.93	60	6.65	1001	298	421.4	166.3
E1- 78-79 core - 3	43.5	145.9	22.29	124.5	52.7	6.97	78.2	12.95	85.2	16.23	40	4.28	18.22	1.74	438.7	185	363.9	3.76
E1- 78-79 core - 6	1100	1810	173	664	137	14.8	137.9	20.3	130.4	27.3	75	9.38	48.5	5.27	761	139.5	380.4	61
E1- 78-79 core - 7	2910	4530	422	1575	262.3	29	249.4	33.97	209.6	41.72	112.1	13.73	71.7	8.16	1177	168.7	416.9	207
E1- 78-79 core - 9	2410	3760	347	1310	232	25.7	231.9	32.3	200.4	39.72	106.8	13.31	66.3	6.89	1120	129.6	411	139
E1- 86-88 core - 1	3840	5430	458	1562	219.7	23.2	195	25.7	162.1	33	91.2	11.64	60.8	6.81	936	216.3	399.5	198
E1- 86-88 core - 2	2350	3.70E+03	332	1210	208	22.1	219	30.6	196	39.1	107	13.3	62	7	1140	111.7	321.6	158
E1- 86-88 core - 3	442	790	83.7	363	88.3	10.4	109.4	16.96	113.4	24.6	68.6	8.61	41.4	4.6	674	108.7	384.1	47
E1- 86-88 core - 4	3220	4580	388	1360	206	24	196	27	167.3	31.7	82.8	10.39	52.5	5.43	927	147.3	413.2	167

E1- 86-88 core - 6	4505	6780	586	2051	294.3	29.96	262.3	33.88	199.1	40.08	105.9	13.22	68.3	7.44	1141	221.5	449.8	437.6
E1- 86-88 core - 7	12180	16960	1444	4890	695	116.6	585	69.5	374	63.3	142.1	15.33	71.2	7.51	1831	179.9	430.2	290
E1- 86-88 core - 8	5080	7640	666	2340	326	33.9	280	35	202.5	39.3	102.8	12.6	61.9	6.59	1116	208	429	273
E1- 86-88 core - 9	3400	5280	472	1720	268	29.4	271	37.9	252	56	161	20.9	115	12.8	1640	144.7	391	223
E1- 86-88 core - 10	4569	6890	598	2093	299.9	30.07	271.1	34.49	209.8	40.84	109.8	13.6	71	7.64	1173	244.8	452.6	485
E1- 82-83 - 1	7480	10190	831	2690	379	35	304.4	39.1	239	46.23	127.5	16.28	84.5	9.42	1336	229	485	359
E1- 82-83 - 2	37830	4.89E+04	4130	13800	2311	460	1994	226.1	1115	171	335.7	29.5	127.1	12.81	5220	135.3	412.3	207
E1- 82-83 - 3	1740	2630	259	960	178	19.2	180.6	25.4	163.4	33.5	93.3	11.54	59.2	6.3	948	101.1	432.2	81
E1- 82-83 - 4	5950	8730	754	2594	398.1	38.47	332.1	42.31	253.9	50.29	135.5	16.51	86.6	9.26	1428	218.1	485.3	391.3
E1- 82-83 - 5	5081	7710	670.3	2315	358.2	35.7	295.7	36.55	219.4	43.48	114.8	13.9	71.6	7.5	1221	210.8	475.1	302.9
E1- 82-83 - 6	3970	5960	521	1830	298	30.3	263	34.7	215.7	42.57	117.1	14.07	73.4	7.93	1184	181.8	418.3	300
E1- 82-83 - 7	1076	1620	143.8	516	93	11.35	93.3	13.5	86.9	18.5	52.8	6.77	35	4.69	529	370	427.8	75.3
E1- 84-85 - 1	5280	7330	606	1986	293.9	30.1	243.8	32.25	198.9	39.7	109.1	14.2	75	8.47	1147	262	456.3	261.1
E1- 84-85 - 2	7140	10470	886	2984	451.6	42.37	372.5	48.18	285	56.75	153.2	19.1	98.8	10.45	1602	237.3	494.1	398.5
E1- 84-85 - 3	6030	8990	774.1	2665	422.5	38.89	359.7	47.27	283.2	57	156.1	19.15	98.8	10.4	1640	240.9	487.3	389.9
E1- 84-85 - 4	6120	9330	812	2807	433.9	39.69	359.9	45.26	272.8	54.19	146.6	18.02	93	9.62	1556	212.1	481.2	395
E1- 84-85 - 5	6080	9300	812	2797	422.1	39.33	354	44.67	266.4	53.13	143.8	17.34	90.1	9.46	1522	203.4	472.9	376.5
E1- 84-85 - 6	5640	8590	749	2604	395.4	37.49	335.4	42.67	253.8	50.57	135.9	16.49	84.3	9.07	1425	207.8	456.7	356.4
E1- 84-85 - 7	5670	8700	761	2630	403	38.2	339.9	42.13	251.4	50.48	135.9	16.67	83.1	9.29	1425	220	451.2	373
E1- 84-85 - 8	2902	4918	471.5	1815	313.3	31.49	298.7	40.03	251.5	52.33	146.8	18.63	100.4	11.93	1501	210.2	443.7	420

E1- 84-85 - 9	3720	5740	506	1818	283.2	29.12	247.8	31.41	198.5	38.88	104.6	12.81	67.8	7.46	1098	266	440.2	287
E1- 84-85 - 10	2000	3080	273	984	166	17.5	161	22.5	143.2	28.9	77.2	9.54	49.2	5.65	803	232	397.4	258
E1- 74-75 - 1	1970	3190	294	1102	203.5	20.43	195.3	26.32	167.8	34.5	94.4	11.96	62.3	6.83	1000	166.4	398.2	280
E1- 74-75 - 2	4050	6210	546	1950	306	27.9	285.9	38.9	243.2	49.5	134.9	17.12	89.6	9.99	1416	291	434	675
E1- 74-75 - 4	1172	1785	162	593	107.6	12.53	117.9	17.4	115.7	22.96	62.8	7.52	39.8	4.44	657	249	404.2	203
E1- 74-75 - 6	7690	1.09E+04	890	2990	405	36.9	307	37.2	211.9	39.9	103.7	12.58	64.6	6.73	1102	182	418.4	392
E1- 74-75 - 7	2730	4.00E+03	345	1180	185	18.2	163	21.9	134.7	26.26	68.2	8.37	41.2	4.2	720	259	368.7	131
E1- 74-75 - 8	4060	5680	498	1740	263	26.8	222	29.2	178.4	33.1	87.5	10.75	54.9	5.81	968	199	397.1	208
E1- 74-75 - 9	1235	1880	168	621	110.5	12.6	119	17.15	111.3	23.06	63	7.69	40.2	4.77	648	159.5	395.9	201
E1-N Core																		
Sample Spot	La (ppm)	Ce (ppm)	Pr (ppm)	Nd (ppm)	Sm (ppm)	Eu (ppm)	Gd (ppm)	Dy (ppm)	Ho (ppm)	Er (ppm)	Tm (ppm)	Yb (ppm)	Lu (ppm)	Y (ppm)	Mn (ppm)	Sr (ppm)	Th (ppm)	U (ppm)
E1- 80-81 core- 1	1430	2040	173	599	97.3	13.74	101.5	14.57	95.4	18.4	47.2	5.56	28.8	3.22	512	115.5	262.6	71.8
E1- 80-81 core - 2	1120	1590	138	491	82	10.4	92.3	13	83.4	16.7	43.7	5.23	28.5	3.16	458	141	312.8	62
E1- 80-81 core - 4	108	200	21.9	98	28.1	6.08	42	7.07	47.2	8.44	16.94	1.44	5.14	0.581	191.8	59.9	214.7	3.9
E1- 80-81 core - 5	19.6	75.1	10.85	55.7	20.68	4.51	32.7	6.36	45.1	8.73	19.97	1.69	5.69	0.551	206	53.1	248.7	0.3
E1- 80-81 core - 7	527	772	67.5	245.5	46.7	6.76	53.8	8.81	58.2	11.12	27.2	3.13	16.2	1.83	297	104.5	283.6	27.1
E1-N Rim																		
Sample Spot	La (ppm)	Ce (ppm)	Pr (ppm)	Nd (ppm)	Sm (ppm)	Eu (ppm)	Gd (ppm)	Dy (ppm)	Ho (ppm)	Er (ppm)	Tm (ppm)	Yb (ppm)	Lu (ppm)	Y (ppm)	Mn (ppm)	Sr (ppm)	Th (ppm)	U (ppm)
E1- 80-81 rim1 - 1	3.22	7.75	1.13	6.7	2.76	1.008	8.24	1.92	18.76	5.99	25.13	3.34	20	3.06	207.1	144.7	360.1	0.036

E1- 80-81 rim1 - 2	27.1	50	5.31	22.9	7.92	2.07	13.07	2.87	24.6	6.45	21.3	2.74	15.14	2.28	190.7	675	360.5	0.192
E1- 80-81 rim1 - 3	32.9	61	6.3	30.4	9.1	2.11	14.3	2.83	23.3	6.44	22.8	2.8	16	2.23	202.2	433	340.3	2.17
E1- 80-81 rim1 - 4	8.3	21.2	2.96	14.4	5.7	1.44	10.5	2.19	20.5	6.11	22.37	3	16.3	2.54	190.5	453	320	0.295
E1- 80-81 rim1 - 5	3.39	8.12	1.16	6.81	3.39	0.8	8.07	1.67	16.36	4.76	17.42	2.28	12.6	1.89	163	159.9	367.6	0.0111